Green Thermo-Mechano-Chemical Processing for the Recovery of Lignocellulosic Biomass Components

by

Karelle Seno Guiao

A thesis

presented to the University of Waterloo

in fulfillment of the

thesis requirement for the degree of

Master of Applied Science

in

Chemical Engineering

Waterloo, Ontario, Canada, 2022

Author's Declaration

This thesis consists of material all of which I authored or co-authored: see Statement of Contributions included in the thesis. This is a true copy of the thesis, including any required final revisions, as accepted by my examiners.

I understand that my thesis may be made electronically available to the public.

Statement of Contributions

Some of the contents of the following thesis has been published or will be published in the future. Below is a list outlining the sections of this thesis that has been co-authored and are presented verbatim:

- Chapter 2 outlines a thorough literature review on the reactive extrusion of lignocellulosic biomass, which is adapted from an accepted manuscript entitled, "**Reactive Extrusion as a Sustainable Alternative for the Processing and Valorization of Biomass Components**" to be published in the ***Journal of Cleaner Production*** in 2022. At present time, this manuscript is undergoing the review process, and thus, the contents presented in this thesis are subject to future changes. For this work, I am the first author. A research associate, Arvind Gupta, contributed to the literature review pertaining to nano- and micro-cellulose production, as well as the development of figures. Dr. Mekonnen and Dr. Tzoganakis provided guidance and all authors reviewed and revised the manuscript.
- Chapter 3 is adapted from a previously published manuscript "**Green Mechano-Chemical Processing of Lignocellulosic Biomass for Lignin Recovery, Chemosphere, 293 (2022), 133647,**" in which I am the first author. I was responsible for all investigation, analysis, methodology, visualization, writing, and reviewing. Dr. Mekonnen and Dr. Tzoganakis initiated the project and provided supervision, revision, and editing. All authors contributed to data analysis and discussion.

- Chapter 4 is also adapted from a manuscript that is currently under review for publication in ***Carbohydrate Polymers*** in 2022 titled, "**Green Thermo-Mechano-Chemical Deconstruction of Cellulose Fibers for Cellulose Nanocrystal Production by Reactive Processing,**" in which I am the first author. I was responsible for all investigation, analysis, methodology, visualization, writing, and reviewing. Dr. Mekonnen and Dr. Tzoganakis initiated the project and provided supervision, revision, and editing. All authors contributed to data analysis and discussion.

Abstract

In recent years, there has been a surging demand for sustainable materials due to the environmental issues related to petroleum-derived plastic products. Lignocellulosic biomasses and its various components, such as cellulose, lignin, and hemicellulose, are attractive material alternatives as they are widely available and renewable bioresources. However, the applicability of these various components in materials is currently stunted by their acid-heavy production processes which are not environmentally safe and present serious industrial safety hazards, which counteracts their initial purpose. In addition, some processes are prohibitively expensive and generate low yield. Thus, for more meaningful application, greener and inexpensive processes are necessary.

In this thesis, a reactive batch mixer process involving an ionic liquid, an environmentally friendly solvent, was developed and investigated for the purpose of material, cost, and time efficiency. This reactive process was explored for two different applications pertaining to lignocellulosic biomasses: (1) lignin extraction from wood flour and (2) cellulose nanocrystal (CNC) production from cellulose. For both studies, the primary solvent used was 1-butyl-3-methylimidazolium chloride (BmimCl).

In the extraction of lignin from biomass, high loadings of mixed hardwood flour (MHF) were processed with BmimCl in a batch mixer to solubilize its lignin components. The mixture had a high complex viscosity (approx. 107 Pa·s) at low shear rates and displayed pronounced shear thinning behavior at 50 wt.% MHF loading. A 2^2 factorial design was also implemented to

study the effects of MHF solid loading amount and residence time on lignin extraction yield. A maximum yield of 36.6% was obtained at the maximum solid loading amount and residence time (50 wt.% and 45 min, respectively). The extracted lignin samples were also characterized in comparison with commercial Kraft lignin and lignosulfonate using Fourier transform infrared (FTIR) spectroscopy, ultraviolet-visible (UV-vis), and solid-state carbon nuclear resonance (^{13}C-NMR).

A similar process was also utilized for CNC production from cellulose. In this application, the BmimCl-batch mixer process was implemented with molten oxalic acid dihydrate (OA) to facilitate acid hydrolysis. The influence of OA content and processing time on CNC yield was explored using another factorial design. Through this, a maximum CNC yield (59 wt.%) was obtained with a mixture composition of 1:0.7:0.075 (Cellulose:BmimCl:OA, w/w/w) and processing time of 2.5 min. The produced CNCs were characterized using FTIR and x-ray photoelectron spectroscopy (XPS). Further investigation revealed that the particle size, degree of crystallinity, and thermal stability of the produced CNCs were found to be competitive with those of a commercial CNC product.

In both applications, high yields for lignin recovery and CNC production were achieved at high solid loadings and shorter residence times compared to traditional treatment methods involving ionic liquids. The quality of the lignin and CNC products were also preserved and were determined to be competitive with similar commercial products.

Acknowledgements

First and foremost, I am most grateful to my supervisors, Professor Tizazu Mekonnen and Professor Costas Tzoganakis, who have presented me with the opportunity to pursue my interest in biopolymer research. I have the deepest respect of their knowledge of polymers and polymers processing and their work continues to inspire me. I appreciate your continual guidance and mentorship throughout the pursuit of my master's degree. I also thank the remainder of my committee members, Professor Leonardo Simon and Professor Ali Elkamel, for taking their time to review my thesis and providing insightful feedback.

I would also like to express my appreciation to my colleagues. My master's was completed during an unprecedented time and there were many restrictions, and so I appreciate all the extra efforts you all made to form and develop our friendships. Coming from a materials science background, I am thankful for the support you have provided me in guiding me through chemical engineering. Thank you to Dr. Boon Cheng, Dr. Arvind Gupta, Dr. Hormoz Eslami, Dr. Will Chen, Ewomazino Ojogbo, Binh Trinh, Curtis Seto, Debela Tadele, Hyejin Lee, and Rachel Blanchard. And I especially want to appreciate, Rohan Shorey, Dylan Jubinville, and Azin Adibi, for their never-ending support in and out of the lab.

Next, I want to highlight my new and old friends. To Sophie Campbell, Abigail Vicente, and Alana Guevara, who made my experience in Waterloo the best it could be. To my UofT friends, Medhavi Patel, Julian Rosas, Shaunak Pathane, Aarti Mohnani, Jobey Chua, and Rafia Kouser, who have continuously encouraged me ever since I reached a decision to pursue graduate

studies. To Samantha Johnson and Caitlin Salmon-Eisler, who are my biggest cheerleaders in life. To Angela Mangila, with whom my conversations are endless. And to my life-long friends, Camille Glorioso and Abby Ducay, who will always have my back no matter the distance between us. I am truly thankful to you all.

I also could not have done this without the encouragement of my family. To my second family, the Carlos Family (Merica, Erika, Joyce, and Enrique Carlos), with whom I built some of my brightest memories. To Rene Jayme, Guiane Guiao, and Almah Guiao - home is bright and fun because of you all. To my brother, Karlo Guiao, who brings me laughter and iced coffee. And finally, to my parents, Charina and Angel Guiao, who will always hug me every time I come back home. Your love, support, and never-ending belief in me is what encourages me to constantly improve and try to be the best me. Thank you all for being my home.

Table of Contents

List of Figures

List of Tables

List of Abbreviations

AFM	Atomic force microscopy
AIL	Acid insoluble lignin
AIR	Acid-insoluble residue
AmimCl	1-allyl-3-methylimidazolium chloride
ANOVA	Analysis of variance
ASL	Acid soluble lignin
BS	Barley straw
BmimCl	1-butyl-3-methylimidazolium chloride
BNC	Bacterial nanocellulose
CMC	Carboxymethyl cellulose
CNC	Cellulose nanocrystal
CNF	Cellulose nanofibrils
CNW	Cellulose nanowhiskers
CrI	Crystallinity Index
DI	Distilled

DLS	Dynamic light scattering
EmimAc	1-ethyl-3-methylimidazolium acetate
EmimCl	1-ethyl-3-methylimidazolium chloride
FTIR	Fourier transform infrared
G’	Storage modulus
G”	Loss modulus
HCl	Hydrochloric acid
H_2SO_4	Sulfuric acid
KBr	Potassium bromide
L/D	Flighted length to diameter ratio of an extruder screw
L/S	Liquid to solid ratio
MCC	Microcrystalline cellulose
MHF	Mixed hardwood flour
M_w	Weight-average molecular weight
NaOH	Sodium Hydroxide
NCC	Nanocrystalline cellulose
NMR	Nuclear magnetic resonance

OA	Oxalic acid dihydrate
POM	Polarized optical microscopy
R	NaOH/BS dry matter ratios (%, w/w)
$scCO_2$	Supercritical carbon dioxide
SCFX	Supercritical-fluid-extrusion
SEM	Scanning electron microscopy
SFs	Supercritical fluids
SSE	Single-screw extrusion
SESE	Screw extruder steam explosion
TGA	Thermogravimetric analysis
TSE	Twin-screw extrusion
UV-vis	Ultraviolet-visible
XMG	Xylose, mannose, and galactose
XPS	X-ray photoelectron spectroscopy
XRD	X-ray powder diffraction (XRD)

Chapter 1: Introduction

1.1 Overview and Motivation

The climate crisis and limited supply of fossil fuels creates a need for an alternative to petroleum-based energy and products. In 2022, there are more than 1,500 startups around the world developing new sustainable materials [1]. Bioresources, such as lignocellulosic biomasses, are a key supply in this sector. Lignocellulosic biomasses are plant-based materials that are mostly composed of polysaccharides (cellulose/hemicellulose) and lignin. Some examples of these biomasses include hardwoods, softwoods, sugarcane bagasse, corn stover, and more. Each of its components provide a wide variety of opportunities for valorization and sustainable material application. Cellulose, the most abundant biopolymer in the biosphere, is commonly applied as a filler in composites [2], a dye removal agent in wastewater [3], and Pickering emulsion stabilizers [4] in the form of cellulose nanocrystals (CNCs), cellulose nanofibers (CNFs), cellulose nanowhiskers (CNWs), and bacterial nanocellulose (BNC). Alternatively, hemicellulose is often modified to rid of its hydrophilic nature and applied in medical applications [5], such as wound dressings and drug delivery systems. It has also been grafted and compounded with other materials for bio-adsorbent applications [6]. Further, lignin has value as a filler or matrix for various polymer systems [7], an adsorbent/absorbent [8,9], and an electrode material for supercapacitors [8,10].

Evidently, the components of lignocellulosic biomasses present a varied range of material applications. To recover these components, however, these biomasses require heavy chemical processing. First, the lignocellulosic source is typically pre-treated chemically and/or physically to reduce its recalcitrance, which is then followed by a downstream process for the recovery and purification of a particular component. Acid pre-treatment, specifically with concentrated sulfuric

acid (H_2SO_4), is the most common method employed since acid hydrolysis is a key step for industrial ethanol production from cellulose and hemicellulose [5,11–13]. In the downstream process, acids are also commercially used in the production of CNCs from cellulose [14]. Typically used acids include hydrochloric, phosphoric, maleic, formic, and acetic acids [15]. These acid-based processes are appealing as they are effective at low temperatures and are inexpensive and straightforward to implement [13]. However, these acid-heavy processes also introduce significant challenges, such as equipment corrosion, high toxicity, health and safety concerns, and environmental pollution, in industrial application. Additionally, concentrated acidic processes result in the unintentional degradation of biomass components due to their strong reactivity, especially when combined with heat [5,15]. Therefore, the pre-treatment and valorization of lignocellulosic biomass and its components are inhibited by acid-heavy processing.

One of the main aims of modern research is the development of safer, cleaner, and more efficient manufacturing processes. In biomass processing, more recent studies have explored greener solutions, like dilute acids, ionic liquids, enzymes, liquid hot-water extractions, steam treatments, etc., with the aim of developing and industrializing a more environmentally safe alternative for acid extraction [5,13,14,16,17]. Other investigations have also explored these different solvent systems in combination with mechanical processes such as ball milling [18], extrusion [19,20], steam explosion [21], and more. The introduction of these new processing methods in this field provokes the need for further optimization in terms of processing time and overall costs.

1.2 Research Objectives

This thesis combines an ionic liquid, 1-butyl-3-methylimidazolium chloride (BmimCl), and a mechanical batch mixer method for lignocellulosic biomass processing. In the subsequent analyses, the ionic liquid was used as a green alternative to acidic solvents. On the other hand, the batch mixer was employed as a shear intensive process to facilitate biomass deconstruction at high solid loadings, comparable to an extruder. In combining these two methods, the overall aim of this thesis was to minimize the high costs associated with ionic liquids and reduce processing time. This investigation was employed in two different applications pertaining to lignocellulosic biomasses to highlight its flexibility and industrial potential.

In the first project, BmimCl was processed with mixed hardwood flour (MHF) to solubilize its lignin components, which were then precipitated using a dilute acid for lignin recovery. The main objective of this study was to analyze the effect of solid loading and processing time in the batch mixer on lignin recovery. Additionally, the quality of the recovered lignin was studied and compared with various types of commercially available lignins.

In the second study, a comparable process was employed to produce CNCs. Cellulose was processed with BmimCl and a molten organic acid, oxalic acid dihydrate (OA), in a batch mixer at high solid loadings to facilitate acid hydrolysis. Amorphous cellulose was then removed via a water wash process to produce CNC. The purpose of this project was to determine the influence of OA content and processing time on CNC yield. Similar to the first project, the resulting CNCs were also characterized and compared with a commercial CNC product.

1.3 Thesis Outline

The following thesis is composed of five chapters. The first chapter entail a brief introduction to this work and presents the overall purpose of this thesis. The second chapter presents a thorough literature review of the reactive extrusion processing of lignocellulosic biomasses. Since a batch mixer process is not well-employed in this field of study, the extrusion process was analyzed instead as it is a comparable process. The section highlights the influence of various extrusion parameters on processing, as well as the combination of extrusion with other treatment methods. Next, the third and fourth chapters explore the BmimCl-batch mixer process when applied for lignin recovery from MHF and CNC production from cellulose, respectively. Lastly, the final chapter presents the final conclusions of this work and suggests avenues of future work as well.

Chapter 2: Literature Review

2.1 Biomass Pre-treatment using Extrusion

Extrusion is a thermo-mechanical continuous and inexpensive process often used in metal, food processing, chemical, and polymer industries. Primarily, extruders are employed to homogenize and pump molten polymers through a specifically designed die to develop pellets, sheets, films etc. [22,23]. Additionally, to improve the performance of polymers, the polymer industry has utilized extruders for in-situ chemical reactions as reactive extrusion processes, which further made its space in the pre-treatment of biomasses. Extrusion can be performed using single-screw extrusion (SSE) or twin-screw extrusion (TSE). Both configurations are displayed in **Figure 2.1**. In this process, the material is fed through a hopper, conveyed by a screw that rotates inside a temperature-controlled barrel, and then extruded through a die [24,25]. Key processing variables related to biomass pre-treatment include temperature, screw speed, screw configuration and screw compression ratio (channel depth at the feed to channel depth at discharge ratio) [25].

Depending on the extrusion type, the screw configuration can also vary. For SSE, the screw is typically a single block with a specific flight pattern and pitch. TSE involves two screws that can co-rotating or counter-rotating with respect to each other [23]. The screws can be separated, tangential, partially intermeshing, or fully intermeshing as well [23,26]. Additionally, the screw configuration for TSE can be adjusted depending on what type of process is being performed. Various screw elements such as reverse screws, kneading blocks, mixing gears, and conveying elements can be used. The type of screw elements used and the order in which they are placed can significantly change the mixing behaviour and flow patterns of the machine [24,27]. Of SSE and TSE, TSE is preferred due to its adjustability in terms of mixing and residence time, as well as its overall

heat and mass transfer capabilities [23]. Most commonly, for biomass pre-treatment purposes, fully intermeshing self-wiping co-rotating twin-screw extruders are used [24].

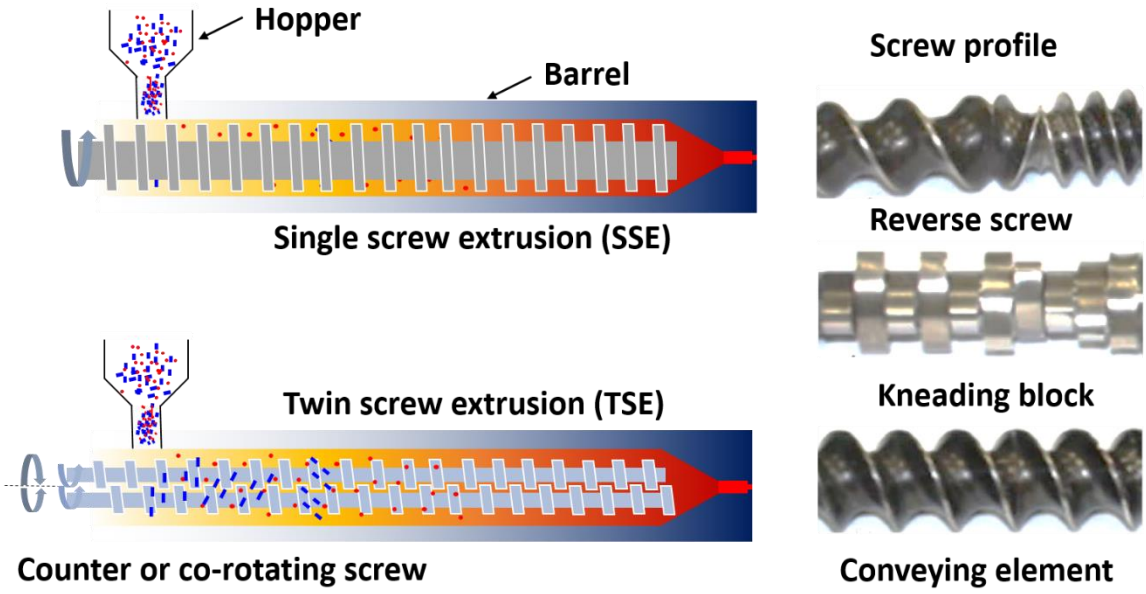

Figure 2.1. A typical single and twin-screw extruder configuration, which includes a motor, a feed hopper, a temperature-controlled barrel, and screws. Pictured on the right are the various screw elements used for a twin-screw extruder setup.

2.2 Extrusion Process for the Pre-treatment of Biomass

Extrusion used in the context of lignocellulosic biomass pre-treatment presents several advantages. First, it is flexible in that it can be combined with chemicals and/or other processes. Extrusion also involves high shear, rapid heat transfer and efficient mixing, all of which improves the effectiveness of the pre-treatment [19]. The extrusion pre-treatment process can also be performed with high biomass loading due to its high shear capabilities, resulting in the successful pulverization and fibrillation of the biomass [24,28]. It also works at moderate temperatures and pH levels, preventing sugar degradation and the generation of toxics [24,29]. The main limitation of biomass pre-treatment using extrusion is its energy consumption, and the capital cost [24]. In

addition, there may be the formation of ethanol fermentation inhibitors, such as furfural and phenolic compounds, under certain conditions of high pressure as well [30].

The way in which extrusion is applied in lignocellulosic biomass pre-treatment varies greatly from study to study. Often, the extrusion process is combined with other pre-treatment technologies to improve the deconstruction of biomasses. Duque et al. classified these different configurations into three main categories: sequence of treatments, reactive extrusion, and extruder modification [24].

The treatment sequence entails the addition of another pre-treatment step before and/or after the extrusion process. In one study, Da Silva et al. impregnated biomass with an ionic liquid (1-ethyl-3-methylimidazolium acetate) prior to extruding the mixture [28]. Reactive extrusion involves the use of chemical or biological catalysts alongside biomass. In fact, most biomass pre-treatments using an extruder are considered a reactive extrusion process due to the presence of water or other chemical reagents used for solubilization. In 2016, Vandenbossche et al. injected sodium hydroxide into the extruder for alkaline pre-treatment, followed by the addition of phosphoric acid for neutralization, the filtrate was removed through output, and an enzymatic solution was finally included for hydrolysis [31]. Lastly, the extruder configuration itself can be modified via the combination of other technologies. For example, Chen et al. designed a screw extruder steam explosion (SESE) apparatus that introduced steam to corn stover inside an extruder and at the end, after pressure is released, the steam explosion occurred [32]. Overall, different extrusion configurations are continuously being explored to determine the most efficient pre-treatment process. These configurations are summarized in **Figure 2.2**, along with the advantages and limitations of biomass pre-treatment using extrusion.

These various methods of extrusion application also facilitate the pre-treatment processing of a wide range of biomasses. Pre-treatment via extrusion has been performed for agricultural wastes,

such as corn stover [33] and sugarcane bagasse [28]. Hardwoods [34–36], softwoods [37,38], and wood-based municipal solid wastes [39] have also been investigated. On the other hand, other non-lignocellulosic biomasses, like algae [40] and animal manure [41], have been pre-treated using extrusion for biodiesel and biogas applications as well and will be explicitly highlighted in a later section.

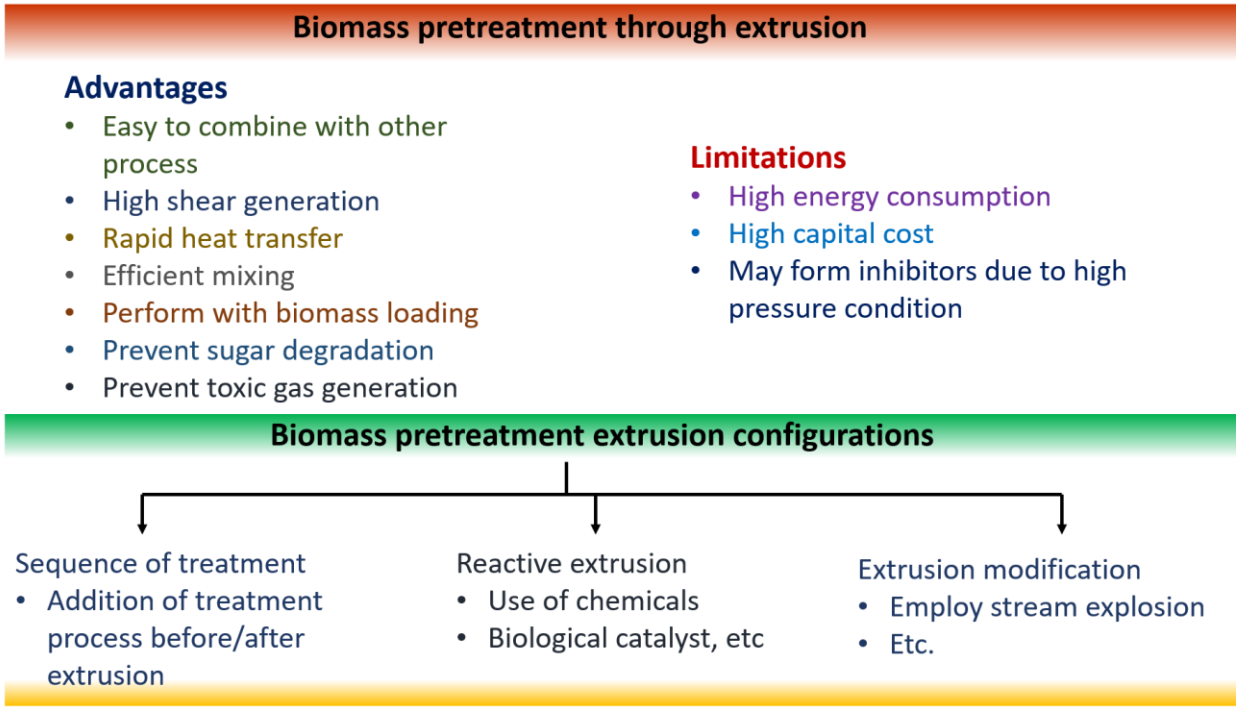

Figure 2.2. The advantages and limitations of the reactive extrusion pre-treatment of biomasses, as well as its various configurations, which have been classified by Duque et al. [24].

2.3 Reactive Extrusion Processing Parameters

The effect of extrusion parameters on the pre-treatment of lignocellulosic biomasses is widely covered in literature [19,20,24,25]. These reviews are often focused on the perspective of lignocellulose preparation for enzymatic hydrolysis which emphasizes sugar recovery for bioethanol conversion. This report will focus on the influence of extrusion parameters on the pre-treatment of lignocellulosic biomass with the aim of fractionation of its main components. However, it is

important to note that the effect of many extrusion variables studied for bioethanol applications still hold true for fractionation because the objective of pre-treatment for both applications is to get rid of the recalcitrance of lignocellulose [42]. Therefore, in this review, the reporting of sugar recovery yields or degree of liquefication obtained from the examined pre-treatment studies serve to emphasize the degree of lignocellulosic mass disruption that directly affects fractionation. Later, the separation and recovery of different biomass components following extrusion are discussed in **Sections 2.5-2.7**.

An advantage of extrusion pre-treatment is the availability of numerous processing variables. Variables include biomass size, liquid impregnation, extruder screw profile, temperature, screw speed, residence time, and the washing and drying of biomass after extrusion. These variables can also be categorized as pre-processing operations, extruder parameters, and post-processing operations, as shown in **Figure 2.3**. The following sections report the effects of each parameter on the pre-treatment process and how they can be controlled to improve it. A summary of the variables of the extrusion pre-treatment processes outlined in this section is provided in **Table 2.1.**

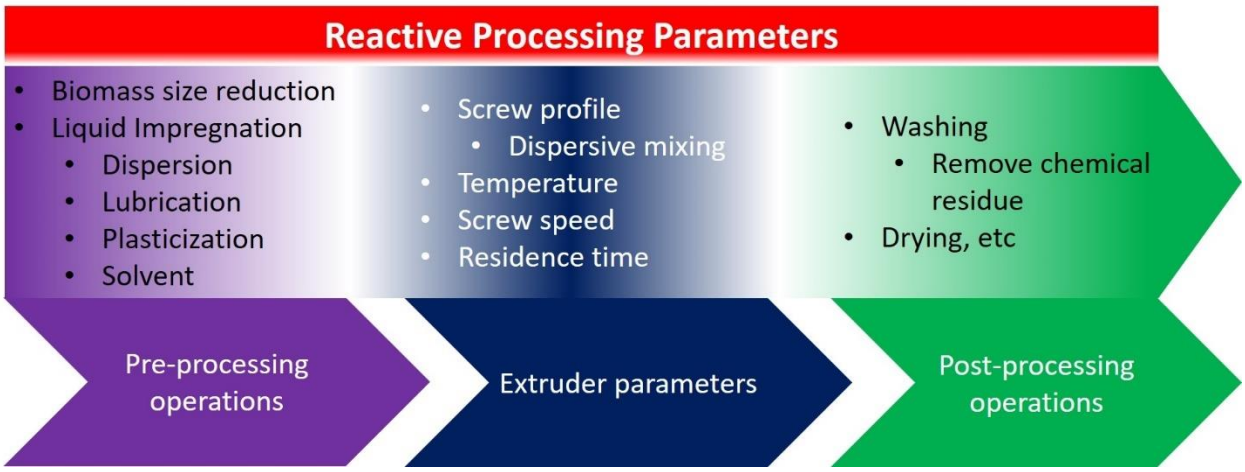

Figure 2.3. The various parameters for a biomass reactive extrusion pre-treatment processes.

Table 2.1. Various extrusion pre-treatment studies and their respective processing variables.

Type of Extrusion	Lignocellulose	Biomass Pre-processing	Screw Length to Diameter Ratio (L/D), Screw Configuration	Screw Speed, Residence Time, and Feed Rate	Additive and Liquid to Solid Composition (L/S)	Temperature Profile	Biomass Post-processing	Sugar Yield at Optimum Processing Condition	Reference
Single-screw Extruder (SSE)	Pine Wood Chips	Milled and sieved, <8 mm	SSE L/D 20:1 Compression ratio, 3:1	100, 150, and 200 rpm 30-90 s depending on rpm	**Additive:** Water 25, 35, and 45% moisture	Single profile 1.100 °C 2.140 °C 3.180 °C	None	Glucose yield – 65.8% Xylose/Mannose/Galactose/ Arabinose yield – 65.6%	37
	Switch grass and prairie cord grass	Milled and sieved, <4 mm	SSE L/D 20:1 Compression ratios 3:1 and 2:1	50, 100 and 150 rpm	**Additive:** Water 15, 25, 35, 45% moisture	Single profile 1. 50 °C 2. 100 °C 3. 150 °C	None	Switchgrass: Glucose yield – 45.25% Xylose yield – 43.86% Prairie cord grass: Glucose yield – 61.42% Xylose yield – 84.25%	43
Co-rotating Twin-screw Extruder (TSE)	Sugarcane bagasse	Milled and sieved; 0.425-1.000 mm biomass size Pre-mixed with IL prior to extrusion	Co-rotating Intermeshing TSE L/D 17:1 Three conveying/reaction zones, two kneading zones, one reverse conveying zone	15 rpm 4 minutes per pass, 1-3 passes	**Additive:** 1-ethyl-3-methylimidazolium Acetate 11.1, 16.6, 25, and 50% solid loading	Single profile 1.80 °C 2.120 °C 3.140 °C 4.160 °C 5.180 °C	Washed with 1 L of distilled water	Glucose yield – 91% Xylose yield – 79%	28
	Douglas-fir	Milled in three steps (coarse, intermediate, and fine)	Co-rotating Intermeshing TSE L/D 40.5:1 Three conveying/reaction zones, two reverse conveying zones	25, 50, 75 rpm	**Additive:** Water 50% moisture	Zone profile 1.25-50 °C 2.25-100 °C 3.25-150 °C	None	Glucose yield – 42.87% Xylose/Mannose yield – 20.99%	44
	Pine Wood Chips	Milled and sieved, <8 mm	SSE L/D 20:1	100, 150, and 200 rpm	**Additive:** Water 25, 35, and 45% moisture	Single profile 1.100 °C 2.140 °C 3.180 °C	None	Glucose yield – 65.8% Xylose/Mannose/Galactose/ Arabinose yield – 65.6%	37

			Compression ratio, 3:1	30-90 s depending on rpm					
	Sorghum bagasse	Milled and sieved, <2 mm Dried overnight at 40 °C	Co-rotating TSE L/D N/A Three conveying/reaction zones, two kneading zones	35 rpm 4 min per pass, 4-10 passes	**Additive:** Deep eutectic solvent (choline chloride: glycerol, 1:2 molar ratio) 30 and 50% solid loading	Single profile 1.150 °C 2.180 °C	Washed with ethanol, freeze dried	Glucose yield – 87.0% Xylose yield – 86.5%	45
	Aspen mechanical pulp	Pre-mixed with distilled water prior to extrusion	Co-rotating Intermeshing TSE L/D 40:1 Three conveying /reaction zones, two kneading zones	250rpm 1, 3, 5, and 7 passes 2.5 kg/h	**Additive:** Water 20, 30, 40 50, 60 and 70% solid loading	Single profile 10 °C	None	*Specific surface area – 18.9 m^2/g *Water retention ability – 216% *Acetyl content – 9.25 mmol/g	46
	Switch grass	Milled and sieved, <4 mm	SSE L/D 20:1 Compression ratios 3:1 and 2:1	50, 100 and 150 rpm	**Additive:** Water 15, 25, 35, 45% moisture	Single profile 50, 100, 150 °C	None	Glucose yield – 45.25% Xylose yield – 43.86%	43
	Prairie cord grass							Glucose yield – 61.42% Xylose yield – 84.25%	43
	Sugarcane bagasse	Milled and sieved; 0.2-2.0 mm	Co-rotating Intermeshing TSE L/D 25:1 Four conveying/reaction zones, three kneading zones Three screw configurations studied	Sugarcane bagasse: 20, 32, 60, 88, 100 rpm 1-10min per pass depending on screw speed and configuration, 1-10 passes	**Additives:** 1.water 2.glycerol 3.ethylene glycol 4. Tween 80 L/S 0-1.0	Single profile Bagasse: 30, 47, 90, 133, 150 °C Straw: 30, 46, 85, 124, 140°C	Washed with water and air-dried	Sugarcane bagasse: Glucose yield – 51.2%	47
	Straw			Straw: 20, 39, 85, 131, 150 rpm 1-10min per pass depending on	**Additives:** 1.water 2.glycerol 3.ethylene glycol 4. Tween 80 L/S 0-1.0	Straw: 30, 46, 85, 124, 140°C	Washed with water and air-dried	Straw: Glucose yield – 68.2%	47

				screw speed and					
	Eucalyptus	Milled and sieved, <2 mm	Co-rotating TSE L/D 24:1 Four conveying/reaction zones, three kneading zones (one forward, two reverse) Two screw configurations studied.	100-300 rpm	**Additive:** NaOH L/S 0.6 -1.5	Zone profile Barrel #1, 50 °C Barrel #2, 70 °C Barrel #3/4 1.75 °C 2. 100 °C 3. 125 °C 4. 150 °C Barrel #5,50 °C	Washing for Configuration B	Glucose yield – 35.8% Xylose yield – approx. 75%	48
	Wheat bran	Milled and separated into 1.041mm>PS >0.132mm and PS<0.132mm	Co-rotating Intermeshing TSE L/D 30:1 Four conveying/reaction zones, three kneading zones (two forward, one reverse)	Wheat bran: 3.7, 5.3, 7 Hz	Additive: 1.Water, 25% or 35% moisture 2.Sodium hydroxide, urea, thiourea mixture (20 and 25% moisture)	Zone profile 1.40-110 °C 2.40-130 °C 3.40-150 °C	None and excess water wash Calcium chloride treatment also performed	Wheat bran: Reducing sugar yield – approx. 67%	49
	Soybean hull			Wheat bran: 3.7, 5.3, 7 Hz	Additive: 1.Water, 25% or 35% moisture 2.Sodium hydroxide, urea, thiourea mixture (30 and 35% moisture)	Zone profile 1.40-110 °C 2.40-130 °C 3.40-150 °C	None and excess water wash Calcium chloride treatment also performed	Wheat bran: Reducing sugar yield – approx. 67%	49

* Enzymatic hydrolysis was not performed, so sugar yield was not obtained. Instead, chemical reactivity was analyzed in terms of specific surface area, water retention ability, and acetylation efficiency.

2.3.1 Pre-Processing Operations

Pre-processing operations refer to the preparation of feed prior to extrusion. This includes biomass size reduction, the impregnation of liquid additives, and moisture control. The influence of these three methods of preparation on the lignocellulosic biomass pre-treatment process are explored.

Size reduction is a prevalent practice prior to the pre-treatment of biomass. In fact, most chemical pre-treatments are not successful without size reduction [50]. While mechanical pre-treatment is involved and particle size reduction occurs during the extrusion processes, biomasses are still often milled prior to extrusion. This may be for practical purposes so that the biomass can be fed inside the extruder barrel, but it also has its advantages. Reducing biomass size increases bio-accessibility and reduces mass and heat transfer limitations during further fractionation or hydrolysis processing [51]. This increase in bio-accessibility is related to the larger external surface area of smaller particle [50]. A chemical pre-treatment study comparing ultrafine and regularly ground poplar wood determined that ultrafine wood had a significantly higher degree of liquefaction at all pre-treatment processing temperatures [52]. However, performing size reduction prior to extrusion pre-treatment involves further high energy consumption. In a study by Gu et al., a three-step milling process was determined for Douglas fir forest residuals in order to pre-condition the biomass prior to extrusion while also considering the energy consumption involved with the milling process [44,53]. While the sugar yield after 30 min of final step ball milling was at a high of 60 wt.%, the energy consumption was also at a high of 2.0 kWh/kg [53]. A ball-milling time of 7 min was determined to be the most energy-efficient for pre-conditioning purposes. Overall, size reduction prior to extrusion is helpful for pre-treatment, but it is limited due to its high energy consumption.

Another pre-processing operation often performed is the impregnation of liquid. Liquid additives are often added to the biomass before extrusion to aid in dispersion, lubrication and plasticization

[54]. Additionally, these liquid additives may be used as solvents in lignocellulose pre-treatment operations to solubilize lignocellulose constituents [24]. When using additives as a solvent, a high liquid to solid ratio (L/S) is preferred (typically 20:1, w/w) [24,28,55]. Da Silva et al. explored the extrusion pre-treatment of sugarcane bagasse at high solid loading and found that the initial rate of enzymatic hydrolysis for 50 wt.% sugarcane bagasse loading mixed with 1-ethyl-3-methylimidazolium, an ionic liquid used as a solvent, was much slower compared to the solid loadings of 11.1, 16.6, and 25 wt.% [28]. Some studies saw little difference in the effect of the L/S ratio, which suggests that the type of solvent is important. In another continuous pre-treatment study involving a deep eutectic solvent made of choline chloride and glycerol mixture (1:2, molar ratio), the glucose and xylose yield of 30 wt.% sorghum bagasse loadings was 85.8% and 84.4%, respectively, while for 50 wt.% loadings, the yield values were similar at approximately 87.0% and 86.5% [45].

When solvents are not used, usually the moisture of the biomass is controlled. The moisture of the biomass directly affects the barrel temperature and rate of shear development, which influences the degree of thermal softening of the biomass [43]. With high moisture content, more slippage occurs, and there is a decrease in friction between material, screw and barrel. Therefore, for water moisture, usually a lower L/S ratio is preferred for pre-treatment purposes [24]. A study by Li et al. compared the reactivity of wet aspen pulp samples with 30 and 60 wt.% solids after performing five extrusion passes for pre-treatment, determining that the defibrillation of the sample with higher solid content was more successful given its better ability to acetylate [46]. Similarly, wet pine wood chips with solid loadings of 55, 65, and 75 wt.% were processed using SSE resulting in total sugar recovery values of approximately 45, 50, and 55%, respectively [37]. In this study, it was

determined that pine wood chips with higher solid content caused an increase in sugar recovery after enzymatic hydrolysis due to the solids contribution in the process shear.

2.3.2 Extruder Parameters

2.3.2.1 Extruder Screw Profile

Depending on the type of extrusion being performed (SSE or TSE), the ways in which the extruder profile can be varied change. The screw for SSE is a single piece consisting of feed, transition, and metering sections typically with a square pitch (when the screw pitch is equal to the screw diameter). While the screw pitch can be constant or variable, in the case of variable pitch designs, the feed and metering sections are square pitch, and the transition section between them has an increasing pitch [54]. Furthermore, sections designed for distributive or dispersive mixing are often added to improve mixing and homogenizing. In particular, dispersive mixing sections introduce high shear stress processes [54]. As aforementioned, most pre-treatment studies are based on TSE, so there is little investigation regarding the influence of SSE profiles on pre-treatment effectiveness. While the influence of section design was not explored, Karunanithy and Muthukumarappan investigated biomass pre-treatment using SSE with varying compression ratios, which is the ratio between the channel depth at the feed to channel depth at discharge [43]. In their study, a screw profile of 3:1 screw compression ratio was determined to be more effective compared to 2:1, with a glucose recovery increase of 12% and 37% for switchgrass and prairie cordgrass, respectively. Additionally, they determined that a higher compression ratio resulted in higher shear force and residence time, causing increase in sugar recovery.

The influence of screw profile for biomass pre-treatment with TSE is more well-studied. The effect of reverse screws in the TSE configuration was investigated by Moro et al. by comparing a screw

design with and without any reverse screws [47]. Reverse screw elements are known to generate backflow in the nip region between two screws, increasing the residence time [56]. When a reverse screw element was added to the last mixing zone, there was an increase of glucose yield from approximately 38% to 59% and an increase of residence time from 1-4 min per pass to 5-10 min per pass [47]. Additionally, zones with reverse screw elements had larger median particle sizes due to the compaction of biomass caused by backflow, but despite this, there was a considerable increase in glucose and xylose/mannose yields at these zones, indicating the opening of recalcitrant structures [44]. Further analysis on TSE screw configuration was performed by Wahid et al. on non-lignocellulosic biomasses, which is explored in more detail in **Section 2.7** [57]. Overall, reverse screw elements provide more exposure to lignocellulose structure, which leads to a more effective fractionation due to the increase in the internal and external surface area of the biomass [44].

2.3.2.2 Temperature

An increase in temperature is well determined to positively effect pre-treatment efficiency [24]. For example, Duque et al. performed alkaline pre-treatment of eucalyptus followed by neutralization using TSE at 125 °C and 150 °C, with the higher temperature displaying higher glucose release (125 °C – 8.3 g / 100 g of the extrudate, 150 °C – 19.4 g / 100 g of extrudate) [48]. Furthermore, in-situ filtration inside the extruder barrel was attempted but was not possible at the highest temperature due to backflow issues caused by the evaporation of the solvent. In the aforementioned study by Karunanithy et al., the high moisture ground pine woodchips were processed at 100, 140 and 180 °C, resulting in an increase from 45% to 55% total sugar yield [37]. Higher temperatures facilitate moisture evaporation and thermal softening, which enhances lignocellulosic biomass disruption. However, in some cases, a maximum temperature threshold was observed due to the type of biomass and catalysts employed in the process [48]. While increasing the temperature of the

processes improves the pre-treatment process, it is limited by chemical, material, and energy constraints. Extrusion processing at higher temperatures could degrade lignocellulose constituents, resulting in the production of fermentation inhibitors.

2.3.2.3 Screw Speed and Residence Time

For extrusion operations, screw speed directly affects the residence time of the biomass. Faster screw speeds are desirable due to high shear generation; however, they lead to a lower degree of fill in TSE and reduced residence time. Once again, in the study by Karunanithy et al., they determined that when screw speed increased from 100 to 200 rpm, the total sugar recovery increased from 45% to 50% [37]. Often, lignocellulosic biomass is also extruded multiple times to increase residence time and improve sugar yield. Kuster Moro et al. examined the glucose yields for extruded sugarcane bagasse and straw for an increasing amount of extrusion passes [47]. They observed that the glucose yield of sugarcane bagasse increased from 32.4% to 36.6% as the number of passes increased from one to three, after, the glucose yield remained consistent. Similarly, for straw, the glucose yield increased from 27.3% to 57.1% as the number of passes increased from zero to ten. Therefore, there exists an optimum balance between screw speed and residence time that must be determined for effective pre-treatment.

2.3.3 Post-Processing Operations

Post-processing operations after extrusion usually entail the removal of solvents or chemicals via a water wash. The purpose of washing the extrudates is to remove chemical residue and enzyme inhibitors [48]. When alkaline treated and neutralized eucalyptus extrudates were washed with distilled water by Duque et al., the glucose release was increased 1.2-fold compared to the glucose release of non-washed extrudates [48]. Mechanical washing operations can also be performed using

a screw-type solid and liquid separator following alkaline extrusion pre-treatment [58]. In doing so, they were able to recycle black liquor twice and developed an opportunity for the recycling of washed water as well. Although, pre-treatment efficiency decreased with increased recycling. Overall, the washing of extrudates with water is a quick way to remove any residues that can directly affect the subsequent fractionation and enzymatic hydrolysis processes [24].

2.3.4 Rheological Considerations

It is also important to understand the rheological behaviour of biomass inside the extruder since it plays a significant role in the pre-treatment process. Senturk-Ozer et al. studied the rheological behaviour of mixed hardwoods pre-treated using extrusion and a set of different solvents, including white liquor (14.2 wt.% sodium hydroxide/NaOH), recycled black liquor, and carboxymethyl cellulose (CMC) [36]. They were initially unsuccessful in extruding biomass suspended in NaOH due to the filtration of the liquid phase, the subsequent collection of solids, poor flow, and the resulting locking of the extruder screws. However, after adding a CMC-NaOH-water mixture with 27 wt.% biomass, extrusion was successful and attributed to its recorded shear thinning behaviour. Additionally, the dynamic properties of the mixture suggested gel-like behaviour, where the storage modulus (G') was higher and parallel to the loss modulus (G") [36]. After black liquor was separated from the extruded mixture, it was recycled and tested to demonstrate improved flowability of the mixed hardwoods since it displayed appealing rheological properties as well. The liquor had a Newtonian plateau at lower shear rates and shear thinning behaviour at higher shear rates.

However, there are not many studies that have explored both the rheological behaviour of the feed and extrudate after extrusion pre-treatment. Instead, valuable rheological information can be referenced from other studies involving incubators or batch mixers. For instance, a study by Kim

et al. compared the rheological behaviour of mixtures of microcrystalline cellulose (MCC), cotton, hemp, and acacia incubated with 1-ethyl-3-methylimidazolium acetate (EmimAc) and 1-ethyl-3-methylimidazolium chloride (EmimCl) [59]. Similar to the behaviour of samples following extrusion pre-treatment, the mixtures show non-Newtonian, shear-thinning behaviour. **Figure 2.4** shows the complex viscosity of various pre-treated biomasses. The lignocellulosic biomasses show typical polymeric, shear-thinning behaviour with high viscosity. The addition of ionic liquid solvents lowered viscosity and caused shear-thinning behaviour at higher shear rates. Overall, the use of solvents decreases the amount of shear present in the extruder, which directly affects the amount of heat generation as well.

2.3.5 Conclusions Regarding Reactive Extrusion Processing Parameters

The effectiveness of the reactive extrusion process depends on its various parameters. Pre-processing parameters, such as size reduction, impregnation of a solvent, or moisture control, aim to increase bio-accessibility or introduce solvents to aid in processing. Extruder parameters dictate the degree of shear intensity through the adjustment of the screw profile, temperature, and screw speed/residence time. And post-processing operations dictate the purity of the extruded product, removing inhibitors to facilitate more effective fractionation or enzymatic hydrolysis. Together, these parameters are the fundamentals upon which a reaction extrusion process should be built and optimized.

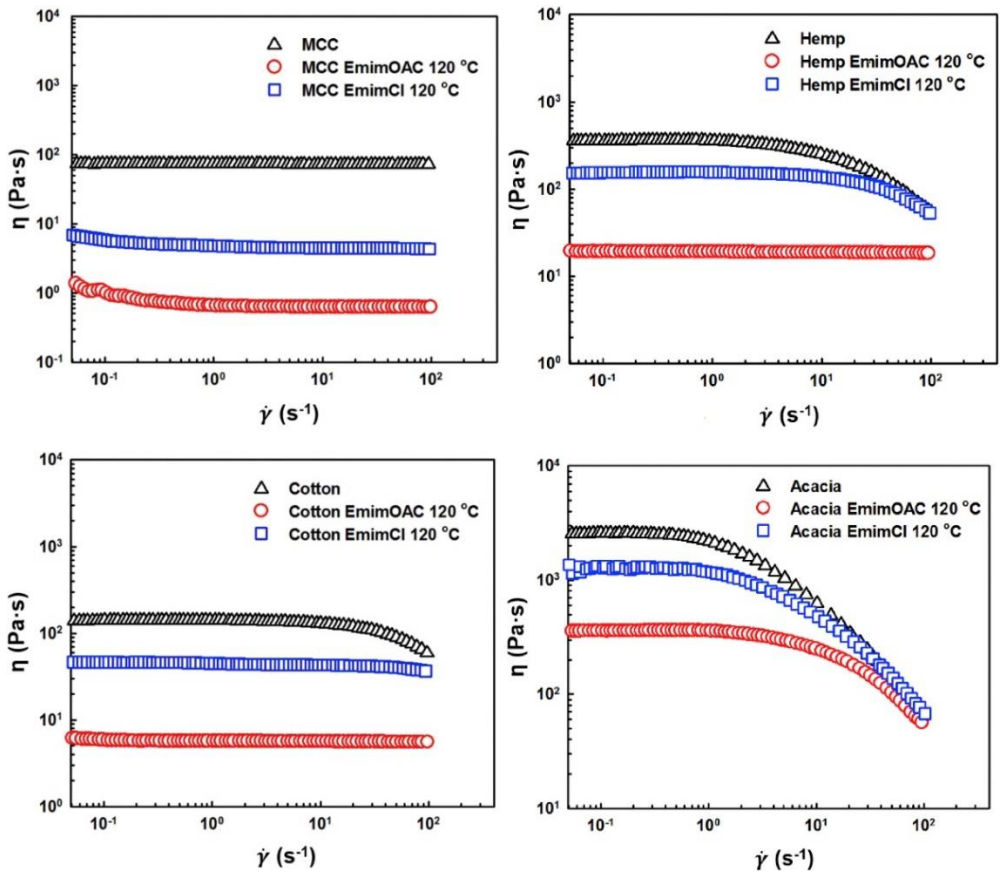

Figure 2.4. Steady shear viscosities of MCC, cotton, hemp, and acacia incubated with 1-ethyl-3-methylimidazolium acetate (EmimAc) and 1-ethyl-3-methylimidazolium chloride (EmimCl) at 120 °C. Adapted from Kim et al. with permission from Elsevier © 2016 [59].

2.4 Extrusion Assisted with Other Treatment Methods

Previously, in **Section 2.2**, the ways in which extrusion can be combined with other pre-treatment processes was highlighted and a few examples were provided. This section outlines these different treatment methods and their effect on pre-treatment efficiency in detail.

Extrusion can be combined with various chemical solvents, such as alkalis, dilute acids, ionic liquids, and supercritical fluids, as well as other technologies, like microwaves, ultrasound, and steam explosion. **Figure 2.5** briefly emphasizes their advantages and disadvantages in terms of

processing for each of these methods, which will also be covered in-depth in their respective sections. Below, **Table 2.2** summarizes of related studies mentioned in this review involving identified processes that can be combined with extrusion.

Extrusion assisted with other methods					
Alkali extrusion	**Dilute acid extrusion**	**Ionic liquid extrusion**	**Microwave/ultra sound assisted extrusion**	**Steam explosion assisted extrusion**	**Supercritical CO_2 assisted extrusion**
Low cost, Direct method for lignin valorization, No sugar generation, low processing temperature. May corrode machinery	Low chemical and operation cost, Considered as green, may prevent corrosion. Cause sugar degradation, may produce inhibitors,	Green processing High cost, lack of recycling, some ionic liquid may be corrosive	Chemical free, Green method, No corrosion. Extra operation cost, Scale-up challenge	Easy recalcitrant structure breakdown, no chemical solvents, low environmental impact. May generate inhibitors due to high temperature	Green solvent, non-toxic, non-flammable, chemically inert, residue free, inexpensive. Additional cost for equipment and energy requirement

Figure 2.5. The methods that can be used to assist with biomass extrusion pre-treatment and their main advantages (green) and disadvantages (red).

Table 2.2. Various extrusion pre-treatment studies involving other pre-treatment methods and their respective processing variables.

Combined Treatment Method Type	Lignocellulose	Configuration with Extrusion	Other Treatment Details	Sugar Yield at Optimum Condition	Reference
Alkaline Assisted Extrusion	Barley straw (BS)	Sodium hydroxide (NaOH) pumped into twin-screw extruder (TSE), followed by water for neutralization and in-situ filtration.	10% w/v NaOH solution 0.6 kg/h biomass feed rate NaOH/BS, 2.5 to 7.5% w/w 50-100 °C 150 rpm 2 min residence time	Glucose yield – 88.9% Xylose yield – 71.0%	60
	Wheat straw (WS)	NaOH pumped into TSE, extrudates acidified with phosphoric acid, and washed with water thrice.	10% w/v NaOH solution 0.6 kg/h biomass feed rate NaOH/WS, 6% w/w 70 °C 150 rpm 2 min residence time 85% w/v phosphoric acid Varying enzyme loadings for enzymatic hydrolysis	Glucose yield – approx. 80% Xylose yield – approx. 90%	61
	Corn stover (CS)	NaOH pumped into TSE, extrudates were heat preserved and then washed with water until neutrality.	NaOH loading per weight of biomass, 4-10% w/w 200 kg/h biomass feed rate NaOH/CS ratio, (2:1) 99 °C, mechanical heat 325 rpm 30 s residence time Heat preservation times of 0-10h	Glucose yield – 85.1% Xylose yield – 69.7%	62
Dilute Acid Assisted Extrusion	Poplar sawdust (PS)	Dilute sulfuric acid (H_2SO_4) pumped into TSE.	0.5-7 wt.% H_2SO_4 13.4 mL/min acid feed rate 0.06 kg/h biomass feed rate H_2SO_4/PS ratio (9:1, 11:1, 13:1) 160-185 °C 60 rpm 10.2 min residence time	Glucose yield – approx. 5% Xylose yield – 89.2%	35
	Rape straw (RS)	Dilute H_2SO_4 pumped into TSE.	1.5-3.5 wt.% H_2SO_4 4.5-6.9 mL/min acid feed rate 0.03 kg/h biomass feed rate H_2SO_4/RS ratio (9:1, 11:1, 13:1) 160-185 °C 19.7 rpm 7.2 min residence time	Glucose yield – approx. 1% Xylose yield – 89.03%	63
Ionic Liquid Assisted	Sugarcane bagasse	Biomass impregnated with 1-ethyl-3-	Manual feeding of biomass and ionic liquid mixture. Refer to **Table 1** for more details.	Glucose yield – 91.0%	28

Extrusion		methylimidazolium acetate (EmimAc) prior extrusion with TSE.		Xylose yield – approx. 75%	
	Pussy willow	Biomass dispersed in an EmimAc and dimethylsulfoxide (DMSO) mixture prior to extrusion with TSE.	DMSO/EmimAc ratio (10:0, 7:3, 5:5, 3:7, 0:10) 15, 25, and 50 wt.% solids 140 °C and 160 °C 2, 5, and 15 rpm	Glucose yield – 99.0% Xylose yield – 99.5%	34
	Mixed hardwood flour	Biomass impregnated with 1-butyl-3-methylimidazolium (BmimCl) prior to batch mixer processing.	**Batch mixer** Roller Rotor 5-50 wt.% solids 150 °C 150 rpm 10-45 min	Lignin yield – 36.6%	64
Supercritical Fluid Assisted Extrusion	Sorghum	Biomass extruded using supercritical carbon dioxide ($scCO_2$) and TSE.	**Pre-Conditioner** 10 kg/h steam flow rate 20 kg/h water flow rate 199rpm **Extruder** 75 kg/h feed rate 5 kg/h steam rate 2 kg/h carbon dioxide injection rate 30-90 °C, varied zone temperatures 300 rpm	Glucose and xylose yield - N.A. Ethanol yield – 17.87%	65
Microwave Assisted Extrusion	Switchgrass and big bluestem	Biomass extruded using a single screw extruder (SSE) and extrudates are heated using a microwave.	**Extruder** Moisture based (20 wt.% solids) 176-180 °C 155 rpm **Microwave** Moisture based (25, 50, and 75 wt.% solids) 180, 450, and 720 W 2.5, 5, and 10 min	Glucose yield – 52.6% Xylose yield – 75.5%	66
Ultrasonic Assisted Extrusion	Rice hull	Biomass extruded using steam and TSE. Extrudates were soaked in a citrate buffer and then treated with ultrasonic waves.	**Extruder** Moisture based (25-33 wt.% moisture) 120-160 °C 250-400 rpm **Ultrasonic Bath** 35 °C 0.5-2.5 h	Glucose yield – approx. 291.59 mg/ g rice hull Xylose yield –approx. 88.87 mg/g rice hill	67
Steam Explosion Assisted Extrusion	Barley straw	Biomass were steam exploded and then extruded using TSE and an alkaline. Extrudates were then acidified and	**Steam Explosion** 10 mg of H_2SO_4 /g of biomass 180 °C, 9 bar 3.5 min **Extruder**	Glucose yield – approx. 75% Xylose/ Mannose/	68

		washed with water once.	NaOH/BS, 8% w/w 2.5 kg/h biomass feed rate 100 °C 150 rpm 1 min residence time	Galactose/ Arabinose yield – approx. 10%	
	Corncob	Biomass were steam exploded and then extruded using TSE and water.	**Steam Explosion** Moisture based (50 wt.% solids) 205 °C pH 4.8 5 min **Extruder** 4 kg/h biomass feed rate Water/Corncob ratio 1.2:1 100 °C 100 rpm	Glucose yield – 88.41% Xylose yield – N.A.	69

N.A. – Not Available

2.4.1 Alkaline Assisted Extrusion

As aforementioned, liquid additives can be used in order to enhance the effectiveness of extrusion pre-treatment. An alkaline, such as sodium hydroxide (NaOH), is often used due to its ability to solubilize lignin and reduce the recalcitrant structure of lignocellulose [60]. To apply alkaline solutions in an extrusion system, it is pumped into the extruder shortly after feeding the biomass. A typical alkaline-extrusion pre-treatment configuration can be seen in **Figure 2.6** [60]. After alkaline-extrusion pre-treatment, the mixture is neutralized. The neutralization process can be performed inside the extruder, as shown in **Figure 2.6**, but it has also been accomplished on mixtures shortly after extrusion [61,62,70]. Lastly, following neutralization, the solid and liquid fractions of the biomass-alkaline mixture are separated. This procedure leaves a high lignin and hemicellulose content filtrate and a solid residue that is cellulose-rich.

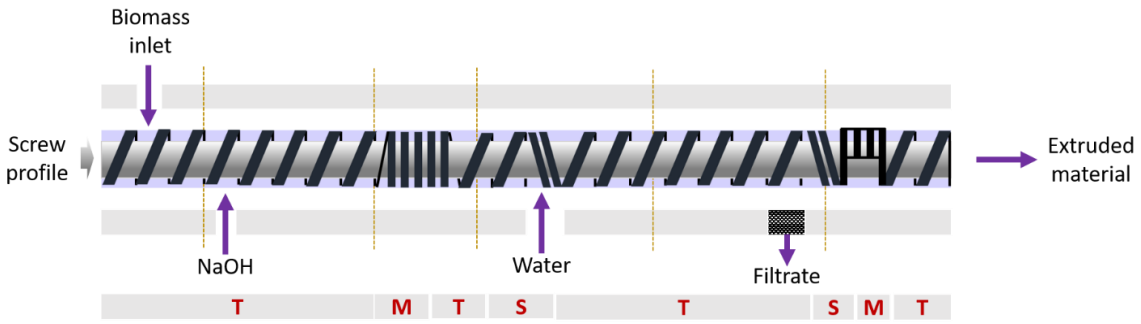

Figure 2.6. Twin-screw configuration for an alkaline extrusion system, where T is a transport zone, M is a mixing zone, and S is a shearing zone. Re-drawn from Duque et al. [60].

The addition of alkaline additives to an extrusion system improves the overall effectiveness of the biomass pre-treatment. In a study by Duque et al., they used the extruder-NaOH configuration in **Figure 2.6** to pretreat barley straw (BS) at varying temperatures and NaOH/BS dry matter ratios (R) (%, w/w) [60]. In their extrusion setup, NaOH addition, neutralization with water, and filtration

were performed continuously. The study concluded that 2.5% R was insufficient to effectively remove lignin from BS, suggesting that the NaOH content was too low. At the highest processing temperature of 100 °C and at higher R, the AIL content of the pre-treated BS at 5 and 7.5% R were 13.2 and 12.1%, respectively, compared to the untreated BS, which had 15.2% AIL content [60]. The removal of lignin suggests a reduction in biomass recalcitrance and implies improved enzymatic hydrolysis performance. When further investigated, increasing R to 5% resulted in higher enzymatic yields, reaching a maximum of 90.3% glucose yield at 100 °C [60]. However, experiments at 7.5% R and higher temperatures of 75 and 100 °C resulted in lower enzymatic yields, possibly due to condensation or repolymerization reactions. Nonetheless, alkaline-extrusion pre-treated biomass had higher glucose and xylose yields compared to untreated biomass, showing overall improvement.

Similar results were obtained by other researchers. Coimbra et al. also reported an increase of cellulose content (from 37.8% in untreated straw to 46.9% in extrudate) and lignin removal of 22% after alkaline extrusion [61]. In the study, alkaline extrusion was performed with wheat straw using a 10% NaOH solution at 70 °C and NaOH to dry wheat straw weight ratio of 6:100. Unlike Duque et al., neutralization with phosphoric acid and filtration were performed only after alkaline extrusion. An alternative study on corn stover biomass pre-treated with alkaline extrusion followed by neutralization and filtration was performed by Liu et al. [62]. At what was determined to be the most optimal processing conditions (0.06 g NaOH/g biomass, 1 h heat preservation time), 71% of lignin was removed [62]. The most optimal processing parameters also considered enzymatic hydrolysis yields for fermentable sugar production. At these conditions, glucan and xylan yields were 83% and 89%, respectively [62]. Both studies further support the fact that alkaline pre-treatment of biomass is generally effective for lignin removal.

The introduction of alkaline chemicals in the extrusion pre-treatment process presents various advantages and disadvantages. Due to the high solubility of lignin in alkaline solutions, alkaline extrusion can be used as a low-cost and direct method for the valorization of lignin [68]. Following alkaline extrusion, lignin can easily be precipitated from the alkaline filtrate by increasing its acidity. For bioethanol production purposes, alkaline extrusion can also be conveniently combined in tandem with bio-catalytic enzymatic hydrolysis [71]. Furthermore, alkaline extrusion does not require high processing temperatures and generates little to no sugar degradation products, such as 2-furaldehyde and 5-hydroxymethyl-2-furaldehyde (furfural and HMF, respectively) [60,72]. However, depending on the alkaline concentrations, the solutions can also corrode the extruder machinery [62,72].

2.4.2 Dilute Acid Assisted Extrusion

Like alkaline extrusion, dilute acids can be used to aid the pre-treatment process of lignocellulosic biomass. Most commonly, dilute sulfuric acid (H_2SO_4) is used in these types of applications. The application of dilute acid in the extrusion process is also similar NaOH addition, with the injection of the solution using a pump after the feeding of biomass. Unlike alkaline extrusion, neutralization and filtration do not follow dilute acid extrusion. Additionally, dilute sulfuric acid is specifically used for its effective isolation and hydrolysis of the polysaccharidic components, and so relevant studies typically focus on the use of pre-treatment for biomass conversion into ethanol.

Kim et al. investigated the bioconversion of poplar sawdust into ethanol using dilute acid extrusion followed by simultaneous saccharification and fermentation [35]. In the study, they determined that xylose, mannose, and galactose (XMG) sugar yields increased with increasing sulfuric acid concentrations and temperatures, as shown in **Figure 2.7**. In the figure, it can be observed that once a certain sulfuric acid concentration is reached, the XMG yield reaches a maximum and

continuously decreases thereafter. For example, at 180 ℃, the temperature at which the highest sugar yield was obtained, the sugar yield increases from approximately 45% when sulfuric acid concentration is 0.5% to almost 90% when the sulfuric acid concentration is 4.5%[35]. From there, the sugar yield decreases due to degradation. Choi and Oh received observed similar sugar yield behaviour in their study on the pre-treatment of rape straw using dilute acid extrusion [63]. At lower temperatures of 150 and 155 ℃, the sugar yield of pre-treated rape straw continuously increases as acid concentration increases, reaching approximately 75% yield. However, at higher temperatures (160-170 ℃), sugar yield increases to a maximum of 80-90% and decreases at higher acid concentrations due to degradation. Overall, the results from both studies indicated that the combination of high temperatures and acid concentrations sufficiently disrupts the structure of lignocellulose, resulting in a high sugar yield. However, this behaviour is limited due to sugar degradation.

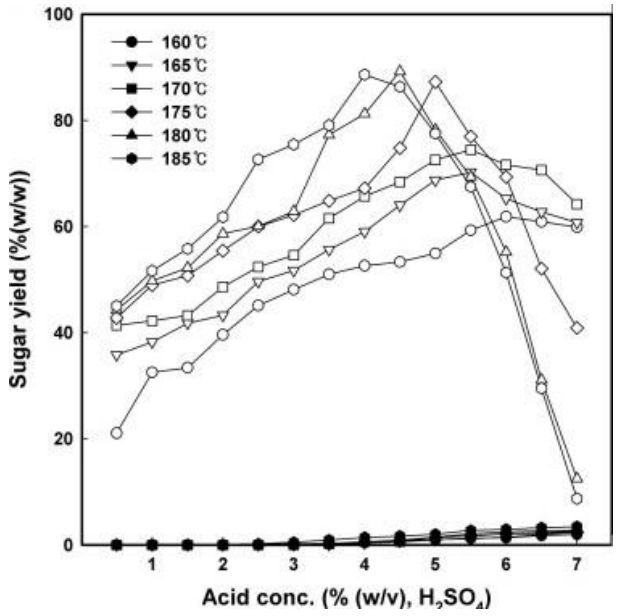

Figure 2.7. The effect of sulfuric acid concentration and temperature on sugar yield of poplar sawdust pre-treated with alkaline extrusion. Glucose yield is represented by the closed symbols and XMG yield is represented by the open symbols. Adapted from Kim et al. with permission from Elsevier © 2013 [35].

The cost and benefits for dilute acid extrusion are comparable to alkaline extrusion. Both processes are simple overall and require relatively low chemical and operation costs [35,73]. Since dilute acid is generally neutral in pH, its related operations may be considered as green and machine corrosion can be prevented as well [73]. However, higher temperatures and degree of acidity can limit saccharide recovery from the biomass, causing sugar degradation and inducing the release of fermentation inhibitors [63].

2.4.3 Ionic Liquid Assisted Extrusion

Ionic liquids are considered "green" solvents that have demonstrated great potential for lignocellulosic biomass pre-treatment. This is because, ionic liquids have characteristic low volatility, high thermal stability, low flammability, and recyclability [34]. In extrusion processes,

instead of feeding ionic liquids into the extrusion system like alkalines and dilute acids, biomasses can be impregnated with ionic liquid at pre-determined ratios before the extrusion. These biomass-ionic liquid mixtures are then fed directly into the extruder for processing. In operation, ionic liquids can act as an efficient solvent and plasticizer [55,74]. Furthermore, the solubilization of the different components of lignocellulosic biomass also varies depending on the type of ionic liquid used. Some ionic liquids prefer lignin solubilization, polysaccharidic solubilization, or both [75,76].

Earlier, a study exploring the extrusion pre-treatment of sugarcane bagasse with 1-ethyl-3-methylimidazolium by Da Silva et al. was highlighted in the context of investigating the influence of the L/S ratio [28]. In that study, there was a low degree of delignification, with a maximum of 18.1% lignin removal. Additionally, increasing the solid loading did not aid in maximizing the amount of delignification. However, looking at glucose, yields of 86.7% to 92.9% were observed for bagasse loadings of 11.1 to 25 wt.%, while at 50 wt.% bagasse loadings, the maximum glucose yield was 76% [28]. For comparison, untreated sugarcane bagasse had a glucose yield of less than 20%. Another study by Han et al. explored pussy willow wood powder using the same ionic liquid and achieved maximum glucose and xylose yields of 99.0% and 99.5%, respectively, at 15% solid loading, 160 °C, and 5 rpm [34]. Similar to Da Silva et al., they also identified that lower solid loadings were more successful in terms of saccharification yield.

The main advantage of using ionic liquids as a solvent is their green nature, as aforementioned. Their non-volatile nature prevents its evaporation into the atmosphere and any inhalation of toxic fumes by animals and humans [77,78]. Additionally, its low volatility makes for easier lifecyle monitoring. Some ionic liquids, such as 1-allyl-3-methylimidazolium chloride, have also been found to completely solubilize lignocellulosic biomass [28,79,80]. To do so, however, large ionic liquids loadings (95 wt.%) and long processing times (1-24 hr) are typically required [55,75,81,82]. The

next biggest challenge associated with ionic liquids is their high cost and the lack of recycling processes currently available [15]. Lastly, some ionic liquids contain halogen anions which makes them corrosive, toxic to some organisms, and not entirely environmentally friendly [77,78,81]. Nevertheless, the application of reactive extrusion processing with ionic liquids is advantageous compared to other pre-treatment methods also using ionic liquids as the mechanical capabilities of extrusion allows for the processing at higher solid loadings and lower processing times, which results in lower overall costs.

2.4.4 Supercritical Fluid Assisted Extrusion

Supercritical fluids (SFs) are substances that surpass a critical temperature and pressure, resulting in the coexistence of the gas and liquid phases of the material. Some common SFs for biomass pre-treatment applications are supercritical water and supercritical carbon dioxide ($scCO_2$) [42]. Though, in most practices, these supercritical fluids are applied in a batch reactor for the supercritical fluid explosion of biomasses.

Extrusion assisted by supercritical fluids is a commonly applied approach in polymer processing, especially for foaming applications [83–85] and viscosity reduction of polymer blends [86]. However, to the best of the authors' knowledge, there has only been one instance in which SFs were used in conjunction with extrusion for lignocellulosic biomass pre-treatment. In 2006, Zhan et al. pre-treated sorghum pellets using a supercritical-fluid-extrusion (SCFX) process for ethanol production, causing an increase of 41.6% in free reducing sugar contents [65]. Since the study focused on ethanol production, the main response variables studied were ethanol yield and fermentation efficiency. During the fermentation of sorghum, various sorghum loading concentrations were explored. For all concentrations, there was at least a 4% increase in ethanol

yield and fermentation efficiency after SCFX processing, with a maximum of 17.87% ethanol yield and 91.57% fermentation efficiency [65].

SFs are appealing since they are green solvents that are non-toxic, inexpensive, chemically inert, non-flammable, and residue-free [85,87]. SFs can also perform various tasks in an extrusion system as it can be applied as a plasticizing agent, expansion agent or, often, both. As aforesaid, SFs lies in between the state of a liquid and a gas. Its liquid-like properties allow it to behave as a more effective solvent than gases, while its gas-like properties encourage higher diffusion rates [88]. These behaviours significantly improve the plasticizing ability of CO_2 and can promote higher solid loadings during biomass pre-treatment.

Additionally, its ability to act as an expansion agent after releasing pressure at the end of the extrusion process is comparable to the supercritical fluid explosion process. Lastly, scCO2 has mild temperature and pressure requirements (31°C, 7.38MPa), which allows for the processing of temperature-sensitive materials, which is especially critical for biomass pre-treatment applications [85,87]. $ScCO_2$ removal is also simple as it only requires depressurization, leaving no residue. The main disadvantage of applying supercritical fluid-assisted extrusion is the material, equipment, and energy cost requirements associated with scCO2 injection. Additionally, it is not yet well explored for biomass pre-treatment applications.

2.4.5 Microwave and Ultrasound Assisted Extrusion

Aside from applying chemical solvents, other technologies have also been used to improve the extrusion pre-treatment process. Particularly, microwave and ultrasound technologies have been investigated. These treatments are implemented directly following the extrusion of biomasses.

Karunanithy et al. applied microwave-assisted extrusion to switchgrass and bluestem [66]. In the study, they focused on applying a sequential extrusion and microwave treatment for sugar recovery. At the determined optimal microwave power and exposure time, significant improvements were made in terms of glucose, xylose, and total sugar recovery for both switchgrass and bluestem. For switchgrass, compared to the extrusion-only control sample, the yields increased by 16.1%, 15.3%, and 15.1%, respectively [66]. Similar observations were seen with bluestem. While the effect of microwave assistance on sugar recovery was moderate compared to extrusion, the introduction of microwave pre-treatment after extrusion improved sugar yields overall.

Alternatively, Zhang et al. pre-treated rice hull via extrusion followed by an ultrasonic bath [67]. Uncommonly, the study measured the expansion degree of the rice hull samples to optimize extrusion conditions due to the existing positive linear relationship between expansion degree and sugar yield. They explored ultrasound operation parameters, deducing that increasing ultrasound pre-treatment time only had a significant effect on the improvement of reducing sugar yields until 1.5 h, after it slows down, lowering efficiency. After optimizing the pre-treatment process, they observed that the reducing sugar yield for a sequential extrusion and ultrasound treatment after 72 hours of enzymatic hydrolysis was 381.59 mg/g rice hull, which is 1.38 times higher than just pre-treatment by extrusion and 4.40 times higher than rice hull that was not pre-treated [67].

Ultrasound and microwave pre-treatments are advantageous since they are chemical free and green methods [67]. Thus, there is no risk of corrosion to equipment and environmental harm. Furthermore, microwave pre-treatments typically require the biomass to be washed free of fermentation inhibitors after; however, this is not necessary for sequential microwave and extrusion pre-treatment [66]. Consequently, introducing ultrasound and microwave technologies also establishes

extra costs to the pre-treatment process and presents challenges with regards to industrial scale-up [75].

2.4.6 Steam Explosion Assisted Extrusion

Steam explosion entails the treatment of biomass with steam at high pressures, which is then released, causing the biomass to rupture. Steam explosion is performed prior to the extrusion pre-treatment of biomass to break down its structure and improve chemical accessibility.

A study by Oliva et al. explored steam explosion and reactive extrusion of barley straw [68]. The barley straw was pre-impregnated with sulfuric acid, steam-exploded, and extruded with NaOH. Steam explosion results in an increase in cellulose and lignin content, explained by corresponding hemicellulose solubilization. Once the steam-exploded biomasses were processed, similar to Duque et al. and Coimbra et al., there was a further increase in cellulose content (55.1% to 64.2%) and a slight decrease in hemicellulose (8.8% to 6.8%) and lignin content (32.1% to 29.3%) [68]. Hemicellulose solubilization increased bio-accessibility, improving lignin extraction and ethanol production. After processing, 32% of the lignin was recovered from the alkaline filtrate via precipitation and ethanol production increased by 66% compared to a solely steam explosion pre-treatment [68]. Through this, the effectiveness of the combined pre-treatment process was demonstrated.

A different investigation by Zheng et al. looked into the pre-treatment of corncob residue after a steam explosion and subsequent extrusion [69]. Their study explored two types of extruder configurations in which one setup achieved 7% xylose removal and the other achieved 80% xylose removal. High xylose removal was achieved through the addition of more kneading elements in the screw design, the operation at a temperature higher than 30 °C, and the use of water as an additive. Overall, they determined that glucose conversion was consistently higher with the

extruder obtaining 80% xylose removal and, at optimized enzymatic hydrolysis conditions, the steam exploded and extruded corncob residues measured a glucose yield of 90% [69].

The ability of steam explosion to simultaneously break down the recalcitrant structure of lignocellulosic biomass of varying particle sizes is very advantageous in pre-treatment [68]. Like microwave and ultrasound technologies, steam explosion is also often performed without chemical solvents and has a low overall environmental impact. However, steam explosion application causes hemicellulose degradation and can generate fermentation inhibitors due to the high processing temperature [29,68]. Although, the use of an acid catalyst in steam explosion aids in lowering processing temperatures and preventing biomass degradation [68].

2.4.7 Conclusions Regarding the Addition of Other Treatment Methods

Other treatment methods involving different solvents and technologies are commonly combined with the reactive extrusion process. Different solvents, like alkalines, dilute acids, and ionic liquids aim to solubilize different components of biomass, enabling chemical deconstruction. Supercritical fluids are multi-functional with solubilization, plasticization, lubrication, and expansion properties. Alternatively, microwave, ultrasound, and steam explosion technologies improve the pre-treatment process via heating, agitation, and expansion caused by depressurization, respectively. The combination of these other methods introduces different avenues for exploration for more productive lignocellulosic biomass pre-treatment.

2.5 Reactive Extrusion for Lignin Production

While lignin is typically burned as fuel, it would be more environmentally and economically advantageous to extract it for further use in material applications. Lignin can be applied as a nanoparticle for wastewater dye adsorption [89], modified for dispersion in elastomers to improve

its mechanical properties [90,91], and used as a plasticizer for concrete [92]. This section explores how lignin is extracted and its quality after biomass extrusion pre-treatment processing.

The primary purpose of the optimization of extrusion parameters and the addition of other processing methods in the pre-treatment process is to reduce the overall recalcitrance of lignocellulosic biomasses for bioethanol production and/or fractionation. This reduction materialized through the physical and chemical separation of cellulose, hemicellulose, and lignin during the reactive extrusion process. Previously mentioned in the introduction of **Section 2.3**, successful lignocellulosic biomass disruption is most often measured through sugar recovery yields due to bioethanol production. Since lignin accessibility is also dictated by the degree of biomass disruption, the formerly reviewed literature regarding the effect of extrusion pre-treatment remains true overall for lignin recovery applications. However, due to the preferential solubilization of some components by different solvents discussed in **Section 2.4**, the downstream operations for lignin recovery can differ. Solvents for cellulose and hemicellulose dissolution result in lignin rich solid residue. However, solvents that aim to solubilize lignin require further processing for lignin extraction, which is discussed in the next section.

2.5.1 Lignin Extraction Processes

The lignin released from the biomass matrix in the pre-treatment process is often dissolved in a solvent. In reactive extrusion, this solvent can be processed with the biomass in the extruder or applied as a post-treatment. Some common lignin extraction solvents include NaOH [64,68,93], dioxane-water (96%) [45], and acetic acid (90/10 v/v) [94]. Of these highlighted studies, Oliva and group had extruded acid-catalyzed steam-exploded barley straw with NaOH [68]. After the dissolution of lignin in a solvent, filtration or centrifugation is performed to separate cellulose-rich residue from lignin-rich liquid fractions. Lignin is then precipitated from the solvent. In the case

of NaOH as a solvent, an acid, like H_2SO_4 and hydrochloric acid (HCl), is added to increase the pH of the solution and precipitate the lignin [64,68,93]. Similarly, with acetic acid, water can be used to precipitate lignin [94]. For a dioxane-water system, the solution is roto-evaporated, and the lignin extracts are freeze-dried [45].

While the lignin extraction process seems straightforward, it presents its own set of challenges as the lignin extraction yield is often low. Therefore, the lignin recovery process would directly benefit from an improved biomass pre-treatment process that effectively deconstructs the structure of biomass so that the lignin is easily accessible by these various highlighted solvents. Thus, further progression in reactive extrusion biomass processing methods and technology can improve lignin recovery yield.

2.5.2 Quality of Lignin Following Reactive Extrusion and Extraction

Lignin recovery is viable and appealing, however, most extrusion pre-treatment studies do not try to extract lignin, so there is a lack of analysis on the effects of pre-treatment on the quality of lignin recovered from extrudates. Typically, only the lignin content of the biomass or the amount of delignification is reported [28,31,95].

Aside from the measurement of delignification, only a handful of studies have extracted lignin after extrusion pre-treatment and characterized it. Most commonly, Fourier transform infrared (FTIR) analysis has been used to confirm the nature of the extracted lignin. Oliva et al. used FTIR to confirm the presence of peaks in the lignin region for a precipitated lignin sample collected from pre-treated barley straw [68]. Tian et al. also determined that the chemical structure of lignin from eucalyptus and aspen before and after liquid hot water extraction did not alter much using FTIR, as shown in **Figure 2.8** [94]. They observed that adsorption bands 1425 (aromatic skeletal vibrations), 1328 (S ring breathing and G ring substituted in position 5), and 1218 cm^{-1} (C–O

stretching in phenols and ethers) are stronger after pre-treatment, which indicates that more guaiacyl (G) and syringyl (S) units of lignin were produced [94]. An increase in unconjugated carbonyl groups due to oxidation was also observed around 1700 cm^{-1} for both biomasses. Overall, FTIR analysis reveals the chemical structure and any modifications of the lignin due to the extrusion pre-treatment process and the chemicals used.

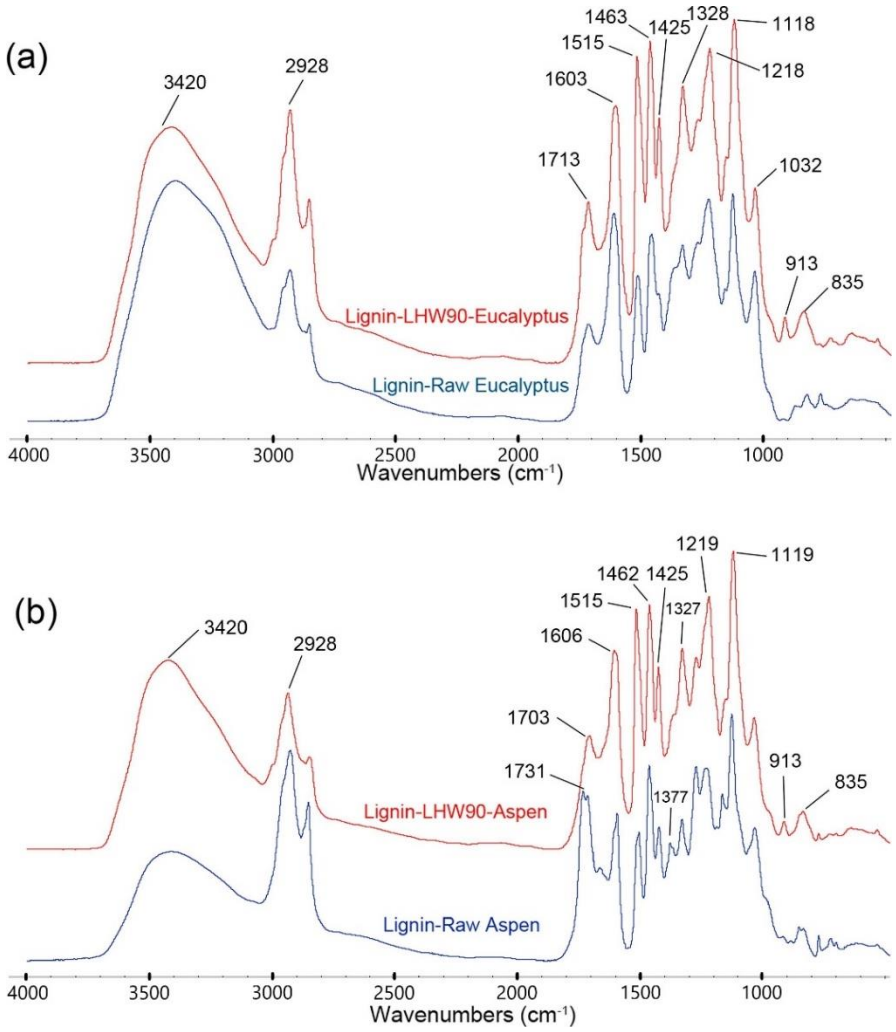

Figure 2.8. FTIR spectra for lignin extracted from eucalyptus after pre-treatment with liquid hot water extraction followed by extrusion. Adapted from Tian et al. with permission from Elsevier © 2019 [94].

Nuclear magnetic resonance (NMR) has also been used to characterize extracted lignin samples. Wu et al. used 2D ^{1}H-^{13}C NMR to compare lignin extracted from rice straw that was extruded and mildly steam exploded to raw rice straw, as shown in **Figure 2.9** [93]. In their study, they observed that the aromatic unit ratios for the extrusion and expansion of rice straw and husk remained similar to their respective raw biomasses. For instance, the raw rice straw had a S:G:H ratio of 0.28:0.59:0.13, which is similar to the processed rice straw with a ratio of 0.3:0.55:0.15 [93]. On the

other hand, Ai et al. used a similar technique and noticed that the S:G:H ratio of the bagasse went from 0.33:0.63:0.04 to ratios of 0.52:0.47:0.01 and 0.46:0.53:0.01 for biomass extruded at loadings of 30% and 50%, respectively [45], when processing with deep eutectic solvents.

The quality of lignin can also be further assessed by evaluating the type and number of interunit linkages present in the lignin using NMR. In the study by Wu et al, they determined that the majority linkage in raw rice straw and husk was *β-O-4* and did not change significantly after expansion pre-treatment, remaining at approx. 60-65% and 80-85%, respectively [93]. They did not observe any changes to the linkage composition of lignin. Alternatively, Ai et al. observed that the majority linkage in sugarcane bagasse lignin decreased from 42.7% *β-O-4* linkage to 30.1% and 23.5% after extrusion processing for 30% and 50% sugarcane bagasse loading, respectively [45]. However, Guiao et al. observed the opposite in their investigation [64]. In their study, there were no indications of the cleavage of the *β-O-4* linkage in the ^{13}C-NMR spectra of the extracted lignin from mixed hardwood flour. The presence of the *β-O-4* linkages after the reactive extrusion pre-treatment of biomass varies across research studies, suggesting that the type of biomass, the extrusion pre-treatment conditions, and the solvents used are all significant factors in determining its possible cleavage.

Next, the molecular weight of the extracted lignin after extrusion pre-treatment has also been explored. The investigation by Wu et al. established that the weight-average molecular weight (M_w) of lignin from rice straw and husk after extrusion and subsequent expansion was 1220-1800 Da [93]. The obtained M_w of the extracted lignin was on the lower end of the expected M_w range since alkali, ball-milled, and organosolv lignin from wheat straw generally ranges from 1000-5000 Da [96]. Ai et al. also determined that the M_w of untreated sugarcane bagasse was 6109 Da and decreased to 3479 and 3252 Da at 30% and 50% loadings, respectively, after extrusion pre-

treatment with deep eutectic solvents [45]. These results suggest that the extrusion pre-treatment of lignocellulosic biomass leads to lignin depolymerization, supporting their previous observation of the β-O-4 linkage. It is likely that the intensive shearing process involved with extrusion cleaved the β-O-4 linkages in the lignin macrostructure, leading to a decrease in molecular weight.

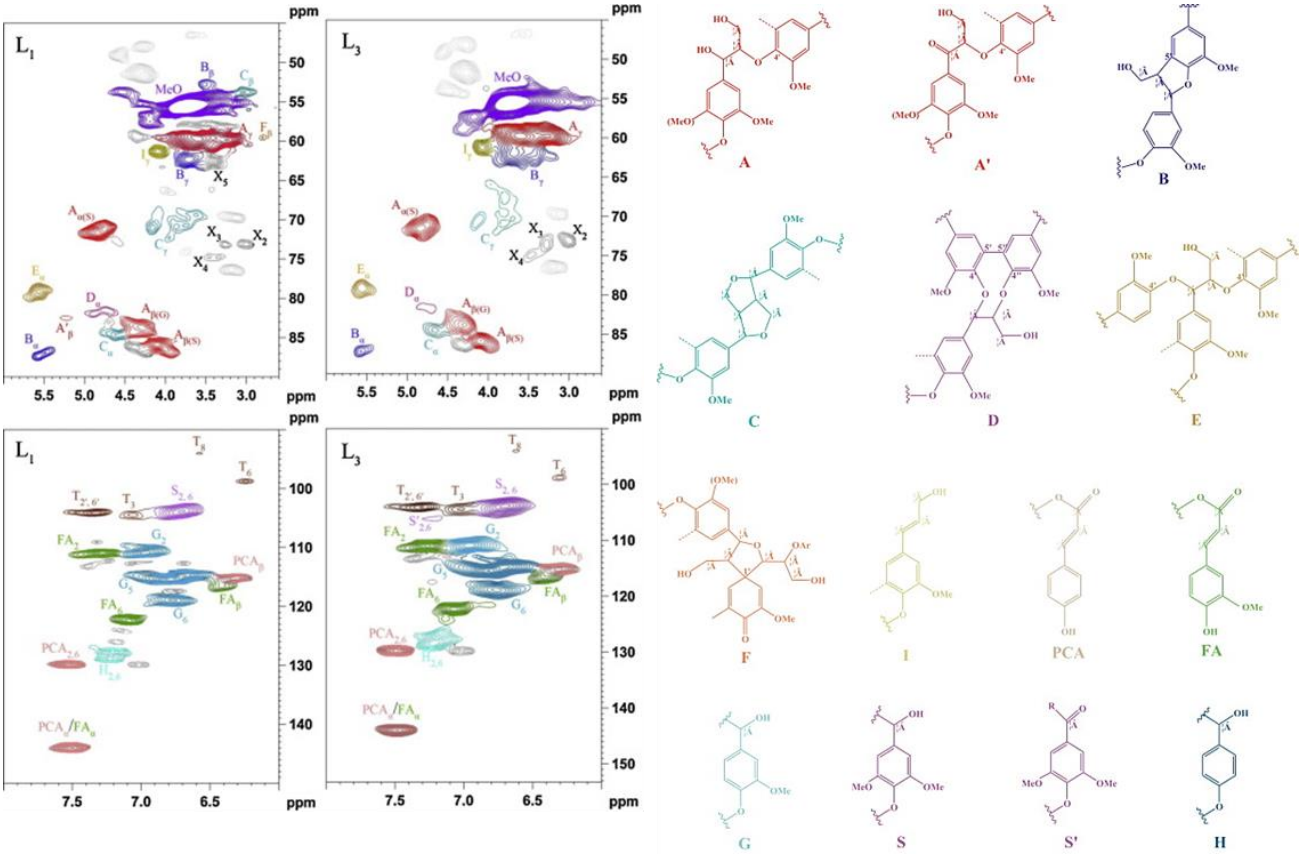

Figure 2.9. 2D ^{1}H-^{13}C NMR of lignin from raw rice straw (L_1) and expanded rice straw with 20% water content (L_3), along with relevant structural units and linkages. Adapted from Wu et al. with permission from Elsevier © 2013 [93].

The reactive extrusion pre-treatment process serves as a primer for lignin fractionation and its subsequent valorization. The process deconstructs the lignocellulosic biomass so that its lignin components are accessible and can be recovered. However, lignin recovery is not yet well explored

in research involving reactive extrusion pre-treatment. Therefore, its influence on lignin yield and quality is not well-determined and must be further investigated in future work.

2.6 Reactive Extrusion for Nano- and Micro-cellulose Production

In addition to lignin, the reactive extrusion process is also promising for the production of other high-value products, such as nano- and micro-cellulose. In the last decade, nano- and micro-sized celluloses gained special attention due to their renewability, biodegradability, safety, superior oxygen barrier properties, and mechanical and colloidal properties [17]. However, typical processes to produce nanocellulose, such as cellulose nanocrystals (CNC) and cellulose nanofibrils (CNF), involve several processing operations that may require large amounts of hazardous and non-environmentally friendly solvents and chemicals [12,97]. Moreover, these wet processes are conducted by utilizing dilute cellulose dispersions, which further reduces the process efficiency as it requires energy-consuming downstream processes. [14]. Additionally, the concentrated mineral acid-based process does not directly permit the utilizing of the side products, such as simple sugars, oligosaccharides, and amorphous cellulose fragments, for bio-fuel or other industrial applications to offset the process cost since further purification of sugars is necessary [98]. Several mechanical operations, such as grinding [18,99], homogenizing [100,101], and micro-fluidization [102] have been attempted to fabricate nano-sized cellulose, however, they are high energy-consuming operations and can be expensive as a consequence [97].

As discussed in the previous sections, the reactive extrusion of lignocellulosic materials is an efficient and relatively straightforward process. The generation of high shear forces and pressure during the extrusion process accelerates the hydrolysis process and reduces the reaction time to generate nano- and micro-cellulose. Further, it is a continuous industrial process that reduces the excess use of acidic solutions and the addition of other mechanical treatment processes. A general

process used for industrial production of microcrystalline cellulose (MCC) involving reactive extrusion is provided in **Figure 2.10** [103].

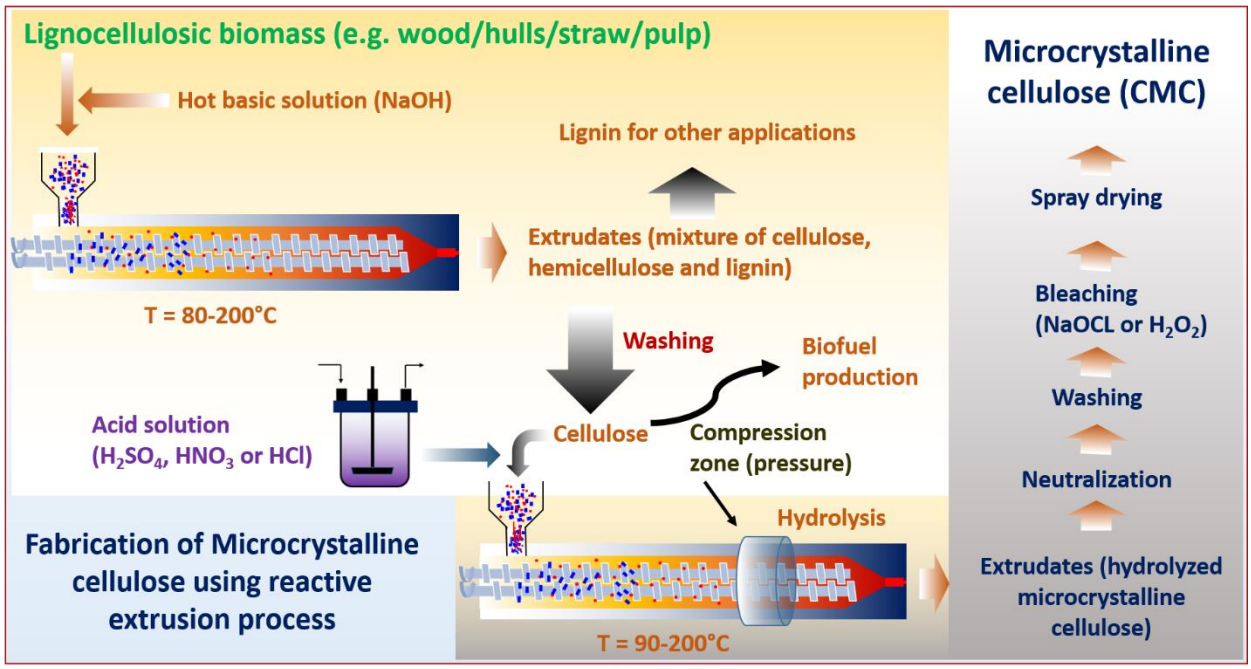

Figure 2.10. Processes involved in the fabrication of cellulose microcrystals through reactive extrusion.

Reactive extrusion is a recent advance in thermo-mechanical processing that shows promise in the efficient fabrication of micro- or nano-sized cellulose. Cellulose is a bunch of compacted fibers with crystalline and amorphous domains [104]. To achieve nano-sized cellulose, various approaches can be adopted. In reactive extrusion, the defibrillation of cellulose is achieved by the kneading and compression processes inherent to the extruder, then a low amount of plasticizer or chemicals is added to dissolve amorphous domains to produce highly crystalline nano-sized cellulose, such as CNC. Like the reactive processing of biomass described in the previous sections, the twin-screw extrusion process allows for flexibility in controlling shear stress, temperature, mixing/compression of the material, etc. Overall, the use of extrusion for cellulose processing

results in the efficient production of nano-sized cellulose at high solid loadings, which is more industrially applicable and ultimately helps reduce costs incurred by transportation, storage, and chemical usage.

Several studies, listed in **Table 2.3**, have focused on the defibrillation or modification of cellulose using an extrusion process [105]. For instance, Ho et al. [106] have reported that the fibrillation of pulp fibers using TSE resulted in producing high solid content (33-45 wt.%) nanocellulose even after several passes through the extruder. They also concluded that the fibrillation of cellulose could only be performed for 14 passes through the extruder due to the undesired generation of heat during processing. Multiple extruder passes were also found to be responsible for cellulose degradation, reduction in degree of polymerization, and slight decrease in crystallinity. In another work, Merci et al. [107] extracted microcrystalline cellulose from soybean hulls through a single screw reactive extrusion process. They used sodium hydroxide to extract cellulose, followed by the addition of sulfuric acid to dissolve amorphous cellulose, and ultimately, obtained microcrystalline cellulose. Recently, a similar approach was also adopted by Mali and group to produce cellulose nanofibrils (CNF) using SSE from soybean hulls [108] and oat hulls [109]. Their study explored the pre-treatment of hulls with peracetic acid and hydrogen peroxide before extrusion processing to effectively obtain CNF. However, these works were predominantly focused on the effect of chemical modification and pre-treatments on lignocellulose [110–112]. A very limited amount of research is available regarding the effect of different extrusion process parameters on the production of cellulosic materials.

In a research investigation targeting the fabrication of CNF from eucalyptus pulp, Rol et al. [113] specifically mentioned the TSE screw profile they used for defibrillation cellulose. The profile consisted of three shearing zones with reverse elements, which were applied to retain the pulp and

increasing the residence time. To increase the amount of shear, they also used different degrees of disk orientation (30°, 60° and 90°). Additionally, they examined the effect of the number of passes on the size of fabricated cellulose at low temperatures (~10°C). It was observed that increasing the number of passes improves the fibrillation of cellulose, leading to particle size homogeneity and transparency. They found that seven passes through the mechanical extruder lead to CNF film with more than 90% transparency, which is an indication of the nanocellulose generation. Before extrusion, they pre-treated the eucalyptus pulp either enzymatically or using TEMPO oxidation. It was further concluded that the extrusion process needed 63% less energy compared to other grinding processes to produce nano-fibrillated cellulose. Overall, they determined that pre-treatment followed by extrusion led to the production of transparent nano-fibrillated cellulose at high solid contents (~20%). However, similar to Ho et al., they also observed fiber degradation with increasing number of passes based on the degree of polymerization, which presents a challenge. Similar extrusion conditions and screw profiles have been used by the same group to defibrillate cellulose pulp using TSE for the production of modified nano-cellulose species, such as phosphorylated cellulose [114], cationic CNF [115], and destructured CNF hydrolyzed by enzymes [116].

Based on these studies, a common thread pertaining to the effect of cellulose extrusion is observed. An increase in extruder pass amount is noted to be influential on various cellulose properties. With a few authors highlighting its positive influence on particle size reduction and film transparency, as well as its unfavourable influence of degree of polymerization and degradation [106,113]. The influence of extruder pass amount is minimal on the degree of crystallinity of the cellulose as it reduces by less than 5% when the number of passes is less than seven in both studies by Ho et al. and Rol et al. At higher amounts of passes, the degree of crystallinity reduces more significantly.

Therefore, the amount of passes a material undergoes in an extruder is significant in determining the quality of the cellulosic product being produced.

The type of extruder screw profile used also determines the amount of shear and compression stresses introduced on the materials during processing. In thermoplastic polymer processing, the extrusion screw profile can be optimized depending on the need. If simple molding is required, a conveying profile can be employed, whereas, if more than one polymer with additives is involved, the compression profile can be adjusted, or a combination of reverse elements could be introduced. Applying mixing and reverse mixing screw elements generates the desired shear and compression necessary for blending. Bras and his group [117] have simulated different screw profiles to optimize the extrusion passes for the nano-fibrillation of cellulose (**Figure 2.11**). They found that a screw containing six shearing zones composed of left-handed staggered disks imparted three times higher strain and produced CNF in one pass. The computer simulation of TSE processing allows for the efficient optimization of extruder design and the minimization of passes for CNF fabrication.

It is understood that a TSE process can be employed to produce nano- and micro-sized cellulose using different lignocellulosic biomasses. Using this method, a two-stage extrusion process can be performed, where the first stage focuses on cellulose pulp extraction and is then followed by a second stage for its defibrillation. TSE is capable of drastically reducing the use of different chemicals. Furthermore, optimization of the screw profile can effectively reduce the number of passes biomass requires for effective processing, which ultimately decreases processing time and saves cost. The production of nanocellulose with high solid content also helps in the reduction of transportation and storage costs. Additionally, the use of TSE gives liberty in tuning different extrusion parameters. However, developing nano-cellulose requires low temperature extrusion, which would need further cooling equipment as an expense. Moreover, the industrial production

of nano-cellulose using an extrusion process is still in its preliminary stages. Therefore, the process requires further optimization of extrusion parameters, such as temperature, screw speed, feed rate, screw profile, and use of green solvents, to produce nano-cellulose with suitable properties at a fair cost.

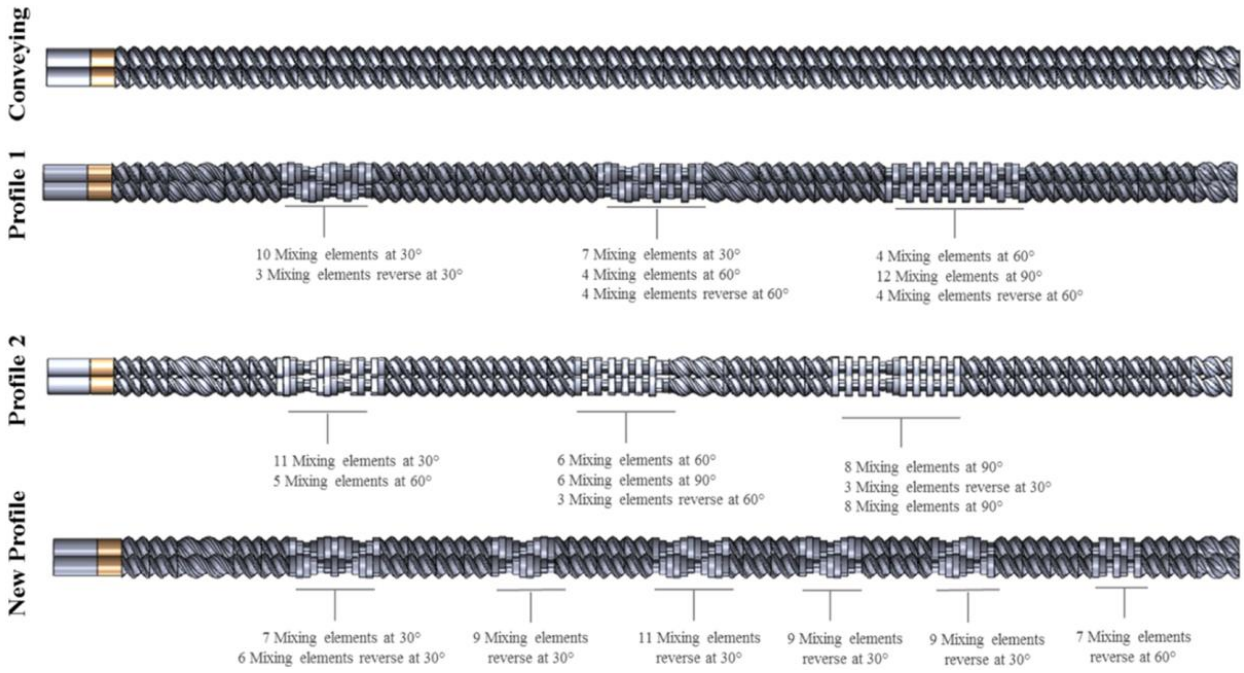

Figure 2.11. Different screw profiles designed for optimum shear generation and defibrillation of cellulose to produce nanocellulose. Adapted from Rol et al. with permission from American Chemical Society © 2019 [117].

Table 2.3. Nano- or micro-cellulose production using extrusion and its properties.

Sl. No.	Lignocellulose	Cellulose species	Extrusion parameters	Chemical used	Cellulose properties	Reference
1.	Never dried needle-leaf bleached kraft pulp with solid content of 28wt.%	Nanofibrillated cellulose	Twin-screw Extruder (TSE) (combination of kneading and feeding screws) L/D = 45 0 °C 400 rpm Maximum 14 passes	--	After 10 passes, solid content = ~39 wt.%, fiber size = ~6 µm with diameter 50 nm, discoloration occurred, degree of crystallinity = 75%,	106
2.	Soybean hulls, 0.3 mm particle size	Microcrystalline cellulose	Single-screw Extruder (SSE) L/D = 40 110°C 100 rpm First with NaOH followed by H_2SO_4	Sodium hydroxide (NaOH), sulfuric acid (H_2SO_4), 32% moisture content,	Cellulose content = ~84%, 70% crystallinity, short and rod shaped fibers with ~13 µm diameter and ~50 µm length.	107
3.	Soybean hulls pre-treated with acetic acid and hydrogen peroxide	Nanofibrillated cellulose	Two-step SSE L/D = 40 110°C 100 rpm First with NaOH followed by H_2SO_4	Sodium hydroxide (NaOH), sulfuric acid (H_2SO_4), acetic acid, hydrogen peroxide.	Cellulose content = ~87%, 80% crystallinity, short and rod shaped fibers with ~11 nm diameter.	108
4.	Oat hulls pre-treated with acetic acid and hydrogen peroxide				Cellulose content = ~78%, 73% crystallinity, short and rod shaped fibers with 80-100 nm diameter.	109
5.	Eucalyptus pulp	Nanofibrillated cellulose	Enzymatic pre-treatment or TEMPO oxidation Followed by TSE L/D = 45 10 °C; 400 rpm; Seven passes	TEMPO/sodium bromide (NaBr)/sodium hypochlorite (NaClO), enzyme.	63% less energy demand, high solid content of 20 wt.%, reduced production and transportation cost, size = 25-35 nm, ~90% transparency, young's modulus = 16 GPa, fiber degradation due to heat generation.	113
6.	Bleached eucalyptus kraft pulp with pre-treatment	phosphorylated cellulose fibrils	Phosphorylated cellulose suspensions at 10 wt.% TSE L/D = 40; 10 °C; 400 rpm 1-4 passes	Urea, NaOH, ammonium phosphate dibasic.	Need 4 passes, can be used as fire retardant material,	114
7.	Bleached eucalyptus kraft pulp	Cationic cellulose nanofibrils	Cationization cellulose suspension at 17 wt.% TSE 10 °C; 400 rpm; 1-7 passes	Epoxypropyl trimethyl ammonium chloride, enzyme	Size 50-55 nm, solid content 17 wt.%, 30% less energy consumption, need seven passes, may work as antibacterial substrate.	115
8.	Bleached eucalyptus kraft pulp	Destructured nanofibrillated cellulose using enzymatic hydrolysis.	Cationic and enzymatic cellulose suspension at 15 wt.% TSE 10 °C; 400 rpm; 1-4 passes	Enzyme solution endoglucanase	Crystallinity of 74%, lower energy consumption,	116

2.7 Reactive Extrusion for the Pre-treatment of Non-Lignocellulosic Biomasses

The pre-treatment of lignocellulosic biomasses has been thoroughly reviewed thus far. This section focuses on the reactive extrusion process and valorization for non-lignocellulosic biomasses. Other components of interest in non-lignocellulosic biomass include pectin from various fruits, lipids from algae, and polysaccharides for biogas production. Before the extraction of these constituents, reactive extrusion can be applied to these other biomasses in a similar manner as lignocellulosic biomass for their pre-treatment, as shown in **Figure 2.12**. The benefits of reactive extrusion for lignocellulosic biomass pre-treatment, including high shear, moderate processing temperature, and superior mixing and heat transfer, are applicable across all biomasses [19,24,29]. Some applications of reactive extrusion for the pre-treatment of non-lignocellulosic biomasses are highlighted below and briefly summarized in **Table 2.4**.

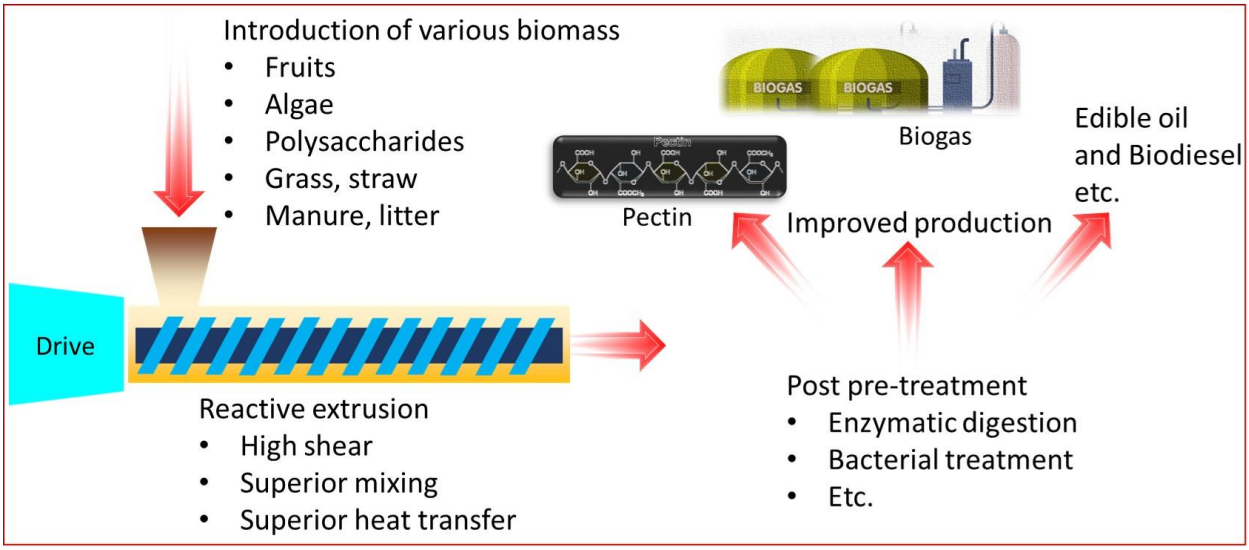

Figure 2.12. Typical reactive extrusion pre-treatment process of non-lignocellulosic biomasses and its subsequent valorization in various applications.

One application is to extract valuable and nutritious components from fruit scraps. For instance, pectin, a polysaccharide commonly used as a thickener, is traditionally extracted from fruits using acids or enzymes. However, acidic extraction is disadvantageous due to possible water pollution, machinery corrosion, and the production of non-consumable fiber-rich residues, while enzymatically digested pectin has a low degree of polymerization overall [118]. Therefore, extrusion pre-treatment has been explored to find a more efficient extraction method.

In one instance, pectin was recovered from commercial lemon fibers by Ralet and Thibault using TSE, obtaining a maximum yield of 29.4% pectin, which is slightly lower compared to the pectin yield of 34.1% using an acidic extraction method [118]. Despite this, the pectin that they extracted had a higher degree of methylation (92 mol% and 81 mol% for TSE and acidic extraction, respectively) [118]. Additionally, minimal other sugars were lost during dialysis using the extrusion pre-treatment method. The authors also proposed some depolymerization of the pectin during the TSE process as molecular weight and intrinsic viscosity decreased as the pectin yield improved. In a separate study, Larrea et al. removed pectin from orange pulp using SSE [119]. They determined that higher temperature, higher moisture contents, and lower screw speeds (i.e., longer residence times) encourage the solubilization of orange pulp components, which resulted in higher soluble dietary fiber values. Additionally, all tested extrusion conditions promoted the amount of orange pulp's total and soluble pectin values. Particularly, maximums of total and soluble pectin values of 43.70% and 16.76%, respectively, were obtained at higher temperatures and low moistures due to increased process severity in terms of shear [119].

The extraction of health benefitting components is another application of reactive extrusion of other non-lignocellulosic biomasses. As previously highlighted, soybean hulls are commonly processed for their lignocellulosic components using reactive extrusion. In addition, their seeds

have been extruded and susbsequently processed with $scCO_2$ in order to obtain contain isoflavones, such as genistein, which are phytochemicals that provide several health benefits [120]. In their study, five variables were related to the scC_{O2} extraction step, including temperature, pressure, ethanol content, co-solvent quantity, and flow rate, were tested and 32 optimal processing conditions were determined. Further details regarding the extraction procedure can be found in **Table 2.4**.

Recently, algae have been processed using reactive extrusion for polyunsaturated fatty acids (PUFA), which have clinical applications. Algae are also regarded as a source of biodiesel and edible oil. It has been found that the extrusion process can be applied in the extraction of valuables from different species of algae by enhancing the cell disruption process [121]. Li et al. found that the pretreatment of microalgae (*Nannochloropsis oceanica*), using a TSE process with a specific die configuration and water content (5%), leads to a significant reduction in time for the subsequent extraction process, decreasing from 10 hours to 20 min [40]. Further, PUFA extraction is improved. The eicosapentaenoic acid contents of the lipid were found to have increased by 37% using one-third of the volume of the solvent compared to lipids extracted from algae without pre-treatment. The pre-treatment using the extrusion process also improves the lipid quality in terms of unsaponifiable content, acid value, and iodine value.

Finally, the pre-treatment of other biomasses, such as straw, grass, manure, litter, etc., using an extrusion process can enhance the biogas production process. The extrusion of biomass accelerates the degradation of slow, degradable organic content and non-degradable content through heavy friction, shear, and mixing [122]. Furthermore, extrusion also helps in depolymerizing cellulose, hemicellulose, protein, and lignin, which increases biomass accessibility for enzymes and bacteria for biogas production [123]. Chen et al. has reported enhanced specific methane production to 227.3 L/kg of rice straw after extrusion pretreatment [123]. In a systematic study, Hjorth et al. observed that

methane production was enhanced by 70% in 28 days after the anaerobic digestion of barley straw [41]. Moreover, combining alkali solvents with the extrusion of rice straw enhanced methane production [48,124,125]. Zhang et al. reported that using sodium hydroxide during extrusion pre-treatment changes the physical properties of biomass, including water holding capacity, specific surface area, specific porosity, and crystallinity index, which leads to improved biogas production by 54% [124]. In another work, Wahid et al. have also suggested reverse elements' usability in a TSE screw profile for methane production [57]. They found that a screw configuration with kneading and reverse screw elements significantly enhances the availability of sugar present in wheat straw for bacterial consumption, leading to increased methane production.

Reactive extrusion for non-lignocellulosic biomasses presents an opportunity for the efficient extraction of other valuable resources aside from cellulose, hemicellulose, and lignin. Identical to lignocellulosic biomasses, reactive extrusion can be performed with either TSE or SSE, and it can also be combined or in sequence with various solvents, such as alkali solvents and $scCO_2$. The high shearing capabilities of reactive extrusion, sometimes supported by these chemical processes or other technologies, is advantageous for processing all types of biomasses due to the resulting heavy degree of deconstruction. In this way, there is increased accessibility to the desired component(s), regardless of the subsequent process needed to retrieve it. And thus, reactive extrusion as a pre-treatment for all biomasses is feasible and reasonable, especially for fractionation or component extraction purposes.

Table 2.4. Reactive extrusion of non-lignocellulosic biomass and the conventional component extracted for valorization.

Biomass	Desired Component	Processing Conditions	Maximum Yield and Respective Processing Conditions	Reference
Commercial lemon dietary fibers	Pectin	TSE; Water added, 20-50 wt.% of dry matter 24, 32 kg/h biomass feed rate L/D = 18; 90-115 °C; 150, 240 rpm Two screw configurations	Pectin Yield = 29.4% (99 °C, 240 rpm, 20 wt.% of dry matter in water added, 32 kg/h)	118
Orange pulp	Pectin	SSE 22-38 wt.% moisture Compression ratio, 3:1 L/D = 20; 4.2 kg/h; 83-167 °C; 126-194 rpm	Total Pectin Yield = 43.70% (125 °C, 30 wt.% moisture, 160 rpm) Soluble Pectin Yield = 16.76% (167 °C, 30 wt.% moisture, 160 rpm)	119
Soybean	Genistein	**Extrusion Pre-treatment** Extruder Unknown; 85 °C; 260 rpm **$ScCO_2$ Extraction** Step 1 – 70 °C, 25 MPa, 3 h Step 2 – 40-80 °C, 20-40 MPa, 0-100 % ethanol, 30-70 mL ethanol/methanol co-solvents, 9-13 kg/h Step 3 - 70 °C, 25 MPa, 3 h	Genistein Yield = 0.094% (ScCO2 Extraction Step 2 Conditions: 60 °C, 40 MPa, 0% ethanol, 70 mL co-solvents, 9 kg/h)	120
Algae (*Nannochloropsis oceanica*)	Eicosapentaenoic acid	TSE 5-30 wt.% moisture 50-150 °C; 100 -250 rpm 5 different die configurations (A-E) Screw to die distance, δ, 0-4 mm	Lipid yield = 15% (Extrusion - Die C, δ = 4mm, 5% water content. Lipid Extraction – 60 °C, 30:1 w/w solvent to biomass, 20 min)	40
Rice Straw	Cellulose and hemicellulose for methane production	TSE L/D = 3.75; 120 rpm Varying methane production variables	Specific methane production = 227.3 L/g VS of rice straw	123
Barley Straw, Grass, Solid fraction – screw-pressed manure, Solid fraction – flocculated and filtered manure, and Deep litter	Cellulose and hemicellulose for methane production	TSE L/D = 1.3	Approx. Methane Yield after 90 days Barley Straw = 370 L/kg VS Grass = 200 L/kg VS Solid fraction – screw-pressed manure = 280 L/kg VS Solid fraction – flocculated and filtered manure = 350 L/kg VS Deep Litter = 290 L/kg VS	41
Rice Straw	Cellulose and hemicellulose for methane production	**Extrusion Pre-treatment** TSE; No other details provided **NaOH Pre-impregnation** 35 °C; 3-120 h; Solid-to-liquid ratio, 1:6 Alkaline loading rate, 1.5-6.0%	Specific methane production = 288 mL/g VS	124
Wheat straw and Deep litter	Cellulose and hemicellulose for methane production	TSE; L/D = 40; 18 kg/h; 600 rpm Five screw configurations (Mild kneading, Long kneading, Reverse, Kneading and reverse, Kneading with reverse)	Methane Yield after 90 days Wheat Straw = 327.3 NL/kg VS (Configuration: Kneading and reverse) Deep litter = 306.9 NL/kg VS; (Configuration: Long kneading)	57

2.8 Future Trend and Challenges in the Reactive Extrusion of Biomass

Extrusion pre-treatment methods for the processing of biomasses are not yet exhaustively explored. Investigations involving newer solvents, such as ionic liquids (Da Silva et al., 2013; Han et al., 2020), organosolv (Brudecki et al., 2013), biocatalyst enzymes (Gatt et al., 2018), or supercritical carbon dioxide (Zhan et al., 2006), are emerging as areas of interest in extrusion pre-treatment. These solvents are appealing for industrial applications as they are considered more environmentally friendly compared to common biomass pre-treatments, typically involving mineral acids and caustic solutions (Gu et al., 2013; Kumari and Singh, 2018). However, the effectiveness of these solvents with regards to extrusion pre-treatment needs to be further assessed in future work. Furthermore, since the extrusion pre-treatment system is very adaptable, a variety of combined and sequential pre-treatment processes involving extrusion have yet to be studied. Recently, microwave (Gao et al., 2019; Karunanithy et al., 2014) and ultrasonic (Debiagi et al., 2021; Zhang et al., 2020) treatment of the biomass following extrusion are used to improve conversion yield as these methods are simple, effective, and chemical-free. Overall, the extrusion process is still lagging in terms of performance compared to acid, and alkaline pre-treatment, and many improvements can be made.

A few challenges hold back the implementation of extrusion pre-treatment at an industrial scale. First, there is a lack of analysis regarding its economic feasibility. The pre-treatment of biomass is a broad area of study as the steps that follow pre-treatment can vary. As aforementioned, enzymatic hydrolysis for the biomass conversion into bioethanol using the extrusion process is the most common biomass valorization process. Due to this, economic feasibility studies for extrusion pre-treatment are mostly focused on biofuel production (Souza et al., 2021; Yoo, 2011). However, the valorization of the other components of these biomasses is highly desirable and has gained

attention in recent years. Therefore, economic feasibility studies for the fractionation of the main biomass components and subsequent generation of high-value co-products need further investigation.

In addition to the lack of complete economic analysis, there are also some critical difficulties involved with the newer research areas in extrusion pre-treatment. Green solvents, like ionic liquids, are costly, making them difficult to apply industrially. Ionic liquids can cost from $2.70-$31.80 USD/g (Luo et al., 2013). Furthermore, the addition of other technologies, such as steam explosion or supercritical fluid incorporation, with the extrusion process can also add capital and energy costs to the process (J. Chen et al., 2014; Karunanithy et al., 2014). These emerging areas of interest must also be taken into consideration concerning process cost.

Another area for improvement in extrusion pre-treatment is the amount of energy consumed during the process, which also contributes to cost. Like cost analysis, energy consumption assessment during extrusion pre-treatment is lacking and is only present for studies aiming for biofuel production (Hjorth et al., 2011; Souza et al., 2021). In those studies, energy input and output are closely monitored as there is a possibility to generate energy from the side – and by-product streams to counteract the energy consumption of the process used to make the biofuel and make the process energetically profitable. For studies involving the valorization of other components, a similar analysis is required for the process to be scalable.

While the extrusion pre-treatment process is appealing due to its continuity, high throughput, and high solid loading capability, current research is not yet sufficient for industrial-scale applications. Further studies must be performed to determine an optimum pre-treatment method involving extrusion processing that is effective, environmentally friendly, low energy, and inexpensive.

Chapter 3: Green Mechano-Chemical Processing of Lignocellulosic Biomass for Lignin Recovery

3.1 Introduction

As a renewable resource for material applications, lignocellulosic biomass helps alleviate environmental concerns related to petroleum-derived plastic products. Non-renewable resources, such as fossil fuels, are associated with plastic pollution, human and animal health and safety due to petrochemical by-products, and global climate change [126,127]. Lignocellulosic biomasses are considered an appropriate alternative to fossil fuel-based products due to their extensive availability, renewability, and sustainability. In addition, they are a great source of natural macromolecules, such as cellulose, hemicellulose, and lignin. Lignocellulosic biomasses are directly derived from the forestry and agricultural industry residues.

Currently, lignocellulosic biomass residues are mostly burned as sources of energy. In 2019, biomass accounted for about five quintillion joules of energy generation, which is about 5% of the total primary energy use in the United States [128]. However, there has been some progress towards the valorization of biomass components instead of its use as a direct source of fuel. Most commonly, cellulose and hemicellulose are used in bioethanol production. The sugars and starch derived from cellulose and hemicellulose can constitute up to 90% of the required feedstock for bioethanol [11]. The application of lignin is not as well explored in comparison. At present, lignin is used as an additive in concrete mixtures, binder in animal feed, or as dispersants in dyes and crop protection products [13]. Furthermore, there is ongoing research studying the depolymerization of lignin as its aromatic building blocks can provide material benefits in terms of rigidity, hydrophobicity, and fire resistance [13] and the carbonization of lignin for functional applications [89].

Yet, the application of lignin is limited by technological maturity, lignin recovery scale-up costs, and the difficulty in isolating and controlling its recalcitrant structure [13,129].

There is a variety of lignin grades available industrially, all with varying isolation processes. Present industrial sources of lignin include kraft lignin, sulfite lignin, soda lignin, and organosolv lignin. Prior to the isolation of lignin, a pre-treatment process is performed on lignocellulose which dictates the type of lignin produced and its characteristics. Pre-treatment prepares lignocellulose for further processing by increasing porosity, surface accessibility, and reducing its overall recalcitrance [42]. Pre-treatment and processing methods can be physical, chemical, physico-chemical, biological, and combinations. Subsequently, solvent and by-product recovery follow the pre-treatment processes, leading to the production of biomass derivatives such as paper, bioethanol, high-quality lignin, etc. [130].

Most of the highlighted types of lignin are a direct result of established pulping processes. Unfortunately, the processes for these common types of lignin usually involve corrosive solvents (e.g., sodium hydroxide, sodium sulfide, various sulfites, soda-anthraquinone, etc.) that are not safe for the environment [13]. Moreover, most processes result in lignin derivatives not desired in some material applications requiring higher purity. As an alternative, newer studies explore the application of ionic liquids, which are considered as green solvents that can retain the inherent molecular structure of lignin during the processing of lignocellulosic biomass. Generally, ionic liquids are considered environmentally friendly due to their low volatility, high thermal stability, and their reusability [131]. While the low volatility of ionic liquids prevents its evaporation into the atmosphere and inhalation by humans and animals, it can still be introduced into soil and aquatic environments, in which it has been identified to be toxic to some organisms [77,78]. Therefore, extra precaution must still be performed to the life cycle of ionic liquids when designing processes

involving its use. These solvents are characterized by their small inorganic anion and large organic cation pairs, and they typically demonstrate a low melting point (below 100 °C). Ionic liquids are also considered designer solvents since these ions can be tailored according to the desired application [131]. Some common ionic liquids include: 1-butyl-3-methylimidazolium chloride (BmimCl), 1-ethyl-3-methylimidazolium chloride (EmimCl), 1-allyl-3-methylimidazolium chloride (AmimCl), and 1-ethyl-3-methylimidazolium acetate (EmimAc) [75].

Clearly, the properties of ionic liquids make them desirable for application as solvents in the lignocellulosic biomass pre-treatment processes. However, there are several factors that limit their application. First, ionic liquids are costly, ranging from 2.70-31.80 USD/g [75]. Additionally, ionic liquid processing often requires high amounts of ionic liquid loading (~95 wt.%), which is not feasible for industrial applications due to its high cost [55,81,82]. For this reason, the recycling of ionic liquids after pre-treatment is desirable, however, research is currently lacking [75,132]. Furthermore, the use of ionic liquids for lignocellulose deconstruction is not yet optimized, and in most cases, the processes require a long period of time (1 to 24 h) [55,75,81,82]. As such, higher solid loadings and lower processing times would greatly benefit the application of ionic liquid processing of lignocellulose biomass on an industrial scale.

A few studies have been carried out and have found some success with the high solid loading processing of biomasses with ionic liquids. To achieve this, these studies implemented larger volume equipment with higher shear capabilities and used it in combination with ionic liquid solvents. For instance, Da Silva et al. and Silveira et al. used a twin-screw extruder and supercritical carbon dioxide, respectively, to treat sugarcane bagasse with EmimAc [28,133]. Alternatively, Liang et al. combined ionic liquid processing with acidolysis in a reactor to process various municipal solid waste blends at 10 and 15 wt.% solids [134].

Comparatively, more studies have been performed involving high biomass loadings with hydrothermal pre-treatment methods [135]. Batch operation modes for hydrothermal pre-treatment include liquid hot water and steam explosion processes. In two studies in 2010 and 2012 by Romani et al., *Eucalyptus Globulus* was pre-treated with hot water between 210-230 °C at solid loadings in the range of 4-16 wt.% inside a stirred reactor [136,137]. Even higher solid loadings of Norway spruce wood (~30 wt.%) was processed with mild steam explosion inside an autoclave by Jedvert et al. [138]. Hydrothermal pre-treatment can also be performed continuously. For example, a study in 2019 explored a pilot scale continuous tubular reactor in which various biomasses, such as sugarcane bagasse and corn stover, were pre-treated at 10 wt.% at 180 °C for 20 min. The main advantage of hydrothermal pre-treatment methods compared to ionic liquid assisted methods is the lack of chemicals involved, which is advantageous in terms of machinery corrosion prevention and cost [29,135]. However, these processes have high energy demand due to the high amounts of pressure and water involved [29,135]. These previous investigations with water as a solvent can act as a point of reference for ionic liquid processing and its possible scale-up in the future.

To further understand ionic liquid processing at high solid loadings, in this study, mixed hardwood flour (MHF) is processed with BmimCl in a mechano-chemical process using a high shear batch mixer. BmimCl was selected to be studied in this investigation since it is widely investigated and relatively cheap compared to other ionic liquids which are known to be more successful in the solubilization of biomass components, such as EmimAc [82,132]. The influence of biomass loading amount and processing time on the effectiveness of ionic liquid processing of biomass was determined, emphasizing lignin recovery. Successful processing was measured based on the amount of lignin extracted from the biomass. Additionally, the rheological behavior of the biomass and ionic liquid mixtures was also investigated to understand the performance of the mechano-

chemical process. The extracted lignin samples were also characterized in detail and compared with commercial lignin products.

3.2 Materials and Methods

3.2.1 Materials

Mixed hardwood flour (MHF) (mesh 165) was obtained from Ontario Sawdust (Holland Landing, Ontario, Canada). 1-butyl-3-methylimidazolium chloride (BmimCl) was purchased from Hangzhou Satort Biopharma Co., Ltd (Zhejiang, China). The BmimCl has a melting point of 73 °C and is hygroscopic, so opened containers were stored in a desiccator. Sodium hydroxide (NaOH) pellets (≥ 97.0%) and potassium bromide were purchased from Sigma-Aldrich. Hydrochloric acid (HCl, ACS reagent grade, 36.5-38%) and sulfuric acid (H_2SO_4, ACS reagent grade, 95-98%) were purchased from Fischer Scientific Canada. Dealkaline lignin powder (L0045), or sodium lignosulfonate, and Amallin^{TM} Kraft Lignin were acquired from TCI Chemicals and West Fraser (Hinton, Alberta, Canada), respectively.

3.2.2 Methods

3.2.2.1 Mechano-chemical processing of wood flour with BmimCl

Prior to any processing, the MHF was dried at 80 °C overnight in a tray covered with perforated aluminum foil. After drying, the moisture of the MHF was measured to be 2-5 wt.% using a Sartorius moisture analyzer. The MHF was then manually pre-mixed with melted BmimCl in a beaker at various solid loadings (**Table 3.1**) in 50 g increments to ensure homogeneous mixing for a total weight of 150 g. The processing of the MHF – BmimCl blends was then performed on a Thermo Scientific HAAKE Rheomix Polylab QC Lab Mixer using roller blades. A fixed processing temperature of 150 °C was selected based on the thermal stability of MHF at this

temperature. Thermogravimetric analysis revealed that 150 °C was well below the onset thermal degradation temperature of MHF (approx. 270 °C) and that there is negligible weight loss (< 5 wt.%) at this temperature. The influence of temperature is not explored in this study as its positive influence on biomass pre-treatment is well reported [24,75]. Additionally, a fixed rotor speed of 150 rpm was picked based on batch mixer operation constraints (maximum rotor speed of 200 rpm).

Table 3.1. Batch mixer experimental processing conditions for MHF – BmimCl blends and extracted lignin yield.

Sample Name	Solid Loading Amount	Residence Time	Lignin Extraction Yield
50W-45m	50%	45 min	36.6%
50W-10m	50%	10 min	23.6%
5W-45m	5%	45 min	19.3%
5W-10m	5%	10 min	18.9%
27.5W-m1	27.5%	27.5 min	23.2%
27.5W-m2	27.5%	27.5 min	25.3%
27.5W-m3	27.5%	27.5 min	23.8%

In this experiment, a 2^2 factorial design was performed with three center points, for a total of seven runs. The two factors that varied were the MHF to BmimCl ratio and the residence time. For the MHF to BmimCl ratio, the low and high MHF loading levels with respect to BmimCl were 5 and 50 wt.%, while the minimum and maximum residence times of 10 and 45 min, respectively**,** were tested. Thus, the center points had an MHF loading of 27.5 wt.% and a residence time of 27.5 min,

as shown in **Table 3.1**. The low end MHF loading amount was chosen since 5 wt.% solid loading is a common loading amount explored in ionic liquid pre-treatment studies [55,81,82], while the high end was selected due to torque constraints that are introduced at high solid loadings. Residence time values were grounded on the idea of applying a similar analysis using an extruder instead of a batch mixer in a future study. Residence time in an extruder is determined by the number of times a material is passed through the extruder, where one pass in a lab scale extruder at a slow speed is approx. four minutes [28,45,47]. The maximum residence time of 45 min was determined to be a feasible amount of manual extruder passes (equivalent to approx. 10 passes). The processed samples were then collected, cooled to room temperature, and stored in airtight containers until further use. A regression model was also developed based on lignin extraction yield, and analysis of variance (ANOVA) was performed using Minitab 14.

3.2.2.2 Lignin Extraction

Lignin was extracted from MHF with and without mechano-chemical processing. Samples processed at 5 wt.% MHF solid loading are liquid and solidify after cooling to room temperature and so, to prepare the processed samples for extraction, these samples were kept in an oven at 80 °C for six hours to allow for the melting of BmimCl. Samples processed at 27.5 and 50 wt.% MHF solid loading are solid, either like hard clay or powder, and these samples were ground using a coffee grinder. 50 g of each processed sample were then added to a beaker with 500 mL of 0.1 N NaOH aqueous solution. For unprocessed MHF, 2.5 g of the sample was taken, which is equivalent to the amount of wood in 50 g of a 5 wt.% MHF solid loading sample. The alkaline-biomass mixture was processed overnight on a hot plate (70 °C) under magnetic stirring, centrifuged (3,800 rpm for 5 min) to remove the cellulose-rich solid residue and to recover the alkali-soluble lignin supernatant. The supernatant (Supernatant 1) was then acidified to a pH of 2 using 1 N HCl on a

hot plate (70 °C) under agitation (400 rpm) for 30 min to precipitate the lignin. The acidified mixture was then centrifuged, and the precipitated lignin residue was recovered.

The extracted lignin was washed with 40 mL of acidified water (pH 2, using 1 N HCl) to remove any remaining ionic liquid residue. A vortex mixer (2700 rpm for 30 s) was used to thoroughly wash the lignin inside the centrifuge tube. The acidified water washings were removed after centrifuging (4,000 rpm for 10-20 min). Similarly, the cellulose-rich solid residue was washed with 160 mL of acidified water.

Finally, the washed lignin and residue samples were quantitatively transferred into separate aluminum pans using distilled (DI) water and dried at 80 °C overnight. The weight of the extracted lignin was measured after drying. Extracted lignin and residue were stored in vials and polyethylene bags, respectively, at room temperature. A schematic representation of the described mechano-chemical processing of lignocellulosic biomass and subsequent lignin extraction is presented in **Figure 3.1**.

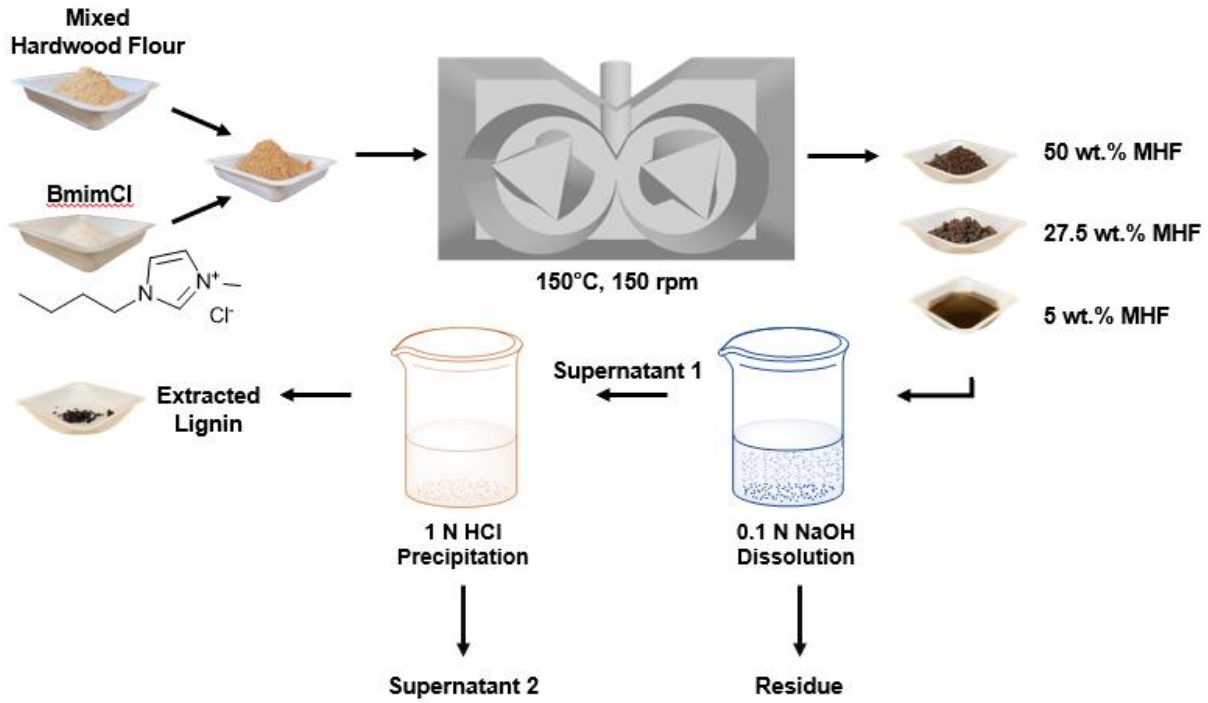

Figure 3.1. A general diagram of the mechano-chemical processing of 1-butyl-3-methylimidazolium chloride (BmimCl) and mixed hardwood flour (MHF) and the following lignin extraction procedure.

3.2.2.3 Characterization

Polarized Optical Microscopy (POM)

To investigate the physical structure of MHF before and after batch processing and lignin extraction, polarized optical microscopy (POM) was used. For this study, the Olympus BX53 upright microscope was used with an Olympus SC100 color camera and U-TV-0.5XC-3 camera adaptor. A magnification lens of 20x was used for all images. For sample preparation, 25 mg of each sample was dispersed in 20 mL of distilled water at room temperature. An aliquot was then taken from the mixture and dried at 80 °C overnight. Samples were analyzed on top of a clean glass slide.

Parallel Plate Rheometry

The viscosity and rheological behavior of the MHF and BmimCl mixtures after mechano-chemical processing was characterized using a parallel plate rheometer (TAI AR2000, TA Instruments, New Castle, DE, USA). Pure BmimCl, ground (≥ 27.5 wt.% MHF loading), and melted (5 wt.% MHF loading) samples were compressed into sheets, and a circular die was used to cut disks sized 25 mm in diameter. Melted and BmimCl samples were solidified in a refrigerator prior to disk cutting. The disks of high MHF loading samples had a thickness of 1.2 mm, while BmimCl and low MHF loading samples had a thickness of 2.5 mm to accommodate the melting of the ionic liquid. A frequency sweep was performed from 0.05 to 1000 rad/s at 150 °C for all samples. The strain was kept constant at a value in the linear viscoelastic region of that specific sample. For high MHF loading samples, the strain was kept at 0.1% strain, while low MHF loading samples and pure BmimCl were held at 5% strain. Lastly, the gap was kept at approx. 1 mm.

Determination of Lignin Extraction Yield

After drying of the extracted lignin, its yield with respect to the amount of lignin initially present in MHF was calculated using the following equation:

$$Percentage\ Lignin\ Extraction\ Yield = \frac{E}{m \times w \times \bar{L}} \times 100 \qquad (3.1)$$

where E is the mass of dried extracted lignin (g), m is the mass of the processed sample (50 g), w is the mass fraction of MHF in the processed sample (0.05, 0.275, or 0.5), and $\bar{L}$ is the average fraction of lignin in MHF determined in the following section.

Determination of Total Lignin Composition of MHF

To determine lignin yield, the percentage of lignin in MHF ($\% L$) must be determined. Soxhlet extraction was performed using boiling ethanol placed in an oil bath for over 16 h to remove

extractives inside MHF. The ethanol extractives-free MHF was left to air dry. The moisture content of MHF after drying was determined using a Sartorius moisture analyzer to calculate its oven-dry weight (*ODW*).

The lignin fraction in MHF was determined following ISO 21436-2020 procedure B to determine acid-soluble lignin (ASL) and acid-insoluble lignin (AIL) [139]. Briefly, 0.5 g of ethanol extractives-free MHF is stirred in 10 mL of 72% H_2SO_4 in a water bath at a temperature of 20 °C. The mixture was occasionally stirred with a glass rod over the course of 2 h. The mixture was then diluted to 375 mL with DI water and heated to boiling temperature for 4 h while continuously adding hot DI water to maintain a constant concentration of 3% H_2SO_4. After cooling to room temperature, the mixture was centrifuged, and the supernatant containing ASL was collected. The remaining solid pellet, acid-insoluble residue (AIR), was washed with 100 mL of DI water and centrifuged to obtain the water washings. The supernatant was diluted to 500 mL with DI water after the addition of the AIR water washings. To determine ASL, a Cary 300 Bio Ultraviolet-visible (UV-vis) Spectrophotometer was employed to measure the absorbance of the supernatant at 205 nm using a 1 cm glass cuvette and 3% H_2SO_4 as blank. The solution was further diluted to ensure that the absorbance values were within the range of 0.2-0.7 absorbance units. The dilution factor was recorded, and the percentage of ASL in MHF was calculated using **Eq. (3.2)** below:

$$\% \, ASL = \frac{A \times D \times V}{\varepsilon \times b \times ODW} \times 100 \tag{3.2}$$

where *A* is the absorbance at 205 nm, *D* is the dilution factor, *V* is the volume of the solution prior to dilution (500 mL), ε is the average absorption coefficient of lignin from various types of wood (110 L/g·cm), *b* is the path length of the cuvette (1 cm), and *ODW* is the calculated oven-dry weight of the ethanol extractives-free MHF sample in mg. To determine AIL, the AIR was further washed

three times with 50 mL of DI water. The washed AIR was then quantitatively transferred into a weighed ceramic crucible and dried at 80 °C overnight. The weight of dried AIR was recorded. To correct for ash content, the AIR was placed in a furnace at 525 °C until no black charring remained (3-5 h). The weight of the remaining ash residue was recorded. The following equation was then used to determine the percentage of AIL in MHF:

$$\% AIL = \frac{AR - ASH}{ODW} \times 100 \tag{3.3}$$

where *AR* is the weight of dried AIR in mg, *ASH* is the weight of the ash in mg. The *% L* in MHF was determined as follows:

$$\% L = \%ASL + \%AIL \tag{3.4}$$

The procedure to determine *% L* was performed in triplicate, with the average of the three results ($\% \bar{L}$) being used to calculate lignin extraction yield in **Eq. (3.1)**.

Fourier Transform Infrared (FTIR) Spectroscopy

To analyze the chemical structures of MHF, the extracted lignin, and commercial lignin, Fourier transform infrared (FITR) spectroscopy was employed. In this study, a Thermo Scientific Nicolet FTIR spectrometer was used in transmittance mode at a resolution of 4 cm^{-1} and between wavenumbers of 500-4000 cm^{-1} for 32 scans. The resulting spectra were baseline corrected. To produce samples for the analysis, 3 mg of each sample was homogeneously ground with 200 mg of dried potassium bromide (KBr) powder and compressed into pellet form. Background scans were performed with pure KBr pellets.

Ultraviolet-visible (UV-vis) Spectroscopy

Supplementary confirmation of lignin extraction was determined using ultraviolet-visible (UV-vis) spectroscopy. Extracted and commercial lignin samples were dissolved in 0.01 N NaOH at a concentration of 0.025 mg/mL. Extracted lignin samples were washed thrice with 50 mL of acidic water using a vortex mixer and dried overnight at 80 °C prior to dissolution. The UV-vis spectra were collected using a Cary 300 Bio UV-vis Spectrophotometer between 800-200 nm in glass cuvettes. The blank standard used was 0.01 N NaOH.

Solid state carbon nuclear magnetic resonance (^{13}C-NMR)

Solid state carbon nuclear magnetic resonance (^{13}C-NMR) was performed to further study the chemical structure of the extracted lignin in comparison with commercial lignin. For the analysis, a Bruker Avance III HD 500 MHz machine with solid sample analysis capabilities was used. Samples were analyzed at a magic angle spinning speed of 5 kHz.

Dynamic Light Scattering (DLS)

The zeta potentials of the extracted lignin were also compared with commercial kraft lignin and lignosulfonate. Zeta potential analysis was performed using a Malvern Zetasizer Nano-ZS90 (Westborough, MA, United States). Prior to the analysis, the extracted lignin samples were washed thrice with 50 mL of acidic water using a vortex mixer to remove any remaining ionic liquid and dried overnight at 80 °C. Lignin samples were dispersed in DI water (pH 5) using a sonicator for 30 min and at a concentration of 0.1 mg/mL. After the dispersed samples were left to naturally sediment overnight for stabilization, their zeta potentials were measured at 25 °C inside a folded capillary zeta potential cell (Zetasizer nano series, DTS 1070). The average of three zeta potential measurements was reported for each sample.

Thermogravimetric analysis (TGA)

Thermogravimetric analysis (TGA) of extracted and commercial lignin was completed a Mettler Toledo TGA 2 STAR system. Extracted and commercial lignin was analyzed in 15-20 mg portions under nitrogen gas at a constant flow rate of 30 mL/min. The samples were held at 115 ℃ for 10 min to remove moisture and then heated to 900 °C at a rate of 20 °C/min.

3.3 Results and Discussion

3.3.1 Mechano-Chemical Processing of MHF with BmimCl

The mechano-chemical processing of MHF and BmimCl mixtures resulted in varying temperature and torque behaviors inside the batch mixer, as presented in **Figure 3.2 (a & b)**. While the temperature for all the processes was set at 150 °C, all experiments developed temperatures past 160 °C due to the shear. A maximum temperature of 180 °C was reached by 50W-45m. These higher temperatures result from the high amount of shear being developed between the rotors and the materials during processing. Samples with the highest solid loading experienced a larger increase in temperature due to the increased shearing introduced by the presence of more solid particles. This observation is further supported by the torque behavior inside the batch mixer.

The torque of the batch mixer's rotor indicates the amount of force needed for the rotor to rotate at the set rotation speed (150 rpm) given the temperature and material conditions. From **Figure 3.2b**, the torque values for 5 wt.% MHF samples are very low (1 Nm) due to the high levels of the BmimCl, while 50W-45m and 50W-10m reached a maximum torque of about 20 Nm and 10 Nm, respectively. Additionally, two maxima were observed for 50W-45m. The first maximum at 5 min, found in both 50W-45m and 50W-10m, resulted from the homogeneous blending of the MHF and BmimCl. The second maximum of 50W-45m at 32.5 min could be due to the structural disruption

and swelling of the lignocellulosic biomass by BmimCl. Further analysis of this behavior was studied using a rheological time sweep analysis provided in **Appendix A** (**Figure A1**). Also, there was a sudden decrease in torque and temperature for the same sample at 2.5 min because of the temporary removal of the batch mixer plug. Alternatively, the torque value of 27.5W-m1 reached an upper limit of 5.5 Nm and continuously decreased thereafter. The constant decline after reaching a maximum torque value indicated that MHF particles were sliding past one another with BmimCl acting as a lubricant, and structural disruption was not achieved. Overall, the torque behaviors of the various mixtures demonstrated that higher loadings and longer processing times are required to overcome the recalcitrant structure of MHF.

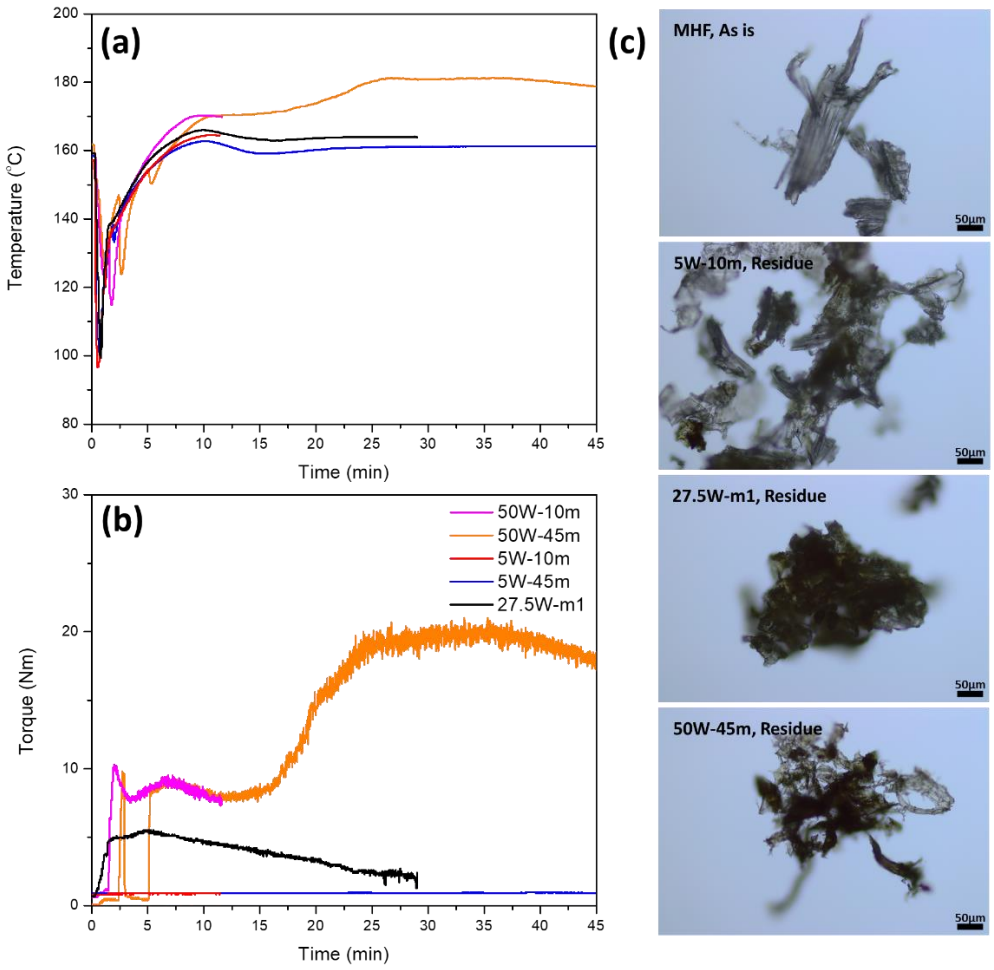

Figure 3.2. (a) Temperature and (b) torque data for batch mixer during the processing of MHF – BmimCl mixtures; (c) POM images of unprocessed MHF and MHF residue after lignin extraction.

After mechano-chemical processing, the MHF and BmimCl mixtures displayed varying behaviors dependent on their compositions and processing conditions. These contrasting natures are illustrated in **Figure 3.1**. Higher MHF loading samples (50 and 27.5 wt.%) were solid, where samples with processing times of 27.5 min or 45 min behaved like hard clay, and samples processed for 10 min acted like powder. The clay-like behavior of the samples with high MHF loading and longer processing times indicated a more thorough integration of BmimCl into MHF. On the other hand, lower MHF loading samples (5 wt.%) were liquid immediately after processing

but solidified as the samples cooled down to room temperature due to the solidification temperature of BmimCl. As a result of their varying natures, the processed samples were prepared slightly differently prior to lignin extraction, as previously highlighted in **Section 3.2.2.2**. The extra melting step required for low MHF loading samples may contribute to further dissolution of the biomass components in the ionic liquid. However, since mechanical stirring was not applied and the melting temperature was low, it is not expected to have a significant influence on lignin extraction yield. Furthermore, the rheological behavior of the differently natured mixtures after processing was also explored in the next section.

Mechano-chemical processing was followed by chemical lignin extraction. The physical effects of these processes on MHF were investigated using POM. The MHF and the obtained residue after processing and lignin extraction were also analyzed in dry state (**Figure 3.2c**). The unprocessed wood samples displayed a fibrous and composed structure, while the processed and lignin extracted MHF residue were disrupted due to the high shear from the process and penetration from BmimCl. For 5W-10m, the residue sample after lignin extraction is flaky with some tendrils. The residue obtained from the midpoint process (27.5W-m1) was imaged to be very agglomerated due to the binding of BmimCl with the wood components and incomplete structural disruption, which was noted from previous torque observations. Lastly, the most processed sample (50W-45m) was very deconstructed with a tangle of tendrils in addition to some agglomeration due to the binding of BmimCl.

3.3.2 Rheological Behaviour of MHF and BmimCl Mixtures

Figure 3.3 (a & b) displays the viscosity and rheological behavior of MHF and BmimCl mixtures after a frequency sweep. The high solid loading samples (≥ 27.5 wt.%) behaved as solids, as observed previously. For these samples, the storage modulus (G') is consistently higher

than the loss modulus (G"). Low solid loading samples (5 wt.%) were opposite in that G" > G', demonstrating liquid-like characteristics.

Additionally, the complex viscosity of higher solid loading samples was significantly higher than ionic liquid-dominated samples. Interestingly, at 50 wt.% solid loading, the viscosity of samples processed for 45 min was slightly lower than the samples processed for only 10 min. This observation indicated the integration of ionic liquid into MHF. However, at 5 wt.% solid loading, the viscosity of samples with longer processing time was higher than those processed for a shorter period. This could be attributed to the destructurization of wood samples into their constituents, such as cellulose, hemicellulose, and lignin. Samples processed for only 10 min were similar to pure BmimCl samples in terms of rheological properties, but slightly more viscous due to the presence of MHF. Moreover, all samples demonstrated shear thinning, which is attributed to the properties of BmimCl and native lignocellulose [59,140]. The 5 wt.% solid loading samples and pure BmimCl also exhibited an abnormal increase in viscosity at higher frequencies. A secondary frequency sweep analysis, provided in **Appendix A** (**Figure A2**), was performed for 5W-45m and BmimCl to confirm the presence of the supposed shear thickening. Further studies must be performed to understand this behavior. Piednoir et al. hypothesized that this apparent shear thickening behavior was not a characteristic of ionic liquids, but was likely due to additional dissipation due to the oscillation of the contact lines between the plate and the sample which is inherent to the parallel plate rheometer geometry [141].

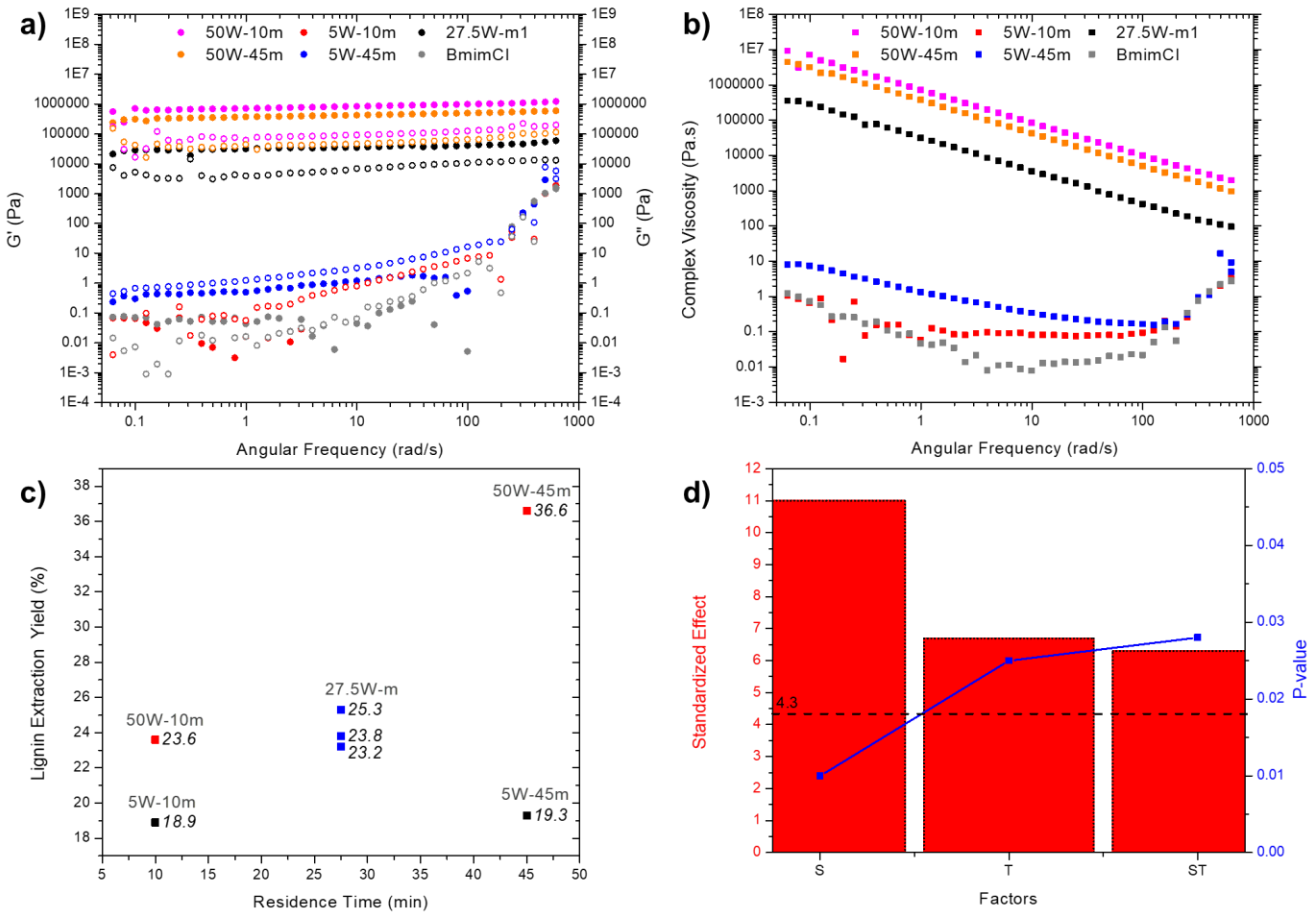

Figure 3.3. (a) Modulus and (b) complex viscosity of various processed MHF and pure BmimCl at 150 °C. Storage modulus (G') are closed symbols and loss modulus (G") are open symbols; (c) A comprehensive plot of lignin extraction yield in relation to residence time in the batch mixer and solid loading amount of MHF processed with BmimCl. The three blue points are the center points of a 2^2 factorial design; (d) Pareto chart and p-values of the sources of variances in the process with a confidence interval of 95%, represented by the horizontal dashed line. All standardized effects were positive. S is solid loading content and T is residence time.

The rheology of high solid loading biomass mixtures with ionic liquids was explored by Cruz et al. [142]. They investigated the shear thinning behaviours of switchgrass and EmimAc mixtures at solid loadings of 3-50 wt.%. Like the rheological properties observed in this study, a significant

increase in viscosity was noted when the biomass loadings were increased. Similarly, at lower loadings (3 wt.%), G" > G' and at higher loadings (10 ≥ wt.%), G' > G" as well. They also determined that, at high solid loadings, the degree of shear thinning enhances. A comparable observation can be made in this study where there was a ~4650x decrease in viscosity for 50W-45m, but only a ~50x decrease for 5W-45m. Overall, the rheological behavior of biomass and ionic liquid mixtures is very dependent on the solid loading amount.

3.3.3 Effect of Processing Variables on Lignin Extraction Yield

The influence of MHF to ionic liquid loading and processing time on lignin extraction using the rheology batch mixer process was explored. The average fraction of total lignin in the MHF was determined to be 28.6 ± 1.4%. This value of % $\bar{L}$ was used as a basis for the calculation of lignin extraction yield in **Eq. (3.1)**. **Table 3.1** displays the lignin extraction yield of BmimCl and MHF samples processed at different conditions, while **Figure 3.3c** provides a comprehensive plot of the data. The lignin extraction yield for unprocessed MHF was determined to be 10.2%, which is significantly less compared to the yields of all mechano-chemical processed samples. The low lignin extraction yield of unprocessed MHF indicates that the lignin recovery process involving lignin dissolution in NaOH and lignin acidic precipitation has little influence in the extraction of lignin from the biomass. Additionally, it emphasizes the effectiveness of the ionic liquid assisted mechano-chemical process.

The following regression model was developed based on the influence of residence time and solid loading (based on coded units) on the yield of the extracted lignin from processed samples:

$$Y = 24.60 + 5.50S + 3.35T + 3.15ST$$

Where, *Y* is lignin extraction yield, *S* is solid loading, and *T* is residence time. The model had an adjusted R^2 value of 96.63%, indicating good fitting. The ANOVA table is presented in **Table A1** in **Appendix A**. From the table, the variance was measured to be 1.17 (or a standard deviation of 1.08%). The p-values of the main effects (*S* and *T*), as well as their interaction (*ST*) in the ANOVA table, were 0.014 and 0.028, respectively. With a set significance level (α) of 0.05, these p-values indicated that the main effects and their interaction were all considered significant (p-values ≤ 0.05). This was further confirmed by the Pareto chart and p-values of the various sources of variance shown in **Figure 3.3d**. Therefore, the effect of solid loading amount, processing time, and their combination are all considered significant in this process. Lastly, curvature on the ANOVA table was not significant (0.607 > 0.05), confirming that, based on the center points, there was not enough evidence to conclude that any of the studied factors having a curved relationship with lignin extraction yield.

Based on **Figure 3.3 (c & d)**, it was observed that an increase in solid loading and residence time were both associated with an increase in lignin extraction yield. Comparing the standardized effects of the various factors, the solid loading amount had a significantly higher positive influence on lignin extraction yield. The large effect of solid loading is attributed to an increase in shear due to a lack of lubrication provided by BmimCl. This behavior is similar to observations made with lignocellulosic biomasses pre-treated with high moisture content and no other solvents. When solvents are not used, a high solid to liquid ratio is preferred to increase the friction in the system [24]. According to other studies, ionic liquid processing with high biomass loadings has been proposed to act as an additive rather than a solvent [28,143].

At 50% solid loading, the effect of residence time was evident. The extraction yield of 50W-45m is significantly larger than 50W-10m. This observation indicated that a longer residence time is

beneficial for lignocellulosic biomass pre-treatment. However, the effect of residence time at low solid loadings is not as apparent due to the lack of shear. An increase in shear can result in greater disruption of the lignocellulosic biomass and lead to an overall decrease in recalcitrance. As aforementioned, ionic liquids act as a solvent at low biomass loadings, so it is likely that the residence times tested in this study are insufficient for the complete dissolution of the lignocellulose. Comparatively, in the study performed by Sun et al., a minimum of 16 h was required in order to solubilize a majority of wood biomass in an ionic liquid [81].

Furthermore, the heat generated by the increase in shear during the processing of the samples with high solid loading led to a higher temperature inside the batch mixer. While the set temperature of the batch mixer was 150 °C, the temperature inside the mixer reached a maximum of about 180 °C when 50W-45m was processed (**Figure 3.2a**). This increase in processing temperature also contributed to the greater lignin extraction yields. It is well known that higher temperatures improve the ionic liquid pre-treatment process but can also degrade lignocellulose [24,81,132]. To confirm that no thermal degradation would occur at 180 °C, a preliminary isothermal TGA was performed to test the thermal stability of MHF, kraft lignin, and lignosulfonate. After an isothermal step at 110 °C for 10 min to remove moisture and another isothermal step at 180 °C for 45 min, the TGA plot for all tested samples plateaued had a weight loss of less than 5 wt.%, indicating negligible thermal degradation.

The effectiveness of lignin extraction in this study is comparable to other ionic liquid processing methods. For ionic liquid processing of biomass performed on a lab-scale, often high amounts of ionic liquid and long processing times are required. Fort et al. were able to extract 20% of lignin from oak, a hardwood, after soaking 5 wt.% of solids in a BmimCl and DMSO-d_6 mixture in 1:3 ratio for 24 h at 100 °C [55]. In another investigation, Lee et al. was able to obtain a delignification

of 32 wt.% after incubating maple hardwood flour with BmimCl at 80 °C and 1 wt.% solid in a nitrogen atmosphere for 24 h and following with alkaline dilution [144]. For a shorter processing period and significantly less amount of ionic liquid, improved delignification was achieved in this study.

A few ionic liquid processing studies have also been performed recently using mechano-chemical processes for the purpose of increasing solid loading. However, the processing and analysis of hardwood materials is lacking. As previously highlighted, a study performed by Da Silva et al. involved the continuous processing of sugarcane bagasse with EmimAc [28]. They achieved a maximum delignification of 18.1% at 140 °C, 11.1 wt.% solids, and one extrusion pass. At 50 wt.% solids, the delignification was significantly lower at 4.8% even after three extrusion passes (approx. 12 min residence time). Compared to the sample of 50W-10min, which had a lignin extraction yield of 23.6%, their achieved degree of delignification is reduced. In another investigation involving the same ionic liquid and biomass, Silveira et al. were able to remove 41% of lignin using a reactor and supercritical carbon dioxide after processing for 2 h at 180 °C, 50 wt.% solids, and 250 bar [133].

Additionally, higher lignin extraction yields from municipal solid wastes have been achieved in a reactor vessel by Liang et al. [134]. Their study was able to solubilize 99% of the lignin from a corn stover and non-recyclable paper blend at 10 wt.% solid loadings using BmimCl. However, this achievement was due to an intensive acidolysis process following ionic liquid processing. Compared to other mechano-chemical processes involving ionic liquids, the lignin extraction yield obtained in this study is high considering the greater solid loading, shorter processing time, and overall simpler process scheme.

3.3.4 Characterization of Extracted Lignin

FTIR was performed to characterize the extracted lignin, as shown in **Figure 3.4**. The FTIR spectrum for all extracted lignin samples was identical. Lignin characteristic bands were found at 3438 cm^{-1} (OH stretching), 2925 cm^{-1} (CH_3 stretching), 2852 cm^{-1} (CH_2 stretching), 1592/1506 cm^{-1} (C=C stretching vibration) and 1269/1227 cm^{-1} (guaiacy/syringyl ring and C-O stretching vibration) [81,145]. The FTIR spectra also showed evidence of BmimCl residue remaining with the extracted lignin, indicating that the current downstream process needs improvement. Some BmimCl characteristic bands at 3438 cm^{-1} (quaternary amine salt formation with chlorine), 3088 cm^{-1} (hydrogen bond between Cl and hydrogen on C2), 1571/1465/1169 cm^{-1} (symmetric ring stretch) are evident [146–148].

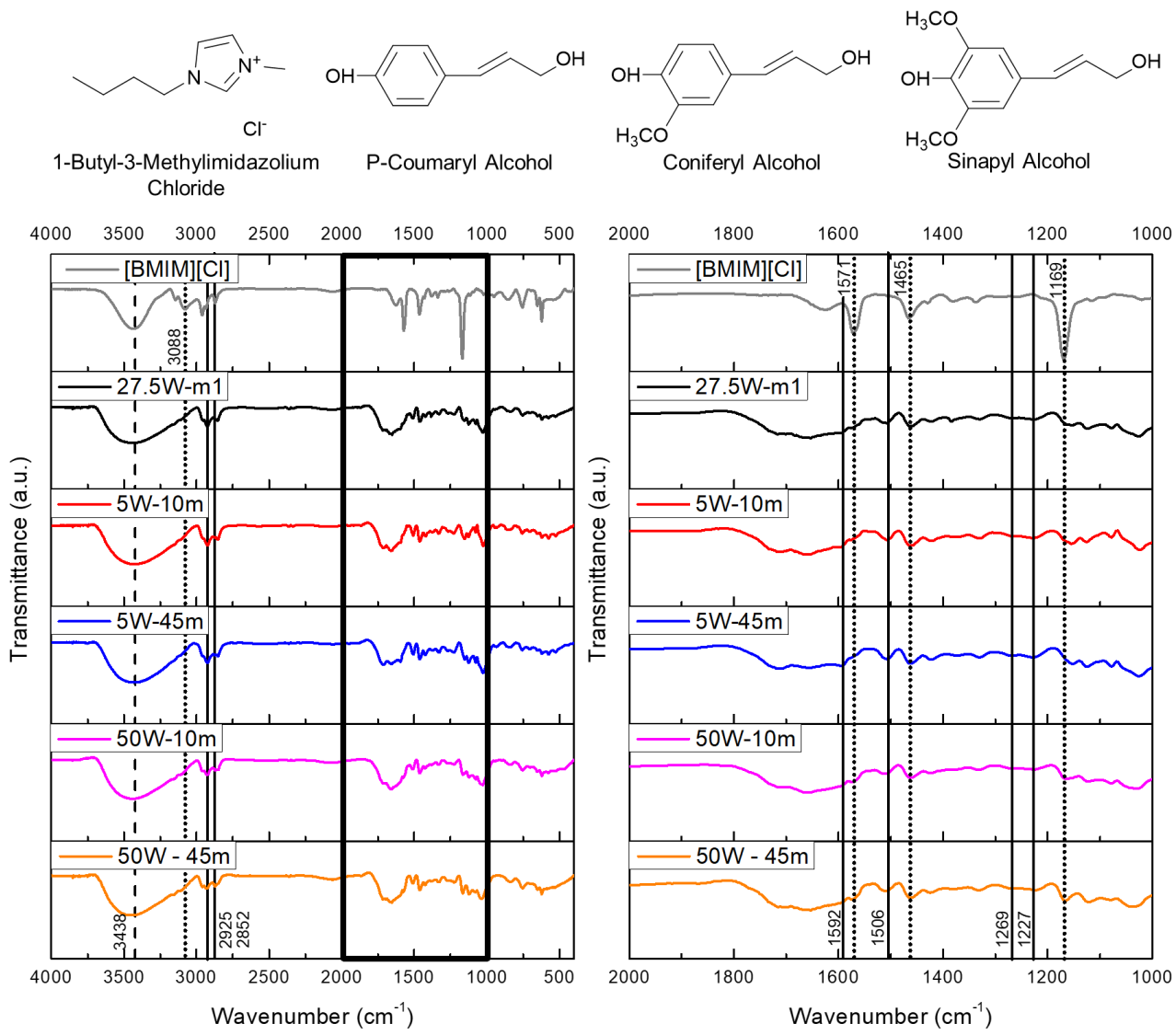

Figure 3.4. FTIR spectrum of ionic liquid and extracted lignin from the processing process. Left is the total spectra and right is the highlighted section of the same spectra. Solid, dotted, and dashed marker lines indicate key features of lignin, ionic liquid, and both, respectively. The chemical structures of BmimCl and the three main lignin precursors are also displayed.

The FTIR and ^{13}C-NMR spectra of wood and commercial lignin are displayed in **Figure 3.5**. Comparing the FTIR spectra of extracted lignin to commercial lignin, the lignin characteristic bands of the extracted lignin samples are not as prominent and sharp, possibly due to noise from

BmimCl residue. **Figure 3.5a** highlights the characteristic bands of cellulose and hemicellulose at 3438 cm^{-1} (OH stretching), 2925 cm^{-1} (CH_3 stretching), 2852 cm^{-1} (CH_2 stretching), 1160 cm^{-1} (C-O-C anti-symmetric bridge stretching vibration), 1110 cm^{-1} (O-H association band), and 1055 cm^{-1} (C-O stretching vibration), the last three of which are not as prominent in the extracted lignin compared to wood [145,149]. Thus, it can be concluded that the extracted samples from MHF were indeed lignin with some ionic liquid residue.

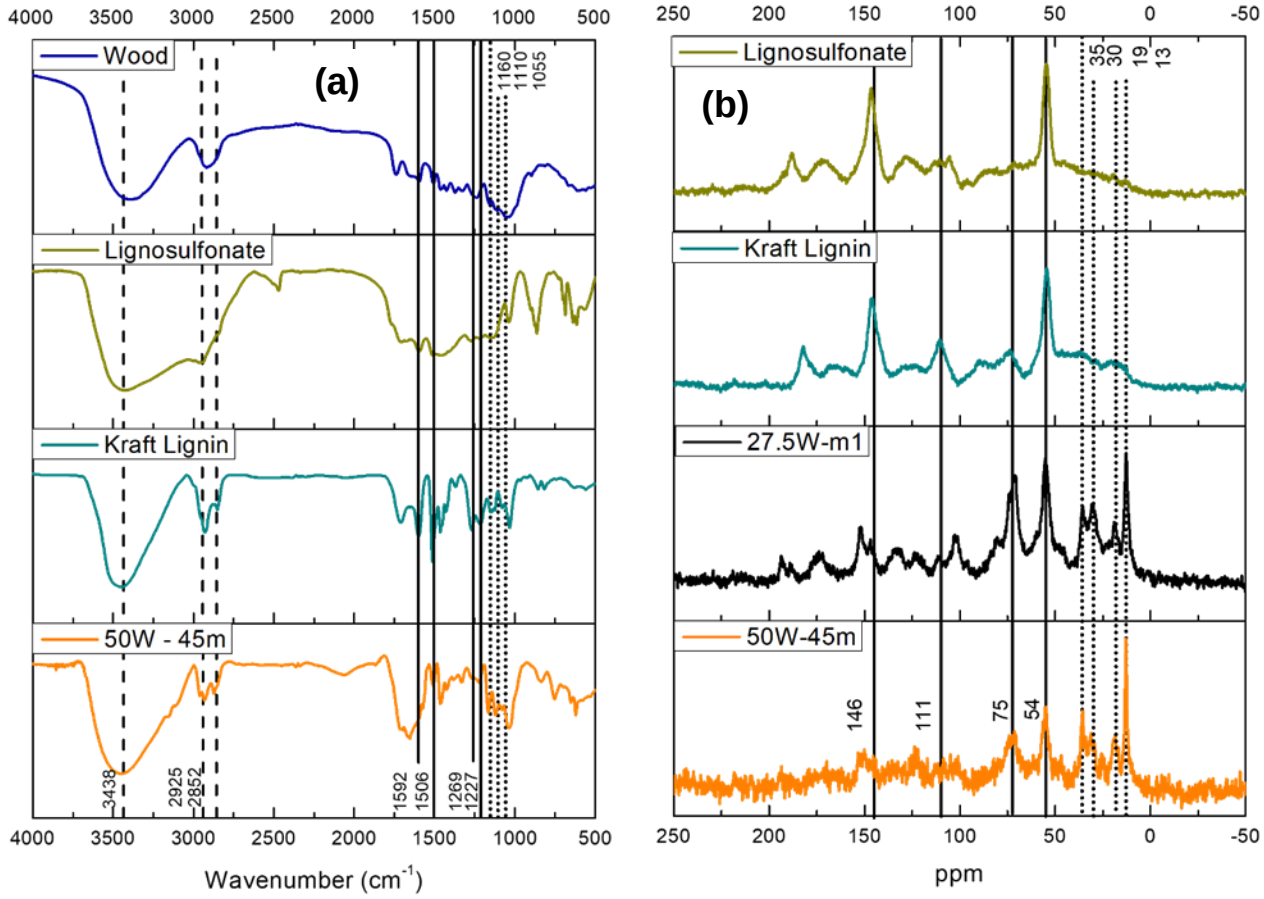

Figure 3.5. (a) FTIR spectra of wood, commercial lignosulfonate, kraft lignin, and extracted lignin. Solid, dotted, and dashed marker lines are characteristic bands related to lignin, cellulose/hemicellulose, and both, respectively; (b) ^{13}C-NMR spectra of extracted lignin compared

with commercially available lignosulfonate and kraft lignin. Solid and dotted lines are peaks related to lignin and BmimCl, respectively.

A similar observation was determined using UV-vis and ^{13}C-NMR. **Figure 3.6a** illustrates that the UV-vis spectra of the extracted lignin were the same as the spectra of kraft lignin and lignosulfonate. All three samples exhibited the main spectral features of lignin. Lignin has absorption bands in three main regions, which correspond to guaiacyl: a sharp peak at 200-208 nm, a shoulder at 227-233 nm, and a maximum at 268-287 nm [150]. Syringyl bands fall in between the second and third bands and can only be identified more precisely using second derivative analysis [150].

The ^{13}C-NMR spectra of the extracted lignin samples were also compared to commercial kraft lignin and lignosulfonate in **Figure 3.5b**. It was noted that the ^{13}C-NMR spectra of the extracted lignin samples (50W-45m and 27.5-m1) had a lot of noise compared to that of the commercial samples. This behavior was attributed to the residual ionic liquid present in the extracted lignin samples, which were also observed during FTIR analysis. Furthermore, the peaks at 13, 19, 30, and 35 ppm, present in both 50W-45m and 27.5W-m1, directly correlate to BmimCl [147,151]. These peaks were not detected in kraft lignin and lignosulfonate.

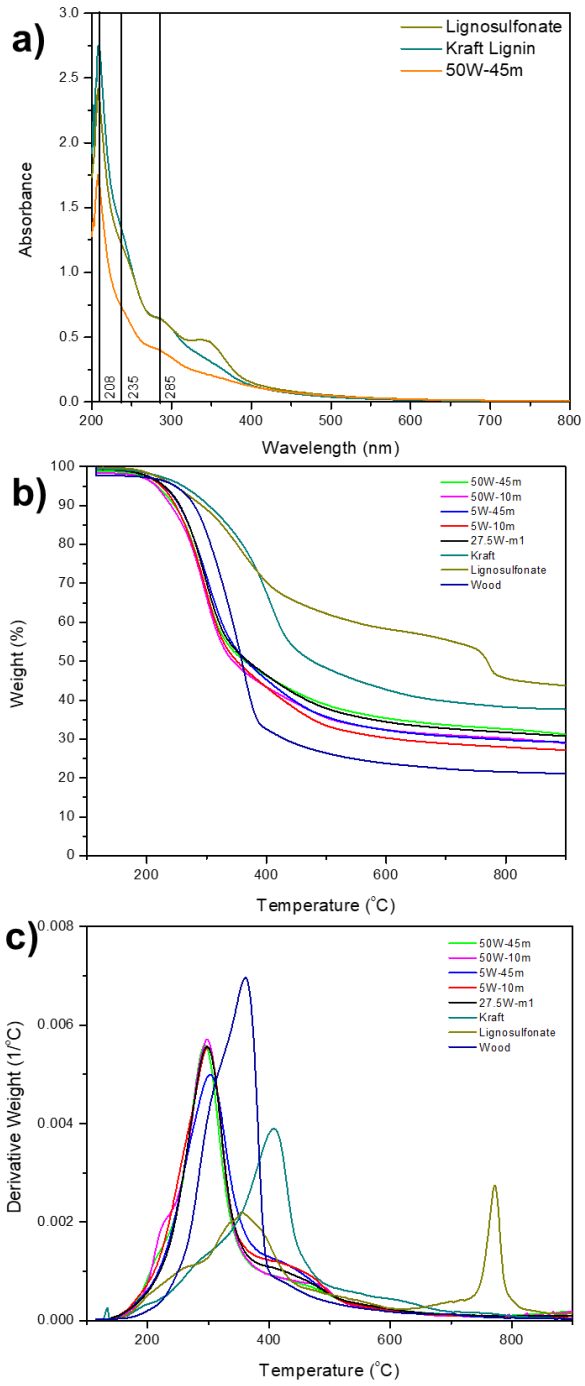

Figure 3.6. UV-vis spectra of extracted lignin compared to commercial kraft lignin and lignosulfonate. Solid lines are characteristic features of lignin; (b) TGA and (c) DTG plots.

Looking more closely at the lignin peaks in the ^{13}C-NMR spectra, characteristic peaks can be found at 54, 75, 111, and 146 ppm [152–155]. The peak at 111 ppm corresponds to syringyl functional groups

in lignin, more commonly found in hardwoods [153]. Both commercial lignin samples studied had strong peaks at 146 and 54 ppm, which relates to C3/C4 guaiacyl non-etherified and methoxy groups, respectively [152–155]. While methoxy groups were strongly present in the extracted lignin samples as well, C3/C4 guaiacyl non-etherified was not as prominent. Furthermore, 50W-45m and 27.5-m1 had significant peaks at 75 ppm, which relates to Cα in the β-O-4 linkage [155,156]. This indicates that the *β-O-4* linkage, a common linkage in lignin that is often attacked and cleaved during most lignin extraction processes, was not cleaved during the mechano-chemical and extraction process employed in this study [157]. This observation may also explain the absence of C3/C4 guaiacyl non-etherified in the extracted lignin compared to the commercial lignin samples. The presence of *β-O-4* may be attributed to two reasons: (1) BmimCl did not chemically associate with lignin, supporting the fact that the ionic liquid did not act as a solvent due to the implementation of high MHF loadings. (2) The processing conditions, specifically temperature and residence time, were subdued enough that depolymerization was not very significant. Correspondingly, the presence of *β-O-4* strongly suggests that the extracted lignin has high molecular weight in this process.

A similar conclusion was made when evaluating the zeta potentials of the extracted lignin. The zeta potentials of extracted lignin (50W-45m), kraft lignin, and lignosulfonate were measured to be -23.4 ± 0.30 mV, -42.2 ± 1.10 mV, and -34.1 ± 0.90 mV, respectively. The zeta potentials for all lignin samples were negative due to acidic functional groups in lignin which are negatively charged in alkaline solutions [158,159]. Comparing the three samples, the zeta potential for the extracted lignin were more neutral compared to Kraft lignin and lignosulfonate. The differences in charge are explained by the varying amounts of acidic groups in the lignin samples. In particular, the thiol and sulfonate groups that are introduced in lignin extraction processes can contribute to

the negative charges of Kraft lignin and lignosulfonate, respectively. The acidic phenolic hydroxyl and carboxyl functional groups also partakes in the zeta potential measurement [158]. As such, the obtained zeta potentials indicated that the extracted lignin had less acidic functional group contents than kraft lignin and lignosulfonate. Generally, phenolic hydroxyl and carboxyl content also decreases with increasing lignin molecular weight [158,160]. Therefore, as previously suggested, the more neutrally charged extracted lignin in this study is likely to be of higher molecular weight.

In addition to the extracted lignin's chemical structure analysis, its thermal stability was compared to commercially available kraft lignin and lignosulfonate through TGA, as shown in **Figure 3.6 (b & c)**. Interestingly, there is little difference in the thermal stability between the extracted lignin samples in this study. The influence of MHF loading and processing time on thermal behavior was not evident. However, the extracted lignin obtained from ionic liquid mediated mechano-chemical processing had significantly lower thermal stability than kraft lignin and lignosulfonate. Looking at the derivative weight loss curve, the main degradation moment for the extracted lignin appears as a sharp peak at about 300 °C with a shoulder on the right starting at 400 °C. Kraft lignin and lignosulfonate have a degradation maximum at 400 °C and 350 °C, respectively. Lignosulfonate also has a second degradation peak at 770 °C because of the degradation of sodium carbonate, which was formed due to the presence of organically bonded sodium cations that are chemically introduced in the lignosulfonate production process [161].

The lower thermal stability of the extracted lignin from the mechano-chemical process may be inherent to the lignin extraction process itself. The thermal behavior of the extracted lignin from MHF was comparable to the lignin extracted from sugarcane bagasse by Tan et al. that used a similar alkaline extraction process [162]. In their study, the extracted lignin began to decompose at 200 °C and had degradation peaks at 290 °C and 370 °C. Furthermore, the weaker thermal behavior

of the extracted lignin has also been proposed to be a result of lower molecular weight distribution [163–165]. However, the ^{13}C-NMR and zeta potential results challenge this assumption due to the heavy presence of the *β-O-4* linkage and lower amounts of phenolic hydroxyl and carboxyl content. Thus, it is difficult to conclusively determine that a lower molecular weight distribution was the cause for the observed lower thermal stability.

3.4 Conclusion

This study investigated lignin extraction from MHF using mechano-chemical processing and ionic liquid at high solid loadings. In terms of rheological performance, MHF and BmimCl mixtures displayed solid-like behavior and high viscosity at elevated solid loadings, which must be considered when working with biomass and ionic liquid processing. Additionally, lignin extraction yield was strongly dependent on solid loading amount due to these higher amounts of shear present at higher loadings. A maximum lignin extraction yield of 36.6% was obtained at 50% solid loading and a residence time of 45 min. The extracted samples were characterized as lignin with some remaining BmimCl residue using FTIR, UV-vis, and ^{13}C-NMR. Future improvements can be made to the current post-processing procedure to collect higher purity lignin.

Chapter 4: Green Thermo-Mechano-hemical Deconstruction of Cellulose Fibers for Cellulose Nanocrystal Production by Reactive Processing

4.1 Introduction

The consumer desire for green products has resulted in a market in which bio-renewable materials are valuable. Cellulose is the foremost biomass in this initiative as it is widely available, renewable, and essentially inexhaustible [166]. Cellulose is present in biomasses such as hardwoods, softwoods, sugarcane bagasse, and wood/forest residues. The natural abundance of cellulose has been capitalized on in various areas of engineering applications, including the production of sustainable nanomaterials.

For instance, nanocrystalline cellulose (NCC) is derived from cellulose for application as an emulsion stabilizer [167–170], a filler for polymers and rubber [171–173], a template for functional materials [167,174,175], and use in functional hybrids with organic and inorganic materials [2,167,176]. Nanocrystalline cellulose is nano-structured cellulose that is inherently crystalline. It is typically categorized as cellulose nanocrystals (CNCs), cellulose nanofibers (CNFs), cellulose nanowhiskers (CNWs), or bacterial nanocellulose (BNC), based on its geometrical shape or method of production [176]. These NCCs can be produced from various biomasses, such as soybean hulls [107,108], corncob [168], wood pulp [177,178], etc., or more directly from cellulose and cellulosic products (microcrystalline cellulose or MCC [179,180], cotton linter [181], filter paper [182], etc.). The most common process for producing most types of NCC is acid hydrolysis with sulfuric or hydrochloric acid [12,14,176]. During hydrolysis, the glycosidic bonds in the amorphous fraction of cellulose are

easily accessible and cleaved. This allows the removal of the amorphous regions of cellulose, leaving only the more crystalline and nano-structured regions.

CNCs are among the most extensively studied and utilized sustainable nanomaterials. The three critical properties of CNCs are colloidal stability, nanoscale dimensions, and high crystallinity index, all of which are necessary for its appeal in various applications [12]. While acid hydrolysis can achieve these properties, mineral acids are not environmentally safe and introduce a lot of industrial safety hazards. Sulfuric acid-based processes are also moderate in CNC yield (30-50%), and due to the presence of sulfate groups, the generated CNCs display poor thermal stability and are challenging to functionalize [183]. Recent studies in the production of CNCs entail the application of aqueous and solid organic acids, which are weaker compared to mineral acids [12]. Explored organic acid solvents include oxalic acid [182,183], maleic acid [183–185], p-toluenesulfonic acid [183], and formic acid [186]. Due to the volatility of aqueous acids and associated safety concerns, solid organic acids, such as oxalic acid dihydrate (OA) [187,188] and maleic anhydride [189], can be appealing for CNC production. Particularly, OA has gained considerable interest as it is biodegradable, non-volatile, inexpensive, and can be produced industrially from biomasses [187].

Ionic liquids are other green solvents that have been explored to produce CNCs. Ionic liquids consist of a small inorganic anion paired with a longer organic cation, known to be easily melted (T_m < 100 °C), and are non-volatile and thermally stable [131]**.** Albeit expensive, ionic liquids can be recovered from aqueous solutions and reused [75,190–192]. Some studies have determined that ionic liquid may be toxic to organisms in soil and aquatic environments [77,78]. However, its non-volatile nature allows for easy monitoring and control of its lifecycle, so accidental discharge can be prevented. When pursued for CNC production, the most commonly studied ionic liquid is 1-butyl-3-methylimidazolium chloride (BmimCl) [179,193]. Unlike acids, ionic liquids do not stimulate

hydrolytic phenomena and can only solubilize cellulose if given enough time [193]. Therefore, ionic liquids are typically used to pre-swell cellulose fibers prior to hydrolysis as a means to increase their accessibility [179,193].

A couple of groups has investigated the combination of swelling with ionic liquids and acid hydrolysis. Fu et al. swelled MCC with BmimCl and subsequently hydrolyzed the fibers with oxalic acid [179]. In another study by Lazko et al., swelling with BmimCl was followed by hydrolysis with dilute sulfuric acid [193]. In both analyses, two steps were performed sequentially. In the latter study, the authors had determined that the simultaneous processing of cotton cellulose with both an ionic liquid and an acid was not efficient. They proposed that the ionic liquid activity was inhibited by the presence of an acid, resulting in no fiber swelling and heterogeneous acid hydrolysis [193]. The improved effectiveness of a two-step process clearly emphasizes ionic liquid's role in increasing fiber accessibility. While the arrangement of ionic liquid and acid was successful, high amounts of both ionic liquid (approx. 90-98 wt.% for swelling) [179,193] and organic acid (approx. 65 wt.%) [179] were needed, and the processing time was long (3-11 h) [179,193].

To resolve these issues, one approach is to implement intense shear processes, such as extrusion or batch mixing. These operations are capable of processing high solid contents at high shear rates, improving accessibility to the cellulose matrix through homogenous mixing and mechanical defibrillation [64,106]. Extrusion of biomasses to produce CNCs has been previously performed as a purely mechanical process [106], but it has also been combined with solvents [107–109,113] or enzymes [113–116] more recently. In these highlighted studies, solid loading ranged from 15-70 wt.%, and 1-14 extruder passes were performed at a screw speed of 100-400 rpm.

The aim of this study was to explore a reactive batch mixing as a one-pot process for CNC production that can save both time and materials. A reactive batch mixer was employed to facilitate

the simultaneous hydrolysis and defibrillation of cellulose using BmimCl and OA. In this study, BmimCl was used as a lubricant/plasticizer and acid carrier – to avoid over-torquing due to high solid contents while also enabling the sorption of OA into the cellulose matrix. The influence of OA loading and processing time on CNC yield was explored. Additionally, the three critical qualities of the produced CNCs (size, stability, and crystallinity) were thoroughly investigated and benchmarked against a commercial CNC product.

4.2 Materials and Method

4.2.1 Materials

Cellulose (Arbocel BE 600-10 TG, avg. fiber length = 18 μm, avg. fiber thickness = 15 μm) was supplied by Rettenmaier Canada Inc. (Markham, Ontario, Canada). The ionic liquid, 1-butyl-3-methlimidazolium chloride (BmimCl) (T_m = 73 °C, stored in a desiccator), was sourced from Hangzhou Sartort Biopharma Co., Ltd (Zhejiang, China). Oxalic acid dihydrate (OA) (T_m = 104-106 °C, T_b = 149-160 °C) was purchased from Sigma-Aldrich. Commercial CNC (CelluForce NCV 100, 4.8 wt.% suspension) was obtained from CelluForce (Montreal, Quebec, Canada). The commercial CNC suspension was diluted to 0.2 wt.% and used as a benchmark for the CNC produced in this study.

4.2.2 Methods

4.2.2.1 Cellulose Nanocrystal (CNC) Preparation

Batch Mixer Processing of Cellulose with an Ionic Liquid and Organic Acid

The reactive batch mixer process with cellulose and subsequent CNC preparation method are summarized in **Figure 4.1**. Prior to processing cellulose, a masterbatch of BmimCl and OA was

produced in 1:1 (w/w) ratio. BmimCl was melted in an oven at 80 °C and an equal amount of OA was added to the solution. The mixture was agitated with a magnetic stirrer for 5 min at 100 °C on a hotplate to ensure that BmimCl remained liquid. As briefly mentioned, in this study, the main role of BmimCl is to act as a plasticizer for processing purposes and as a carrier for OA. Without the ionic liquid, the torque constraints of the batch mixer are surpassed due to heavy solid loading and the resulting amount of shear generated.

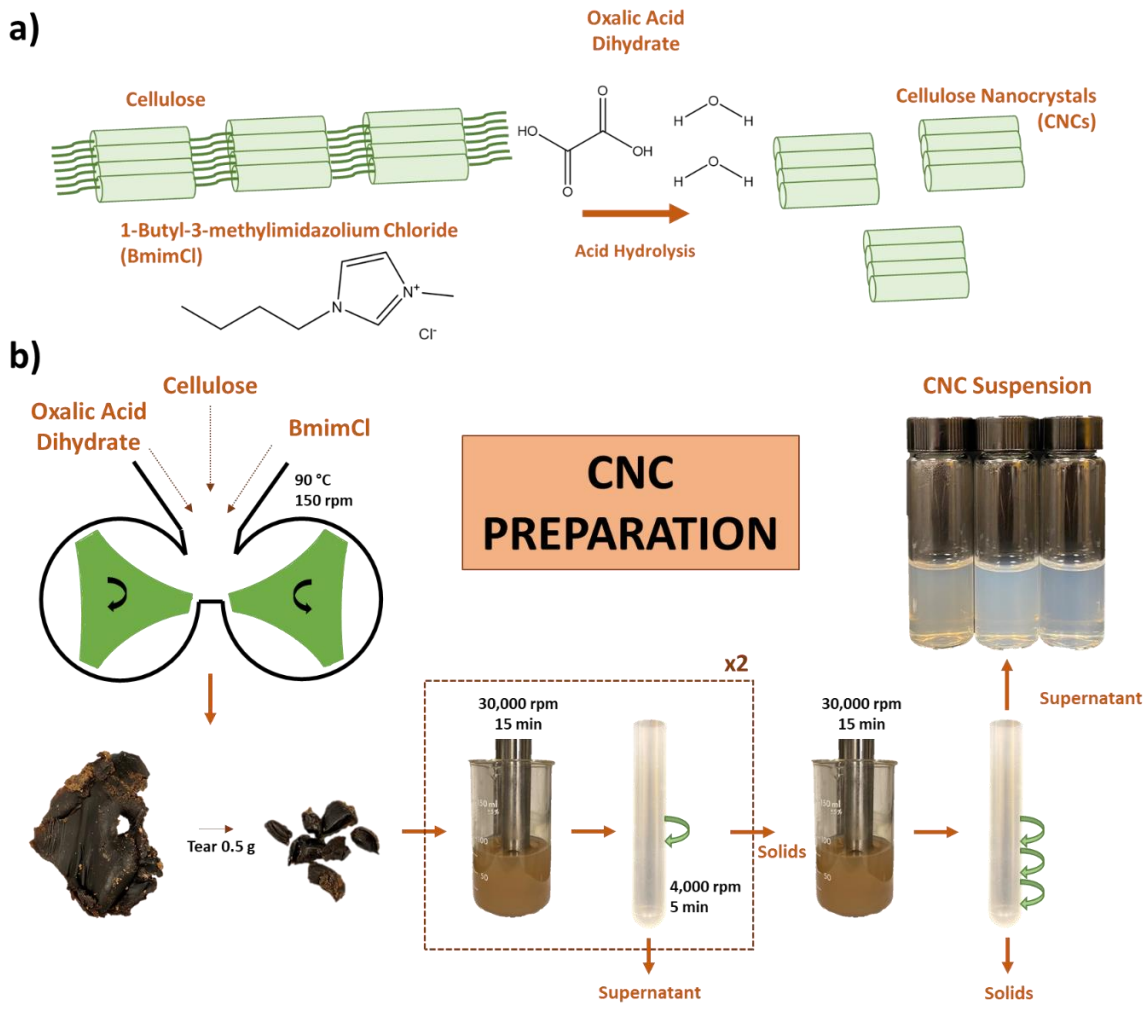

Figure 4.1. (a) Reaction and (b) batch mixer process scheme for the preparation of cellulose nanocrystals (CNCs) from cellulose using 1-butyl-3-methylimidazolium chloride (BmimCl) and oxalic acid dihydrate (OA).

To process cellulose in the reactive batch mixer, 150 g of cellulose was first mixed with the masterbatch based on OA composition, in accordance with **Table 4.1**. Additional melted ionic liquid was added to reach the desired final composition. The mixture was then processed using a Thermo Scientific HAAKE Rheomix Polylab QC Lab Mixer equipped with roller blades. The batch mixer processing temperature and blade rotation speed was set at 90 °C and 150 rpm, respectively. The processing temperature was chosen based on the melting and boiling point of OA, while also considering the increase in actual temperature during processing due to generated shear. Rotation speed was determined based on the maximum speed capabilities of the batch mixer (maximum rotor speed of 200 rpm). After the desired residence time was reached (**Table 4.1**), the process was stopped, and the samples were air cooled and stored in polyethylene bags.

Table 4.1. Experimental processing conditions and their corresponding CNC yield.

Sample Name	Mixture Composition (Cellulose:BmimCl:OA, w/w/w)	Residence Time (min)	Final Torque (Nm)	CNC Yield (wt.%)
0.075-OA-5min	1:0.7:0.075	5	20.6	55.4
0.075-OA-2.5min	1:0.7:0.075	2.5	24.1	59.0
0.025-OA-5min	1:0.7:0.025	5	11.3	52.8
0.025-OA-2.5min	1:0.7:0.025	2.5	23.8	54.5
0.050-OA-3.75min-1	1:0.7:0.05	3.75	20.3	49.8
0.050-OA-3.75min-2	1:0.7:0.05	3.75	22.1	50.5
0.050-OA-3.75min-3	1:0.7:0.05	3.75	20.0	49.5

The experimental 2^2 factorial design is outlined in **Table 4.1**, with three center-points. In this study, OA composition and residence time were the two factors that were varied. OA's maximum and minimum ratio was 0.075 and 0.025, respectively, while the highest and lowest residence time values were 5 and 2.5 min, respectively. The maximum OA composition and residence time variables were determined from preliminary investigations in which higher OA compositions and longer residence times resulted in the severe degradation of cellulose. The minimum OA residence time was selected based on the minimum time required for torque to stabilize during processing. After cellulose processing, CNC yield was determined according to the procedure highlighted in the following section. Minitab14 was then used to perform the analysis of variance (ANOVA) of CNC yield.

Recovery of CNCs

To recover CNCs, the batch mixer processed cellulose was washed thrice to remove any remaining acid and ionic liquid, as described in **Table 4.1**. Briefly, 0.5 g of the processed cellulose was torn into small pieces and added to 72 mL of distilled water. The same water volume was maintained for all washing steps and was based on the volume capacity of the ultracentrifuge, which is used in the final wash. Next, the processed cellulose and distilled water mixture was homogenized using a PowerGen 700 homogenizer with a 10 mm diameter probe at a speed of 30,000 rpm for 15 min with one-minute breaks every five minutes. The homogenized samples were then centrifuged at 4,000 rpm for 5 min. Afterwards, the solid residue was collected and washed again in a similar manner. Finally, the cellulose residue after the second wash was homogenized with 72 mL of distilled water and the turbid mixture was centrifuged at 10,000 rpm for 15 min using an

ultracentrifuge (Beckman Coulter, Optima XPN-100). The supernatant with suspended CNCs and solid residue were collected separately, weighed, and stored in a refrigerator for further analysis.

4.2.2.2 CNC yield determination

The yield of CNCs generated from the process was determined by conducting simple mass balance calculations. For this, the percentage of CNCs in the supernatant of the ultracentrifuged samples was determined using a Sartorius moisture analyzer. 10 g of the CNC suspension was analyzed in the moisture analyzer at a temperature of 105 °C. Three solids percentage measurements were taken and averaged. CNC yield was then calculated using **Eq. (4.1)**:

$$\boldsymbol{Percentage\ CNC\ Yield} = \frac{\boldsymbol{m_s \times \bar{S}}}{\boldsymbol{m_{PC} \times C}} \times \mathbf{100} \qquad (\mathbf{4.1})$$

where m_S is the total mass of the CNC suspension, $\bar{S}$ is the average mass fraction of solids in the CNC suspension, m_{PC} is the mass of processed cellulose (0.5 g), and C is the mass fraction of cellulose in the processed cellulose (0.563, 0.571, or 0.580 – corresponding to 0.075-OA, 0.050-OA, and 0.025-OA, respectively). These mass fractions were calculated based on the fraction of cellulose in the compositional weight ratios presented in **Table 4.1**.

4.2.2.3 Characterization

Fourier transform infrared (FTIR) spectroscopy

Chemical structure analysis of unprocessed cellulose, the produced CNC, and commercial CNC (obtained from CelluForce) was performed using Fourier transform infrared (FTIR) spectroscopy. The produced CNC and CelluForce CNC were dried using a Sartorius moisture analyzer. Approximately 2 mg of each dried sample were collected and ground with 200 mg of dried potassium bromide (KBr) powder and solid pellets were produced. For the analysis, a Thermo

Scientific Nicolet FTIR spectrometer was used in transmittance mode at a resolution of 4 cm^{-1}. The scan was performed between 400-4000 cm^{-1} for 64 scans. A pure KBr pellet was used as background.

X-ray photoelectron spectroscopy (XPS)

X-ray photoelectron spectroscopy (XPS) analysis was carried out to investigate the surface chemistry of the cellulosic materials. A Thermo-VG Scientific ESCALab Microprobe system equipped with a hemispherical analyzer and a monochromatic Al Kα X-ray source was used for measurements. For analysis, CNC suspensions were dried in an oven at 80 °C overnight and ground to produce powdered CNCs. Additionally, CasaXPS was used to determine atomic compositions of the analyzed samples.

Polarized optical microscopy (POM)

Polarized optical microscopy (POM) was used to observe the physical structure of dried CNC and cellulose. An Olympus BX53 microscope with a SC100 color camera and U-TV-0.5XC-3 camera adaptor was used for imaging. Aliquots of dispersed cellulose, produced CNC, and CelluForce CNC were taken and dried on top of a glass slide at 80 °C. All samples were analyzed at a magnification of 20x.

Scanning electron microscopy (SEM)

Scanning electron microscopy (SEM) was performed using a field emission SEM (Quanta FEG-SEM 250, Oxford Instrument) at an accelerating voltage of 20 kV. SEM was performed to closely examine the structure and size of unprocessed cellulose. For sample preparation, an aliquot of dispersed cellulose in distilled water was air-dried on top of carbon tape and sputter coated with gold.

Atomic force microscopy (AFM)

To investigate the structure and size of the produced and CelluForce CNC particles, atomic force microscopy (AFM) was used. An aliquot of the CNC suspensions was placed on a clean glass slide and left to air-dry. The samples were then analyzed using a Veeco Dimension 3100 AFM with a NanoScope IV controller. Images were taken at a size of 1.00 x 1.00 μm^2 and using a scan rate of 0.5 Hz.

Dynamic light scattering (DLS)

Dynamic light scattering (DLS) was employed to determine the particle size and zeta potential of unprocessed cellulose, produced CNC, and CelluForce CNC. DLS was performed using a Malvern Zetasizer Nano-ZS90 (Westborough, MA, United States). The produced CNC suspensions were investigated as is, while unprocessed cellulose was dispersed in water and the CelluForce CNC suspension was diluted with water. All samples were analyzed in the range of 0.2-0.3 wt.% solid loading. A polystyrene disposable cuvette was used for particle size measurements. Zeta potential analysis was performed at 25 °C using a folded capillary zeta potential cell (Zetasizer nano series, DTS 1070). Three zeta potential and particle size measurements were performed, and the average was reported. Suspension stability was also monitored by evaluating the particle size of cellulose and CNC suspensions one week after agitation.

X-ray powder diffraction (XRD)

The crystallinity of the produced CNC samples was compared to unprocessed cellulose and CelluForce CNC using x-ray powder diffraction (XRD). Sample preparation of CNC powder was similar to the preparation required for XPS analysis above. A Rigaku MiniFlex II Desktop x-ray diffractometer was used for analysis in the 2θ range of 5-50°, with a step size of 0.02°, and scan

speed of 1 s/step. XRD operation was performed at 30 kV and 15 mA. The background spectrum from the empty glass sample holder was subtracted from all sample spectra prior to the calculation of the crystallinity index (CrI). The CrI was then calculated using Segal's method:

$$\boldsymbol{CrI = \frac{I_{200} - I_{am}}{I_{200}}\, x\, 100} \qquad (\mathbf{4.2})$$

where I_{200} is the intensity of the global maximum peak corresponding to (200) lattice diffraction at 2θ = 22° and I_{am} is the intensity of the local minimum peak allocated to amorphous band diffraction at 2θ = 18° [194].

Thermogravimetric analysis (TGA)

The thermal stability of cellulose and CNC was also investigated using thermogravimetric analysis (TGA). Cellulose and dried CNC powder were analyzed from 25-600 °C with a ramping rate of 10 °C/min and under a nitrogen flow rate of 20 mL/min.

4.3 Results and Discussion

4.3.1 Thermo-Mechano-Chemical Processing of Cellulose in a Batch Mixer

To deconstruct cellulose, the fibers were processed with BmimCl and OA in a reactive batch mixer. The temperature and torque data from the processing of samples with varying compositions, outlined in **Table 4.1**, are presented in **Figure 4.2**. In this study, the temperature of the batch mixer was set at 90 °C and was measured to have increased during processing for all samples due to the introduction of shear from the cellulose loading. The shear rate in the midpoint of the inner and outer cylinders of the batch mixer was estimated using Bousmina's method [195]. Using a power-law index derived from a previous study by the authors involving the same ionic liquid and a biomass loading of 50 wt.%, the shear rate was calculated to be approx. 7665 s^{-1} [64]. Samples with 0.050-

OA and 0.075-OA reached a similar maximum temperature of approximately 150 °C, while samples with 0.025-OA had a maximum temperature of approximately 160 °C due to higher solid loading. Additionally, the recorded torque data revealed that two maximums were reached for all samples. The first maximum is attributed to the homogeneous blending of cellulose, BmimCl, and OA. The following global maximum is assigned to cellulose's subsequent deconstruction and defibrillation. It can also be seen that, at low OA contents (0.025), the deconstruction/defibrillation of cellulose peaks is delayed compared to the samples at high (0.0750) and center-point (0.05) levels.

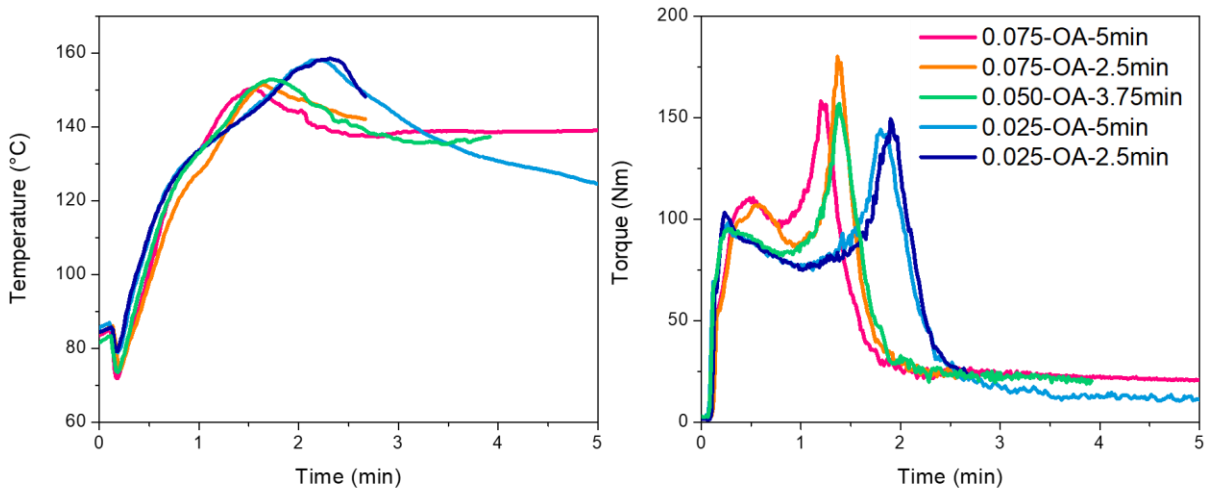

Figure 4.2. Temperature (left) and torque (right) data for the batch mixer during the processing of cellulose with BmimCl and OA.

4.3.2 Effect of Processing Variables CNC Yield

A CNC suspension was recovered following the reactive batch processing and downstream processing. The CNC yield for each experimental condition was determined according to **Eq. (4.1)** and is shown as a function of residence time and OA content in **Figure 4.3a**. The maximum CNC yield obtained in this study was 59.0% for the 0.075-OA-2.5 min sample, while the minimum CNC

yield was 49.5% for 0.050-OA-3.75min-3 sample. Notably, an increase in OA content results in an increase in CNC yield, indicating that higher acid concentrations facilitate cellulose deconstruction. Alternatively, an increase in processing time from 2.5 min to 5 min reduces CNC yield. Longer processing time may have led to the degradation of cellulose, which reduces CNC recovery.

Interestingly, all three center-points (0.050-OA-3.75 min) had minimum CNC yield. The expectation is that samples processed with 0.025-OA should have lower CNC yield compared to the midpoints due to lesser acid loadings. However, this was not the case. It is proposed that the higher measured processing temperatures of the 0.025-OA samples may have contributed to its increased performance compared to the midpoint samples. As previously highlighted, samples with 0.025-OA reached a maximum process generated temperature of approx. 160 °C compared to about 150 °C for the remaining samples. Therefore, there is a sensitive balance between OA composition, processing time, as well as measured processing temperature.

Table 4.2. ANOVA table for CNC yield.

Source	DF	Seq. SS	Adj. SS	Adj. MS	F	P ($\alpha = 0.05$)
Main Effects	2	19.6250	19.6250	9.8125	37.26	0.026
2-Way Interactions	1	0.9025	0.9025	0.9025	3.43	0.205
Curvature	1	51.7001	51.7001	51.7001	196.33	0.005
Residual Error	2	0.5267	0.5267	0.2633		
Pure Error	2	0.5267	0.5267	0.2633		
Total	6	72.7543				

The ANOVA table presented in Table 4.2 and the Pareto/P-values graph in **Figure 4.3b** further support this observation. Based on the ANOVA table, the variance was 0.26 (or a standard

deviation of 0.51 wt.%). A significance level (α) of 0.05 was set for this analysis. Both the main effects of OA composition (C) and processing time (T) are considered significant according to ANOVA (p-values ≤ 0.05). The interaction of the main effects (CT) is measured to be insignificant with a p-value of 0.205. Based on the Pareto graph of the standardized effects, C has a greater effect than T. From the three main factors, only C is positive, which indicates the positive impact of increased OA content on CNC yield, while the standardized effect of T is negative because of the detrimental effect of processing time on CNC yield through degradation. The interaction of C and T is also negative, as evidenced by the minimum yields generated by the center-points. As a result of this interaction, the curvature is considered significant with a p-value of 0.005. Thus, a sufficient linear regression model cannot be produced from the current data.

The CNC yields in this study are considerably higher compared to previous investigations with similar approaches. As previously highlighted, Fu et al. performed a parallel analysis, but in two steps, involving the swelling of cellulose with BmimCl and subsequent hydrolysis with the solvent form of OA at a concentration and loading of 70 wt.% and approx. 75 wt.%, respectively [179]. In that study, a maximum yield of 27.74% was obtained for a swelling operation at 45 °C for 2 h and a hydrolysis step at 90 °C for 7 h [179]. To the best of the authors' knowledge, no other previous study has combined BmimCl and oxalic acid, or its dihydrate form. However, in 2014, Lazko et al. did combine BmimCl and dilute sulfuric acid in a two-stage method like Fu et al. [193]. In their investigation, they could only attain an average CNC yield of 15 wt.% when the swelling was conducted with 98 wt.% BmimCl loading at 80 °C for 1-2 h and hydrolysis with 1-4 wt.% sulfuric acid for 2-16 h [193]. Comparatively, the achieved CNC yield in this study was considerably higher for a significantly shorter time and higher solid loadings, making it appealing for commercial deployment.

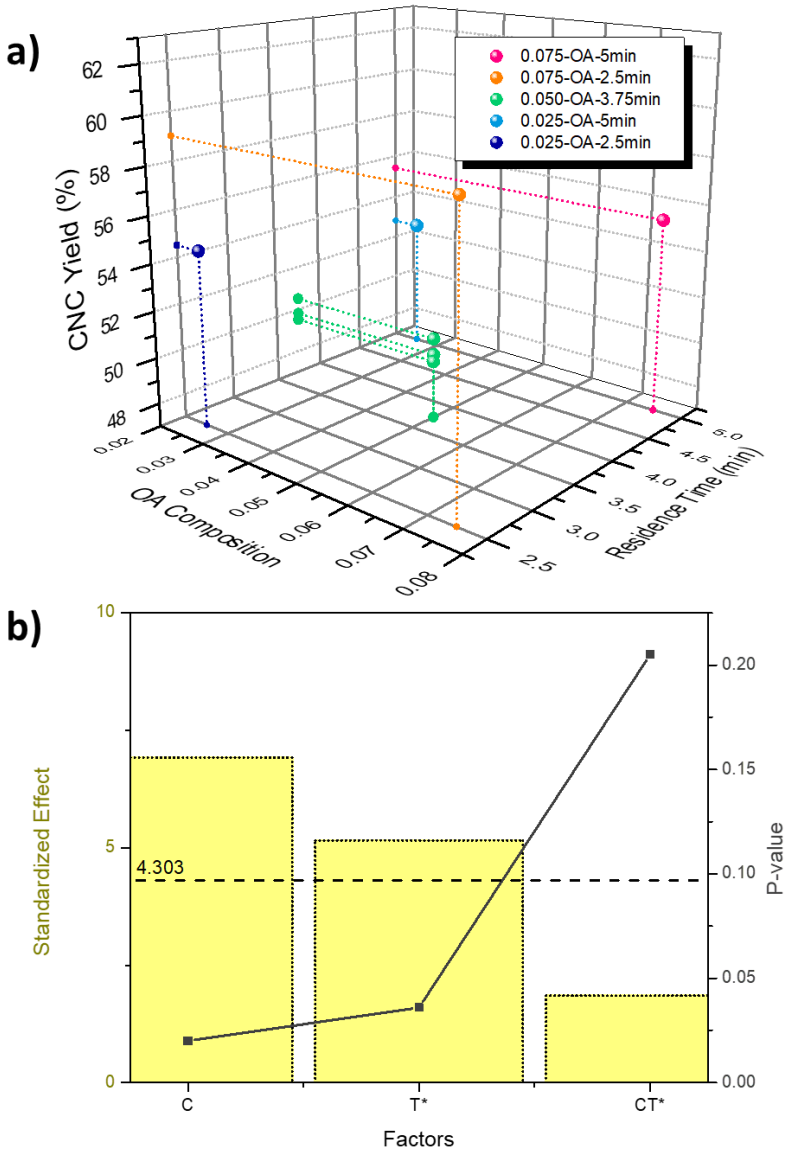

Figure 4.3. (a) A 3D plot of CNC yield against OA composition and residence time. (b) Pareto chart and p-values of the sources of variance with a confidence interval of 95%, represented by the dashed line. C is OA composition and T is residence time. *Negative standardized effect.

Molten OA has been previously studied independently for solvent-free CNC production. In a 2017 study by Li et al., dissolved softwood pulp was hydrolyzed with molten OA for 1 h at 110 °C to produce cellulose oxalate nanocrystals at a maximum yield of 80.6% [187]. Later, the same group

was able to achieve 94% yield after exploring various types of pulps and optimizing the production and washing process [188]. However, in both studies, the OA loading was high at approx. 80 wt.% and the processing time was long (1 h) [187,188]. OA has also been explored for application in its solvent form, oxalic acid. However, processing with only aqueous oxalic acid results in low yield since it is a weak acid. For example, the highest yield obtained by Chen et al. when processing bleached kraft eucalyptus pulp over a selection of organic acids (oxalic, maleic, and p-toulenesulfonic), with various acid concentration ranges (30-80 wt.%), hydrolysis temperatures (80-120 °C), and processing time (0.5-4 h) was only 25% [183].

The high CNC recovery efficiency achieved in this work can be attributed to a few factors. Firstly, a concentrated version of oxalic acid is directly used in the form of OA, which has 29 wt.% water of crystallization. The studies performed by Li and their group suggest that OA is more effective for the hydrolysis of cellulose than diluted oxalic acid in the range of 30-80 wt.%. Next, the homogeneous and shear intensive (approx. 150 Nm in torque and a shear rate of 7665 s^{-1}) mixing of the batch mixer process also promotes the defibrillation of cellulose and increases the accessibility of the amorphous sections of cellulose. And lastly, this occurrence is also enhanced by implementing BmimCl as a carrier for OA throughout the cellulose matrix and as a plasticizer for processing.

4.3.3 Characterization of CNC

4.3.3.1 Chemical Structure of CNC

The chemical structure of commercial CNC was compared with the CNC produced in this study and the unprocessed cellulose using FTIR (**Figure 4.4a)**. The FTIR spectra of 0.075-OA-2.5 min was used as a representative of the generated CNCs since all samples produced in this study displayed similar spectra. The spectra of 0.075-OA-2.5 min, unprocessed cellulose, and

CelluForce CNC were all comparable, with little difference. The bands at 3406 cm^{-1} (OH stretching), 2926 (CH_3 stretching), and 2893 cm^{-1} (CH_2 stretching) are characteristic of cellulosic materials [145,149]. In particular, cellulose has a range of distinct bands between wavenumbers of 1641 and 897 cm^{-1}, which are labelled in **Figure 4.4a** [145,149]. Commonly, CNC produced using oxalic acid dihydrate has a peak at 1739 cm^{-1}, corresponding to the stretching of C=O from the ester carbonyl groups [183,187,188]. This band is often used to characterize cellulose oxalate [187,188]. However, this characteristic band was not observed in the produced CNC samples of this study. The lack of this band is likely due to the significantly lesser amounts of OA (< 5 wt.%) employed in this study. Previous studies involving OA or oxalic acid used loadings from 80-90 wt.% [183,187,188]. The lower OA content resulted in no observed esterification of the CNCs in the FTIR spectra. Therefore, the FTIR spectra of the produced CNC in this study were very similar to the original, unprocessed cellulose from which it was derived.

Additionally, surface analysis of the cellulose and CNC samples was performed using XPS. The overall XPS spectra of the samples are shown in **Figure 4.4b**. The complete spectra revealed that oxygen (O 1s) and carbon (C 1s) are the most prominent elements in the chemical structure of the surface for all the samples. Peaks at binding energies of 164 eV and 399 eV, which respectively relate to S 2p and N 1s, were also monitored, but were not observed. Sulfur was monitored to identify any sulfate groups from the commercial processing of CelluForce CNC and cellulose. At the same time, nitrogen was surveyed to identify any residues from BmimCl. Presumably, both elements were not abundant enough to be measured, and their signals were encompassed in the background noise if present at all. Using CasaXPS, each sample's carbon and oxygen composition was determined and outlined in **Table 4.3**. The processing of native cellulose results in a slight rise in carbon to oxygen atomic ratios.

A closer examination of the C 1s curves also indicated an overlap (**Figure 4.4c)**. The C 1s curve is composed of four different peaks related to various bonding states of carbon. The peaks pertaining to C-C, C-O, C=O/O-C-O, and O-C=O are associated with binding energies of approx. 283.2 eV, 284.9 eV, 286.4 eV, and 288.8 eV, respectively. From initial inspection, some peaks for certain samples are missing or are significantly lesser than others. To clearly explore these differences, the C 1s curves for all samples were deconvoluted and some key samples are highlighted in **Figure 4.4 (d-f)**. Based on these deconvolutions, the concentration of each moiety of C 1s was determined using CasaXPS software in **Table 4.3**.

Table 4.3. XPS analysis of cellulose and CNC samples. Compositions obtained using CasaXPS.

	Sample Composition		**Composition of C 1s after Deconvolution**			
Sample Name	**O 1s (at.%)**	**C 1s (at.%)**	**C-C (at.%)**	**C-O (at.%)**	**C=O or O-C-O (at.%)**	**O-C=O (at.%)**
0.075-OA-2.5min	39.8	60.2	18.6	31.3	49.0	1.1
0.050-OA-3.75min	41.2	58.8	11.8	33.4	37.0	17.8
0.025-OA-5min	40.9	59.1	12.3	33.9	26.9	26.9
Cellulose	43.5	56.5	2.8	21.8	50.7	24.7
CelluForce	42.6	57.4	12.0	31.0	34.8	22.2

Comparison of the C 1s compositions of each sample reveals the effects of the implemented batch mixer process in this study. There are significant differences among the produced CNC samples

in the atomic concentrations of C=O/O-C-O and O-C=O. The CNC samples of 0.025-OA-5 min recorded a slightly higher carboxyl groups (O-C=O) than unprocessed cellulose, which may be due to possible esterification reactions of cellulose with OA. However, there is a considerable reduction in O-C=O associated with increasing OA content. The sample of 0.075-OA-2.5 min decreased by 95.6% in carboxyl groups compared to cellulose. The declines in O-C=O content of 0.075-OA-2.5 min and 0.050-OA-3.75 min were compensated by an increase in other carbon-based functional groups, especially C=O/O-C-O. These changes in composition have been formerly recognized as a result of surface degradation and the removal of low molecular weight oxidized/degraded products [196]. Increases in C-C and decreases in overall oxygen levels have previously been attributed to the possible degradation of cellulose as well [197]. Interestingly, for each produced sample, the number of C-C groups positively correlates with its respective CNC yield (Pearson's correlation coefficient = 0.97). This relationship implies that OA content and processing time also influence the degree of surface degradation in CNC to a similar extent as CNC yield. Conclusively, XPS analysis reveals the sensitive nature of the batch mixer process with BmimCl and OA in this study. Slight changes in OA content incite degradation of carboxyl groups and cause dramatic differences in the surface composition of the resulting CNC samples.

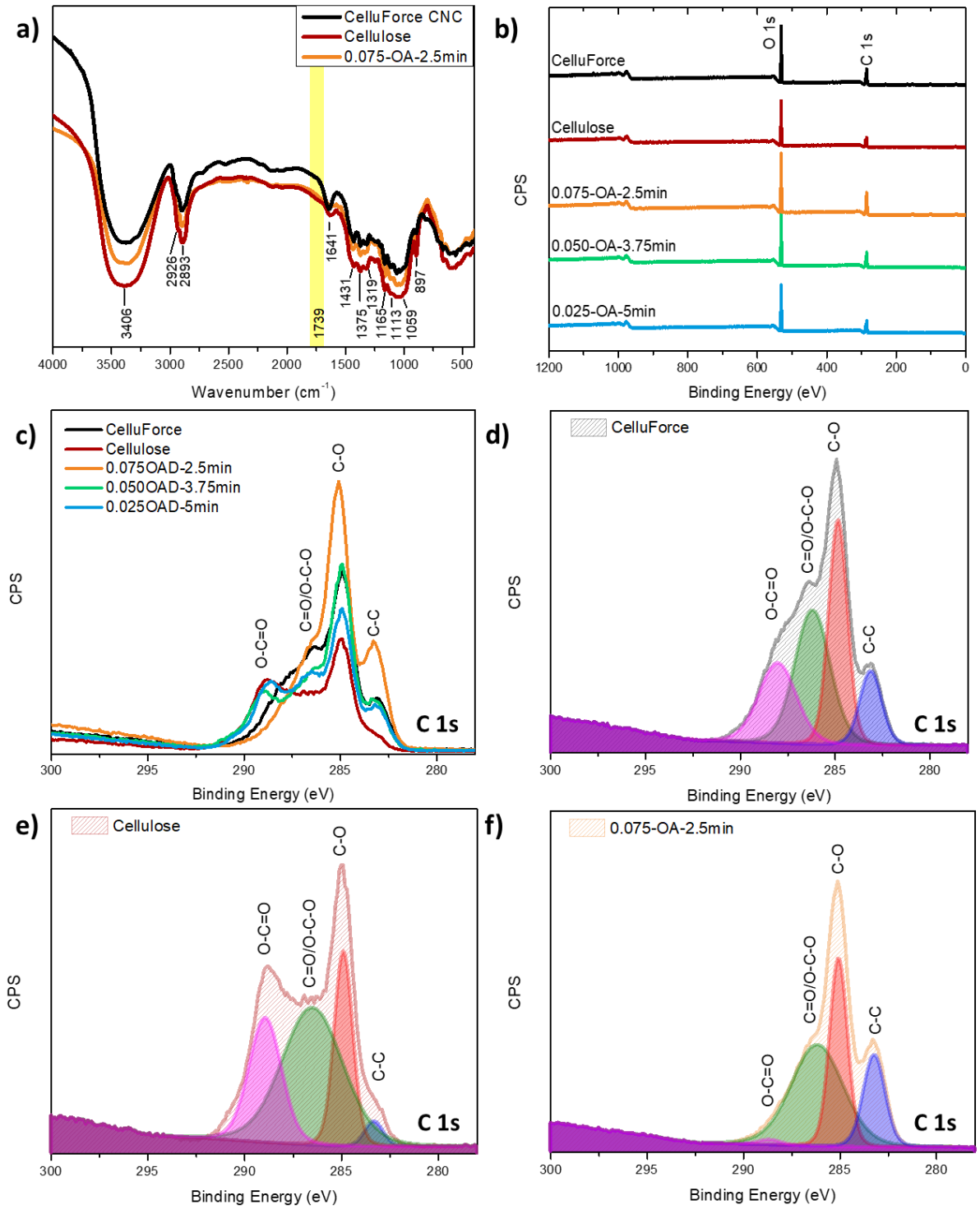

Figure 4.4. (a) FTIR, (b) overall XPS, and (c) overlayed XPS C 1s peak spectra for cellulose, produced CNC, and CelluForce CNC. (d-f) Deconvoluted C 1s peak spectra for key samples.

4.3.3.2 Physical Structure and Crystallinity Index of CNC

POM images of cellulose and CNC were collected to explore their physical structure. After drying an aliquot of cellulose and CNC suspensions on a glass slide, a thin film was formed with a distinct coffee-ring stain in which there was an accumulation of particles at the edge due to uneven drying [198]. Optical and polarized images of these edges for cellulose, 0.025-OA-5 min, and CelluForce CNC are presented in **Figure 4.5**. The unprocessed cellulose particles are variously shaped and display little polarizability (**Figure 4.5.1a and Figure 4.5.1b**). Both developed and commercial CNC samples produced more uniform films composed of nanoparticles unobservable with POM (**Figure 4.5.2a and Figure 4.5.3a**). The polarizing activity of the CNC samples (**Figure 4.5.2b and Figure 4.5.3b**) is indicative of high crystallinity, which is explored later in this section.

To further explore the size and geometric shape of the cellulosic materials at the nanoscale, SEM and AFM were used. Due to the loose nature of cellulose fibers, AFM analysis could not be performed, and alternatively, SEM was utilized. **Figure 4.5.1c** displays the non-uniform shape and size of unprocessed cellulose, with some particles being round and others more fibrous. After processing cellulose in this study, the resulting CNC particles were more uniform and significantly smaller. From **Figure 4.5.2c**, the CNC produced from 0.025-OA-5 min was measured to be < 125 nm in length and < 25 nm in diameter. Comparatively, the CNC obtained from CelluForce in **Figure 4.5.3c** had a higher aspect ratio (approx. < 400 nm in length and < 25 nm in diameter).

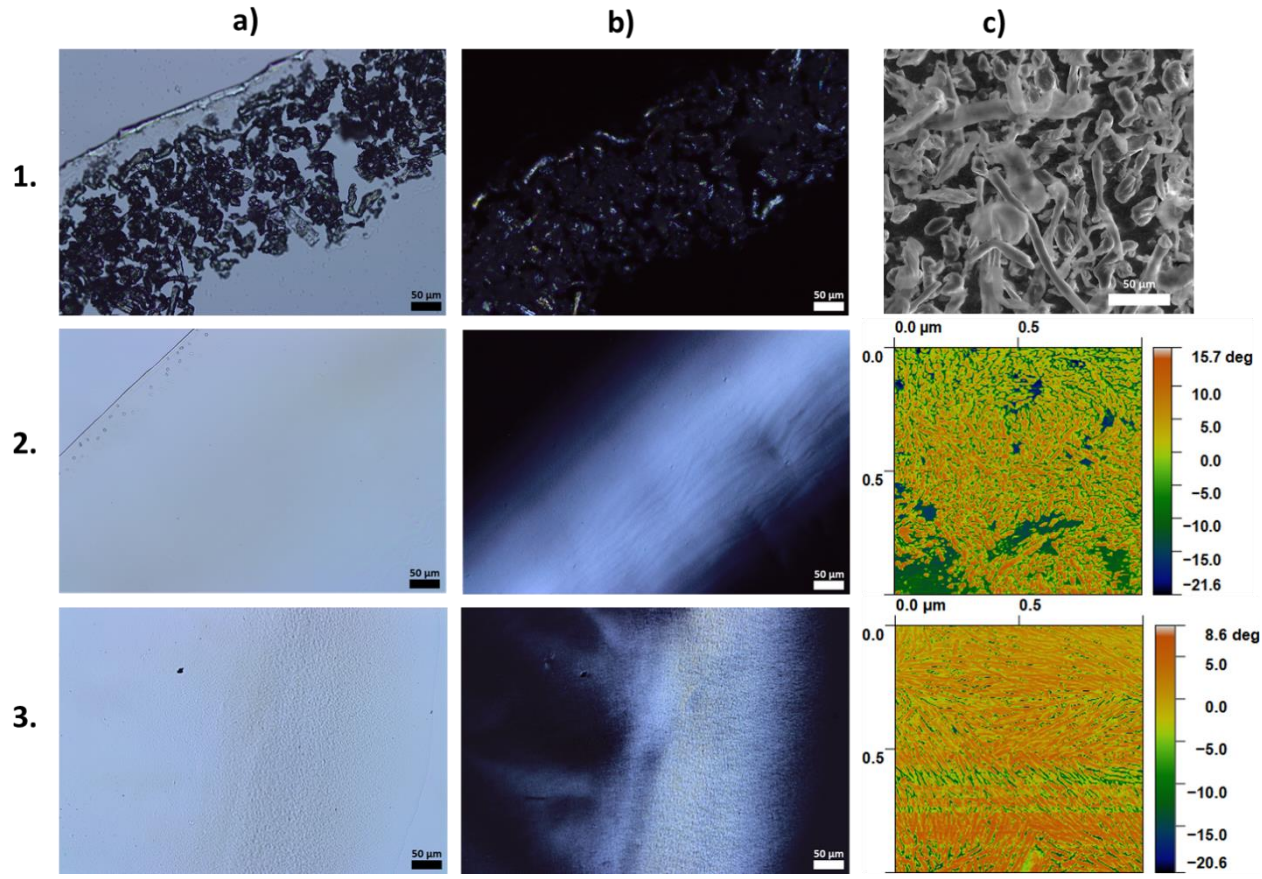

Figure 4.5. Images of (1) Cellulose, (2) 0.025-OA-5min, and (3) CelluForce CNC. Images in column (a) are optical microscope images and (b) are polarized images. Lastly, column (c) presents an SEM image of cellulose (1c) and AFM images of CNC (2c and 3c).

DLS was also used to measure the particle size of the cellulosic materials. The respective particle size distribution plots of each sample are displayed in the top section of **Figure 4.6a** and the measured diameter sizes are also graphed in **Figure 4.6b**. Prior to further analysis, it is important to note that any discrepancies in size between AFM and DLS measurements is due to the unreliability of DLS analysis for the size measurement of polydisperse, non-spherical particles [199]. For example, unprocessed cellulose was determined to be approx. 3 µm in size using DLS, however, supplier specifications provide an average fiber length of 18 µm and average fiber thickness of 15 µm. Despite this discrepancy, overall, it can still be concluded that processing

cellulose with BmimCl and OA results in a significant size reduction of cellulose particles to generate CNCs. The produced CNC in this study were measured to be in the size range of approximately 180-300 nm, depending on the processing conditions. Generally, lower OA content also resulted in larger CNCs size. Based on DLS, the CelluForce CNC sample was also measured to be smaller in size than the produced CNC, although this is inaccurate due to the fibrous, non-spherical nature of CNCs. The previously presented AFM images strongly suggest the opposite with CelluForce CNC being longer and, thus, a higher aspect ratio.

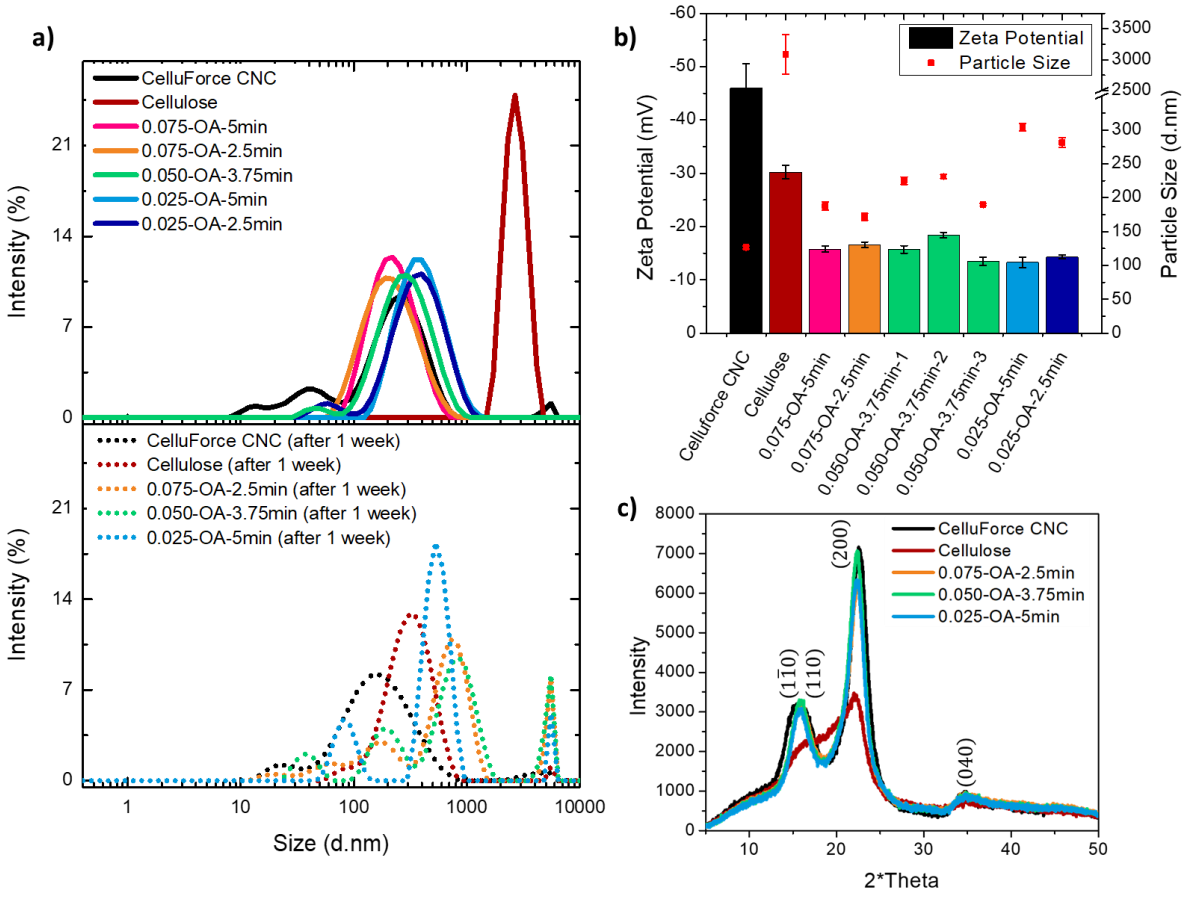

Figure 4.6. (a) Particle size distribution (bottom is one week after agitation), (b) particle size and zeta potential measurements, and (c) XRD spectra for cellulose and CNC samples.

In addition to size, the degree of crystallinity is a vital characteristic of CNC. The crystalline index (CrI) of cellulose and CNCs was determined from the XRD spectra in **Figure 4.6c**. From these spectra, the crystalline peaks of cellulose I were observed at 15.8° (comprising of both 14.9° and 16.5°), 22.4°, and 34.8°, which correspond to the planes of $(1\bar{1}0), (110), (200), \text{and } (040)$, respectively [189,192,200]. Using **Eq. (4.2)**, unprocessed cellulose and CelluForce CNC were calculated to have a CrI of 43.3% and 88.0%, respectively. The CrI of the developed CNC samples were measured to be 82.8%, 87.3%, and 85.6% for the 0.075-OA-2.5 min, 0.050-OAD-3.75 min, and 0.025-OA-5 min, respectively. Thus, the CrI of the developed CNC is very similar to commercially available CNCs.

4.3.3.3 Suspension Stability of CNC

The suspension stability of cellulose and CNC in water can be determined by measuring their zeta potential. Generally, a CNC suspension is considered stable if its absolute zeta potential is more than 30 mV [12,101,201]. If the absolute zeta potential is less than 15 mV, nanocellulose aggregates [201]. The zeta potentials of cellulose, produced CNC, and commercial CNC are presented in **Figure 4.6b**. Unprocessed cellulose and CelluForce CNC had absolute zeta potentials greater than 30 mV, while all the produced CNC samples in this study had between 10-20 mV. The low absolute zeta potential of the produced CNC samples indicates that the suspension can be unstable and is prone to aggregation [201]. However, minimal surface charge also allows for easier chemical modifications since it indicates there are more reactive hydroxyl groups over other stable functional groups [176]. To explore the stability of the suspensions, samples were shaken and left undisturbed for a week at room temperature and their particle sizes were measured using DLS. The resulting distributions are shown at the bottom of **Figure 4.6a**. In the distribution plot, there is a clear increase in the size of the CNC samples produced in this study, as evidenced by the peaks that appear at approx. 5000

nm. After one week, the samples measured significantly higher diameters (320-420 nm greater). The increase in particle sizes was indicative of nanocellulose agglomeration. Comparatively, the commercial CNC suspension, which had a high absolute zeta potential, was stable with an unchanged distribution plot and maintained a low DLS particle size. The unprocessed cellulose experienced a significant decrease in particle size (~10x less) due to the settling of large particles and is irrelevant to zeta potential, as shown in Figure 4.7 **(a & b)**.

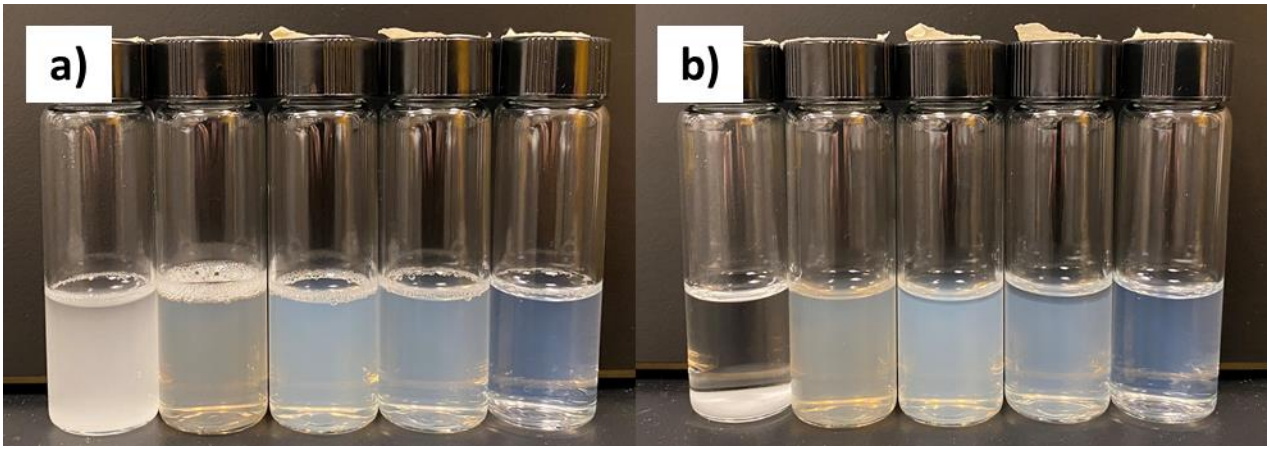

Figure 4.7. Images of cellulose and CNC suspended in water (a) immediately after agitation and (b) one week following. Left to right: Cellulose, 0.075-OA-2.5min, 0.050-OA-3.75min, 0.025-OA-5min, and CelluForce CNC.

The zeta potential of CNCs is related to the types of acids being used in the production of nanocellulose particles. Commercial CNCs are typically produced via sulfuric acid, and as a result, it contains negatively charged sulfate functional groups [12,101,201]. In this study, OA was used, which is a weaker organic acid that contains negatively charged oxalate groups. The differing reactivity of these acids and the employed processing conditions can cause the observed contrasts in this study in terms of zeta potential and suspension stability [183]. This difference was most notable between the produced and CelluForce CNC, however, it can also be observed between cellulose

and the produced CNC. The absolute zeta potential of unprocessed cellulose was larger than the generated CNC samples. It is likely that the cellulose production process could have involved stronger acids and, once it was processed with the OA in this study, the functional groups introduced in its production were removed and/or replaced. Based on the XPS results, this functional group is the carboxyl functional group.

In previous studies, CNCs generated via oxalic acid hydrolysis had similar zeta potentials as CNC developed with a sulfuric acid process [179,183]. In the work by Fu et al., the zeta potential of CNC that had been swollen with BmimCl and hydrolyzed with an oxalic acid ranged from -25 to -40 mV [179]. An alternative study involving oxalic acid hydrolysis at varying acid loading, temperature, and time conditions had zeta potentials in the range of -35 to -45 mV [183]. Evaluating the developed CNC against current research demonstrated that there is a significant difference in absolute zeta potential. The lower absolute zeta potential of the CNC samples in this study was hypothesized to be caused by the comparatively low OA loading (< 5 wt.% for all investigated samples), as well as the possible degradation of carboxyl groups in the native cellulose. Accordingly, less carboxyl moieties are present in the nanocellulose structure, affecting zeta potential values.

4.3.3.4 Thermal Stability of CNC

As an important factor for the material application of CNCs, the thermal stability of the produced CNC samples was analyzed and compared with cellulose and CelluForce CNC. The resulting thermogravimetric graphs of each cellulosic material and their respective derivative plots are presented in Figure 4.8. The derivative TGA graphs showed that the produced CNC samples all experienced the principal point of degradation at approximately 329 °C, despite their varying processing conditions. A secondary local maximum degradation peak, with varying breadths, between 435-450 °C was also observed for these samples. The unprocessed cellulose had a primary

degradation moment at a slightly higher temperature of 342 °C in comparison to the produced CNC and with no secondary peaks. Further, the derivative graphs show that the main degradation point for the commercial CNC samples (296 °C) was lower compared to unprocessed cellulose and all produced CNC samples. The commercial CNC samples also had two secondary degradation peaks at 344 °C and 459 °C.

The primary degradation peaks observed from the derivative TGA graphs for the CNC samples are attributed to the degradation of reactive and accessible amorphous regions of the cellulose [202]. These regions are locations on the structure where oxalate or sulfate groups may have been introduced during the production of the CNC in this study or CelluForce CNC, respectively [188,202,203]. The higher temperature degradation processes, related to the secondary peaks of CNC, are attributed to the breakdown of unreacted, crystalline regions of CNC [202,203]. Multiple secondary peaks in the higher temperature regions may be due to varying levels of crystallinity.

The positions of these degradation peaks are suggestive of the thermal stability of these samples. Based on these observations, cellulose is most thermally stable, followed by the produced CNC, and then the commercial CNC. Assessing the produced CNC with the unprocessed cellulose that it originated from, the thermal behaviour of the samples is comparable (~10 °C difference). This means that the production process of this study was not severe enough to substantially reduce its thermal stability. However, there is a considerable difference in the thermal behaviour of CelluForce CNC due to the sulfuric acid use in its production. It is well noted that the introduction of sulfate groups decreases thermal stability [193,204]. Generally, CNCs produced from mineral acids, such as sulfuric or phosphoric acid, are typically lower in thermal stability compared to organic acids, like oxalic and maleic acid [183].

Overall, the thermal stability of the produced CNC in this study is equal to the thermal behaviour of CNC produced via a similar process except performed in two-steps by Fu et al. (BmimCl swelling followed by oxalic acid hydrolysis), both with a maximum degradation temperature at 329 °C [179]. CNC produced solely with oxalic acid and its dihydrate form had maximum peaks at approx. 370 °C and 350 °C, respectively [183,188]. However, it is difficult to determine whether the difference in thermal behaviour between the samples developed in this study and previous work is due to processing conditions or variation in the cellulosic source. Often, CNC produced from weaker acids maintains a comparable thermal performance to the native biomass [179,183,193].

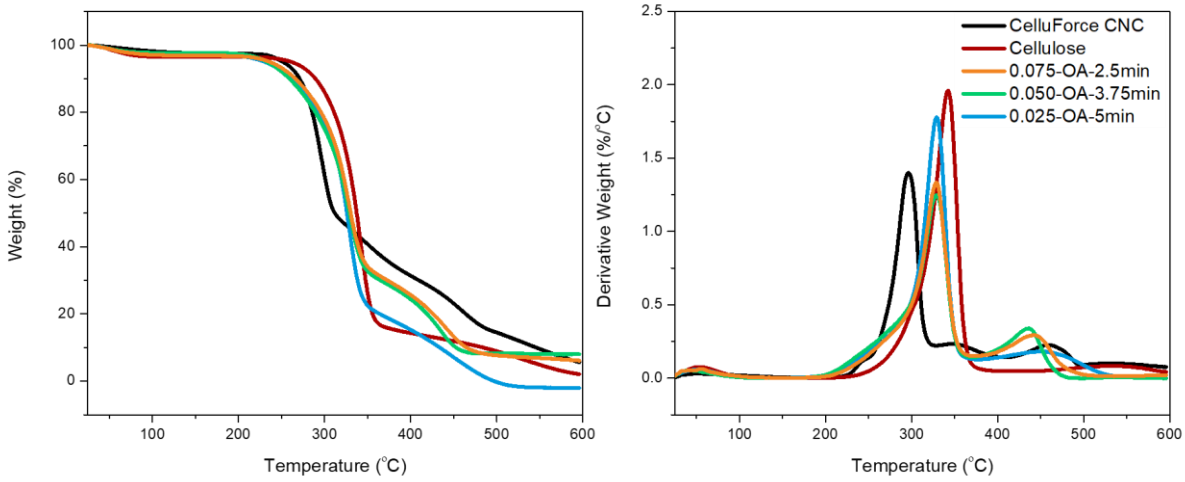

Figure 4.8. Thermogravimetric analysis (left) and its derivative (right) of cellulose, produced CNC, and CelluForce CNC.

4.4 Conclusions

In this study, high yields of CNC were produced in a reactive batch mixer process with BmimCl and OA. It is notable that the implemented process involved higher solid loadings and shorter processing times in comparison to previous similar studies. A maximum CNC yield of 59.0 wt.% was achieved with a mixture composition of 1:0.7:0.075 (Cellulose:BmimCl:OA, w/w/w) and a

processing time of 2.5 min. The resulting CNC was nano-sized and highly crystalline with good thermal stability. However, the CNC suspension had poor long-term stability due to its lower absolute zeta potential measurements. In exchange for suspension stability, the samples were more thermally stable and easily modifiable due to the absence of sulfate groups. The high yield and short processing times observed in this study also indicate an opportunity for a similar application using an extruder instead of a batch mixer for future investigations.

Chapter 5: Concluding Remarks and Future Work

The work presented in this thesis contributes to improve the processing of lignocellulosic biomasses using ionic liquids by reducing costs related to material consumption and processing time. Effective batch mixer processing at biomass loadings greater than 50 wt.% is advantageous in that the amount of expensive ionic liquid being utilized is minimized. Additionally, the intensive shearing capabilities of the mechanical process and the plasticizing effect of BmimCl allows for faster processing. In this thesis, these two aims were both realized in different applications.

Using the BmimCl-batch mixer process, successful lignin recovery (36.6% yield) was achieved at 50 wt.% MHF solid loading and a residence time of 45 min. The extracted biomass was characterized to be lignin with some remaining BmimCl residue using FTIR, UV-vis, and ^{13}C-NMR. When applied for CNC production, a mixture with a composition of 1:0.7:0.075 (Cellulose:BmimCl:OA, w/w/w) processed for 2.5 min in a batch mixer resulted in a maximum CNC yield of 59.0 wt.%. According to FTIR characterization, the produced CNC a had similar chemical structure as CelluForce CNC and unprocessed cellulose. However, XPS analysis revealed that there were slight differences in O 1s and C 1s surface composition. The resulting CNC was also nano-structured, highly crystalline, and great thermal stability compared to commercial CNC.

In both applications, the efficient processing of MHF and cellulose at high solid loadings and minimal processing times suggests an opportunity for feasible industrial application. More specifically, a similar process can be employed using a twin-screw extruder instead of a batch mixer. The shorter processing times implemented in this thesis can be exploited in an extruder, which is continuous and does not allow for long processes. An extruder also maintains a significant

degree of shear during processing like a batch mixer, allowing for high solid loading. The continuity and self-cleaning capabilities of extrusion operations are more appealing in terms of industrial application, and therefore, would be beneficial to explore further in the future.

References

1 StartUs Insights, 5 Top Sustainable Materials Startups You Should Watch in 2022, https://www.startus-insights.com/innovators-guide/5-top-sustainable-materials-startups-2022/, (accessed 18 March 2022).

2 C. Calvino, N. Macke, R. Kato and S. J. Rowan, , DOI:10.1016/j.progpolymsci.2020.101221.

3 M. M. Rahman and S. H. Rimu, *Int. J. Environ. Anal. Chem.*, 2020, **00**, 1–18.

4 H. Dai, J. Wu, H. Zhang, Y. Chen, L. Ma, H. Huang, Y. Huang and Y. Zhang, *Trends Food Sci. Technol.*, 2020, **102**, 16–29.

5 W. Farhat, R. A. Venditti, M. Hubbe, M. Taha, F. Becquart and A. Ayoub, *ChemSusChem*, 2017, **10**, 305–323.

6 Z. Xiang, N. Tang, X. Jin and W. Gao, *Carbohydr. Polym.*, 2022, **278**, 118945.

7 M. N. Collins, M. Nechifor, F. Tanasă, M. Zănoagă, A. McLoughlin, M. A. Stróżyk, M. Culebras and C. A. Teacă, *Int. J. Biol. Macromol.*, 2019, **131**, 828–849.

8 Y. Meng, J. Lu, Y. Cheng, Q. Li and H. Wang, *Int. J. Biol. Macromol.*, 2019, **135**, 1006–1019.

9 Y. Ge and Z. Li, *ACS Sustain. Chem. Eng.*, 2018, **6**, 7181–7192.

10 H. Liu, T. Xu, K. Liu, M. Zhang, W. Liu, H. Li, H. Du and C. Si, *Ind. Crops Prod.*, 2021, **165**, 113425.

11 R. Kumar, S. Singh and O. V. Singh, *J. Ind. Microbiol. Biotechnol.*, 2008, **35**, 377–391.

12 O. M. Vanderfleet and E. D. Cranston, *Nat. Rev. Mater.*, 2021, **6**, 124–144.

13 A. Tribot, G. Amer, M. Abdou Alio, H. de Baynast, C. Delattre, A. Pons, J. D. Mathias, J. M. Callois, C. Vial, P. Michaud and C. G. Dussap, *Eur. Polym. J.*, 2019, 112, 228–240.

14 D. Trache, M. H. Hussin, M. K. M. Haafiz and V. K. Thakur, *Nanoscale*, 2017, **9**, 1763–1786.

15 J. Singh, M. Suhag and A. Dhaka, *Carbohydr. Polym.*, 2015, **117**, 624–631.

16 M. H. L. Silveira, A. R. C. Morais, A. M. Da Costa Lopes, D. N. Olekszyszen, R. Bogel-Łukasik, J. Andreaus and L. Pereira Ramos, *ChemSusChem*, 2015, **8**, 3366–3390.

17 K. J. Nagarajan, N. R. Ramanujam, M. R. Sanjay, S. Siengchin, B. Surya Rajan, K. Sathick Basha, P. Madhu and G. R. Raghav, *A comprehensive review on cellulose nanocrystals and cellulose nanofibers: Pretreatment, preparation, and characterization*, 2021, vol. 42.

18 C. C. Piras, S. Fernández-Prieto and W. M. De Borggraeve, *Nanoscale Adv.*, 2019, **1**, 937–947.

19 J. Zheng and L. Rehmann, *Int. J. Mol. Sci.*, 2014, 15, 18967–18984.

20 E. Gatt, L. Rigal and V. Vandenbossche, *Ind. Crop. Prod.*, 2018, **122**, 329–339.

21 N. Jacquet, G. Maniet, C. Vanderghem, F. Delvigne and A. Richel, *Ind. Eng. Chem. Res.*, 2015, **54**, 2593–2598.

22 C. Tzoganakis and S. Zhu, *Encycl. Polym. Sci. Technol.*, 2012, 1–28.

23 C. Tzoganakis, *Adv. Polym. Technol.*, 1989, **9**, 321–330.

24 A. Duque, P. Manzanares and M. Ballesteros, *Renew. Energy*, 2017, **114**, 1427–1441.

25 C. Karunanithy and K. Muthukumarappan, in *Green Biomass Pretreatment for Biofuels Production*, ed. T. Gu, Springer-Verlag, Berlin Heidelberg, 2013, pp. 31–65.

26 J. L. White, *Twin Screw Extrusion: Technology and Principles*, Hanser Publishers, New York, 1990.

27 G. Shearer and C. Tzoganakis, *Polym. Eng. Sci.*, 2000, 40, 1095–1106.

28 A. S. A. Da Silva, R. S. S. Teixeira, T. Endo, E. P. S. Bon and S. H. Lee, *Green Chem.*, 2013, **15**, 1991–2001.

29 L. Capolupo and V. Faraco, 2016, 9451–9467.

30 D. Kumari and R. Singh, *Renew. Sustain. Energy Rev.*, 2018, **90**, 877–891.

31 V. Vandenbossche, J. Brault, O. Hernandez-melendez, P. Evon, E. Barzana, G. Vilarem and L. Rigal, *Bioresour. Technol.*, 2016, **211**, 146–153.

32 J. Chen, W. Zhang, H. Zhang, Q. Zhang and H. Huang, *Bioresour. Technol.*, 2014, **161**, 230–235.

33 S. Zhang, D. R. Keshwani, Y. Xu and M. A. Hanna, *Ind. Crop. Prod.*, 2012, **37**, 352–357.

34 S. Y. Han, C. W. Park, T. Endo, F. Febrianto, N. H. Kim and S. H. Lee, *Wood Sci.*

Technol., 2020, **54**, 599–613.

35 T. H. Kim, C. H. Choi and K. K. Oh, *Bioresour. Technol.*, 2013, **130**, 306–313.

36 S. Senturk-ozer, H. Gevgilili and D. M. Kalyon, *Bioresour. Technol.*, 2011, **102**, 9068–9075.

37 C. Karunanithy, K. Muthukumarappan and W. R. Gibbons, 2012, 81–99.

38 S. Lee, Y. Teramoto and T. Endo, 2009, **100**, 275–279.

39 M. Green, S. Kimchie, A. I. Malester, B. Rugg and G. Shelef, *Biol. Wastes*, 1988, **26**, 285–295.

40 Q. Li, Z. Zhou, D. Zhang, Z. Wang and W. Cong, *Bioprocess Biosyst. Eng.*, 2020, **43**, 655–662.

41 M. Hjorth, K. Gränitz, A. P. S. Adamsen and H. B. Møller, *Bioresour. Technol.*, 2011, **102**, 4989–4994.

42 E. L. N. Escobar, T. A. da Silva, C. L. Pirich, M. L. Corazza and L. Pereira Ramos, *Front. Bioeng. Biotechnol.*, 2020, 8.

43 C. Karunanithy and K. Muthukumarappan, *Appl. Biochem. Biotechnol.*, 2010, **162**, 1785–1803.

44 B. J. Gu, G. S. Dhumal, M. P. Wolcott and G. M. Ganjyal, *Bioresour. Technol.*, 2019, **275**, 266–271.

45 B. Ai, W. Li, J. Woomer, M. Li, Y. Pu, Z. Sheng, L. Zheng, A. Adedeji, A. J. Ragauskas

and J. Shi, *Green Chem.*, 2020, **22**, 6372–6383.

46 J. Li, M. Thompson and D. J. W. Lawton, *J. Polym. Environ.*, 2019, **27**, 643–651.

47 M. K. Moro, R. Sposina Sobral Teixeira, A. Sant'Ana da Silva, M. Duarte Fujimoto, P. Albuquerque Melo, A. Resende Secchi and E. Pinto da Silva Bon, *Ind. Crops Prod.*, 2017, **97**, 509–517.

48 A. Duque, P. Manzanares, A. González and M. Ballesteros, *Energies*, , DOI:10.3390/en11112961.

49 B. Lamsal, J. Yoo, K. Brijwani and S. Alavi, *Biomass and Bioenergy*, 2010, **34**, 1703–1710.

50 K. Karimi, M. Shafiei and R. Kumar, in *Biofuel Technologies: Recent Developments*, eds. V. K. Gupta and M. G. Tuohy, Springer-Verlag Berlin, 2013, pp. 53–96.

51 A. Barakat, C. Mayer-Laigle, A. Solhy, R. A. D. Arancon, H. De Vries and R. Luque, *RSC Adv.*, 2014, **4**, 48109–48127.

52 Q. Zhai, F. Li, F. Wang, J. Feng, J. Jiang and J. Xu, *Cellulose*, 2019, **26**, 3685–3701.

53 B. J. Gu, J. Wang, M. P. Wolcott and G. M. Ganjyal, *Bioresour. Technol.*, 2018, **251**, 93–98.

54 E. M. Mount, in *Applied Plastics Engineering Handbook*, Canandaigua, 2011, pp. 227–266.

55 D. A. Fort, R. C. Remsing, R. P. Swatloski, P. Moyna, G. Moyna and R. D. Rogers, *Green*

Chem., 2007, **9**, 63–69.

56 M. Chandrasekaran and M. V. Karwe, *AIChE J.*, 1997, **43**, 2424–2431.

57 R. Wahid, M. Hjorth, S. Kristensen and H. B. Møller, *Energy and Fuels*, 2015, **29**, 4030–4037.

58 Y. L. Cha, J. Yang, S. Il Seo, G. H. An, Y. H. Moon, G. D. You, J. E. Lee, J. W. Ahn and K. B. Lee, *Fuel*, 2016, **164**, 322–328.

59 H. Kim, Y. Ahn and S. Y. Kwak, *Biomass and Bioenergy*, 2016, **93**, 243–253.

60 A. Duque, P. Manzanares, I. Ballesteros, M. J. Negro, J. M. Oliva, F. Saez and M. Ballesteros, *Process Biochem.*, 2013, **48**, 775–781.

61 M. C. Coimbra, A. Duque, F. Saéz, P. Manzanares, C. H. Garcia-Cruz and M. Ballesteros, *Renew. Energy*, 2016, **86**, 1060–1068.

62 C. Liu, E. Van Der Heide, H. Wang, B. Li, G. Yu and X. Mu, *Biotechnol. Biofuels*, 2013, **6**, 1–11.

63 C. H. Choi and K. K. Oh, *Bioresour. Technol.*, 2012, **110**, 349–354.

64 K. S. Guiao, C. Tzoganakis and T. H. Mekonnen, *Chemosphere*, , DOI:10.1016/j.chemosphere.2022.133647.

65 X. Zhan, D. Wang, S. R. Bean, X. Mo, X. S. Sun and D. Boyle, *Ind. Crops Prod.*, 2006, **23**, 304–310.

66 C. Karunanithy, K. Muthukumarappan and W. R. Gibbons, *Bioresour. Technol.*, 2014,

153, 393–398.

67 Y. Zhang, T. Li, Y. Shen, L. Wang, H. Zhang, H. Qian and X. Qi, *Ind. Crops Prod.*, 2020, **149**, 112356.

68 J. M. Oliva, M. J. Negro, P. Manzanares, I. Ballesteros, M. Á. Chamorro, F. Sáez, M. Ballesteros and A. D. Moreno, *Fermentation*, 2017, **3**, 1–15.

69 J. Zheng, K. Choo, C. Bradt, R. Lehoux and L. Rehmann, *Biotechnol. Reports*, 2014, **3**, 99–107.

70 J. C. Morales-Huerta, O. Hernández-Meléndez, M. G. Hernández-Luna, O. Manero, E. Bárzana and E. Vivaldo-Lima, *Ind. Eng. Chem. Res.*, 2021, **60**, 12449–12460.

71 V. Vandenbossche, J. Brault, G. Vilarem, O. Hernández-Meléndez, E. Vivaldo-Lima, M. Hernández-Luna, E. Barzana, A. Duque, P. Manzanares, M. Ballesteros, J. Mata, E. Castellón and L. Rigal, *Ind. Crops Prod.*, 2014, **55**, 258–266.

72 P. Doménech, A. Duque, I. Higueras, R. Iglesias and P. Manzanares, *Energies*, , DOI:10.3390/en13174517.

73 J. S. Kim, Y. Y. Lee and R. W. Torget, *Appl. Biochem. Biotechnol.*, 2001, **91**–**93**, 331–340.

74 T. Mekonnen, P. Mussone, H. Khalil and D. Bressler, *J. Mater. Chem. A*, 2013, **1**, 13379–13398.

75 J. Luo, M. Cai and T. Gu, , DOI:10.1007/978-94-007-6052-3.

76 P. Halder, S. Kundu, S. Patel, A. Setiawan, R. Atkin, R. Parthasarthy, J. Paz-Ferreiro, A. Surapaneni and K. Shah, *Renew. Sustain. Energy Rev.*, 2019, **105**, 268–292.

77 J. Flieger and M. Flieger, *Int. J. Mol. Sci.*, 2020, **21**, 1–41.

78 K. S. Khoo, X. Tan, C. W. Ooi, K. W. Chew, W. H. Leong, Y. H. Chai, S. H. Ho and P. L. Show, *J. Clean. Prod.*, 2021, **284**, 124772.

79 I. Kilpeläinen, H. Xie, A. King, M. Granstrom, S. Heikkinen and D. S. Argyropoulos, *J. Agric. Food Chem.*, 2007, **55**, 9142–9148.

80 M. Mora-Pale, L. Meli, T. V. Doherty, R. J. Linhardt and J. S. Dordick, *Biotechnol. Bioeng.*, 2011, **108**, 1229–1245.

81 N. Sun, M. Rahman, Y. Qin, M. L. Maxim, H. Rodríguez and R. D. Rogers, *Green Chem.*, 2009, **11**, 646–65.

82 A. S. Da Silva, S.-H. Lee, T. Endo and E. P.S. Bon, *Bioresour. Technol.*, 2011, **102**, 10505–10509.

83 S. P. Nalawade, F. Picchioni and L. P. B. M. Janssen, *Prog. Polym. Sci.*, 2006, **31**, 19–43.

84 M. Sauceau, J. Fages, A. Common, C. Nikitine and E. Rodier, *Prog. Polym. Sci.*, 2011, **36**, 749–766.

85 M. Chauvet, M. Sauceau and J. Fages, *J. Supercrit. Fluids*, 2017, **120**, 408–420.

86 M. Lee, C. Tzoganakis and C. B. Park, *Adv. Polym. Technol.*, 2000, **19**, 300–311.

87 K. K. Darani and M. R. Mozafari, *J. Biochem. Technol.*, 2009, **2**, 144–152.

88 S. K. Goel and E. J. Beckman, *Polym. Eng. Sci.*, 1994, **34**, 1137–1147.

89 C. Seto, B. P. Chang, C. Tzoganakis and T. H. Mekonnen, *Int. J. Biol. Macromol.*, 2021, **185**, 629–643.

90 R. Shorey, A. Gupta and T. H. Mekonnen, *Ind. Crops Prod.*, 2021, **174**, 114189.

91 B. P. Chang, A. Gupta, R. Muthuraj and T. H. Mekonnen, *Green Chem.*, 2021, **23**, 5337–5378.

92 A. Kalliola, T. Vehmas, T. Liitiä and T. Tamminen, *Ind. Crops Prod.*, 2015, **74**, 150–157.

93 M. Wu, J. Pang, F. Lu, X. Zhang, L. Che, F. Xu and R. Sun, *Ind. Crops Prod.*, 2013, **50**, 887–895.

94 D. Tian, F. Shen, G. Yang, S. Deng, L. Long, J. He, J. Zhang, C. Huang and L. Luo, *Fuel*, 2019, **252**, 589–597.

95 J. Zheng, K. Choo and L. Rehmann, *Biomass and Bioenergy*, 2015, **74**, 224–232.

96 R. Sun, J. M. Lawther, W. B. Banks and B. Xiao, *Ind. Crops Prod.*, 1997, **6**, 97–106.

97 S. Salimi, R. Sotudeh-Gharebagh, R. Zarghami, S. Y. Chan and K. H. Yuen, *ACS Sustain. Chem. Eng.*, 2019, **7**, 15800–15827.

98 V. Oriez, J. Peydecastaing and P. Y. Pontalier, *Molecules*, , DOI:10.3390/molecules24234273.

99 P. Phanthong, P. Reubroycharoen, X. Hao, G. Xu, A. Abudula and G. Guan, *Carbon Resour. Convers.*, 2018, **1**, 32–43.

100 S. Ang, V. Haritos and W. Batchelor, *Cellulose*, 2019, **26**, 4767–4786.

101 H. Wang, M. Zuo, N. Ding, G. Yan, X. Zeng, X. Tang, Y. Sun, T. Lei and L. Lin, *ACS Sustain. Chem. Eng.*, 2019, **7**, 9378–9386.

102 C. G. Otoni, A. S. Carvalho, M. V. C. Cardoso, O. D. Bernardinelli, M. V. Lorevice, L. A. Colnago, W. Loh and L. H. C. Mattoso, *ACS Sustain. Chem. Eng.*, 2018, **6**, 12727–12735.

103 1998.

104 Z. Peter, *Carbohydr. Polym.*, 2021, **254**, 117417.

105 P. N. Bhandari, D. D. Jones and M. A. Hanna, *Carbohydr. Polym.*, 2012, **87**, 2246–2254.

106 T. T. T. Ho, K. Abe, T. Zimmermann and H. Yano, *Cellulose*, 2015, **22**, 421–433.

107 A. Merci, A. Urbano, M. V. E. Grossmann, C. A. Tischer and S. Mali, *Food Res. Int.*, 2015, **73**, 38–43.

108 F. Debiagi, P. C. S. Faria-Tischer and S. Mali, *Cellulose*, 2020, **27**, 1975–1988.

109 F. Debiagi, P. C. S. Faria-Tischer and S. Mali, *Waste and Biomass Valorization*, 2021, **12**, 1051–1060.

110 J. Li, H. Zhang, G. G. Sacripante, D. J. W. Lawton, H. S. Marway and M. R. Thompson, *Cellulose*, 2021, **28**, 1055–1069.

111 J. Li, T. Baker, G. G. Sacripante, D. J. W. Lawton, H. S. Marway, H. Zhang and M. R. Thompson, *Carbohydr. Polym.*, 2021, **270**, 118361.

112 H. Taheri, M. Hietala, T. Suopajärvi, H. Liimatainen and K. Oksman, *ACS Sustain. Chem. Eng.*, 2021, **9**, 883–893.

113 F. Rol, B. Karakashov, O. Nechyporchuk, M. Terrien, V. Meyer, A. Dufresne, M. N. Belgacem and J. Bras, *ACS Sustain. Chem. Eng.*, 2017, **5**, 6524–6531.

114 F. Rol, N. Belgacem, V. Meyer, M. Petit-Conil and J. Bras, *Cellulose*, 2019, **26**, 5635–5651.

115 F. Rol, S. Saini, V. Meyer, M. Petit-Conil and J. Bras, *Ind. Crops Prod.*, 2019, **137**, 81–88.

116 G. Banvillet, E. Gatt, N. Belgacem and J. Bras, *Bioresour. Technol.*, 2021, **327**, 1–8.

117 F. Rol, B. Vergnes, N. El Kissi and J. Bras, *ACS Sustain. Chem. Eng.*, 2020, **8**, 50–59.

118 M. C. Ralet and J. F. Thibault, *Carbohydr. Res.*, 1994, **260**, 283–296.

119 M. A. Larrea, Y. K. Chang and F. Martínez Bustos, *Food Chem.*, 2005, **89**, 301–308.

120 G. Sheng and Q. Zhou, *Appl. Mech. Mater.*, 2012, **178**–**181**, 838–842.

121 M. Wang, H. Cheng, S. Chen, S. Wen, X. Wu, D. Zhang, Q. Yuan and W. Cong, *Energy*, 2018, **142**, 339–345.

122 S. Menardo, V. Cacciatore and P. Balsari, *Bioresour. Technol.*, 2015, **180**, 154–161.

123 X. Chen, Y. L. Zhang, Y. Gu, Z. Liu, Z. Shen, H. Chu and X. Zhou, *Appl. Energy*, 2014, **122**, 34–41.

124 Y. Zhang, X. Chen, Y. Gu and X. Zhou, *Appl. Energy*, 2015, **160**, 39–48.

125 J. Byun, Y. L. Cha, S. M. Park, K. S. Kim, J. E. Lee and Y. G. Kang, *Energies*, , DOI:10.3390/en13215636.

126 N. Laskar and U. Kumar, *Environ. Technol. Innov.*, 2019, **14**, 100352.

127 A. L. Andrady, *Mar. Pollut. Bull.*, 2011, **62**, 1596–1605.

128 U.S. Energy Information Administration, Biomass Explained, https://www.eia.gov/energyexplained/biomass/.

129 O. Yu and K. H. Kim, *Appl. Sci.*, , DOI:10.3390/app10134626.

130 E. C. Achinivu, R. M. Howard, G. Li, H. Gracz and W. A. Henderson, *Green Chem.*, 2014, **16**, 1114–1119.

131 T. V. Doherty, M. Mora-Pale, S. E. Foley, R. J. Linhardt and J. S. Dordick, *Green Chem.*, 2010, **12**, 1967–1975.

132 T. Gu, M. A. Held and A. Faik, *Environ. Technol. (United Kingdom)*, 2013, **34**, 1735–1749.

133 M. H. L. Silveira, B. A. Vanelli, M. L. Corazza and L. P. Ramos, *Bioresour. Technol.*, 2015, **192**, 389–396.

134 L. Liang, C. Li, F. Xu, Q. He, J. Yan, T. Luong, B. A. Simmons, T. R. Pray, S. Singh, V. S. Thompson and N. Sun, *RSC Adv.*, 2017, **7**, 36585–36593.

135 H. A. Ruiz, M. Conrad, S. N. Sun, A. Sanchez, G. J. M. Rocha, A. Romaní, E. Castro, A.

Torres, R. M. Rodríguez-Jasso, L. P. Andrade, I. Smirnova, R. C. Sun and A. S. Meyer, *Bioresour. Technol.*, 2020, **299**, 122685.

136 A. Romaní, G. Garrote and J. C. Parajó, *Fuel*, 2012, **94**, 305–312.

137 A. Romaní, G. Garrote, J. L. Alonso and J. C. Parajó, *Ind. Eng. Chem. Res.*, 2010, **49**, 4653–4663.

138 K. Jedvert, A. Saltberg, M. E. Lindström and H. Theliander, *BioResources*, 2012, **7**, 2051–2074.

139 ISO 21436:2020, 2020.

140 G. L. Burrell, F. Dunlop and F. Separovic, 2010, 2080–2086.

141 A. Piednoir, A. Steinberger, C. Cottin-bizonne, A. Piednoir, A. Steinberger, C. Cottin-bizonne and C. B. A. Non-, *J. Phys. Chem. B*, 2020, **124**, 2685–2690.

142 A. G. Cruz, C. Scullin, C. Mu, G. Cheng, V. Stavila, P. Varanasi and D. Xu, .

143 H. Wu, M. Mora-Pale, J. Miao, T. V. Doherty, R. J. Linhardt and J. S. Dordick, *Biotechnol. Bioeng.*, 2011, **108**, 2865–2875.

144 S. H. Lee, T. V Doherty, R. J. Linhardt and J. S. Dordick, 2009, **102**, 1368–1376.

145 J. Long, X. Li, B. Guo, F. Wang, Y. Yu and L. Wang, *Green Chem.*, 2012, **14**, 1935–1941.

146 K. O. E. L. Mihkel, *Est. Proc. Acad. Sci. Chem.*, 2000, **49**, 1450155.

147 S. A. Dharaskar, M. N. Varma, D. Z. Shende, C. K. Yoo and K. L. Wasewar, *Sci. World J.*, , DOI:10.1155/2013/395274.

148 S. Tait and R. A. Osteryoung, *Inorg. Chem.*, 1984, **23**, 4352–4360.

149 N. Labbé, T. Rials, S. Kelley, Z. M. Cheng, J. Y. Kim and Y. Li, *Wood Sci. Technol.*, 2005, **39**, 61–76.

150 S. Y. Lin and C. W. Dence, *Methods in Lignin Chemistry*, Springer-Verlag, Berlin, 1st edn., 1992.

151 J. G. Huddleston, A. E. Visser, W. M. Reichert, H. D. Willauer, G. A. Broker and R. D. Rogers, *Green Chem.*, 2001, **3**, 156–164.

152 N. Ramezani and M. Sain, *J. Polym. Environ.*, 2018, **26**, 3109–3116.

153 M. Y. Balakshin, E. A. Capanema, R. B. Santos, H. M. Chang and H. Jameel, *Holzforschung*, 2016, **70**, 95–108.

154 H. Wikberg and S. L. Maunu, 2004, **58**, 461–466.

155 B. C. Chen and D. Robert, *Biomass Part B Lignin, Pectin, Chitin*, 1988, **161**, 137–174.

156 R. El Hage, N. Brosse, L. Chrusciel, C. Sanchez, P. Sannigrahi and A. Ragauskas, *Polym. Degrad. Stab.*, 2009, **94**, 1632–1638.

157 Y. Lu, Y. C. Lu, H. Q. Hu, F. J. Xie, X. Y. Wei and X. Fan, *J. Spectrosc.*, , DOI:10.1155/2017/8951658.

158 G. Wang and H. Chen, *Sep. Purif. Technol.*, 2013, **105**, 98–105.

159 Ł. Klapiszewski, M. Nowacka, G. Milczarek and T. Jesionowski, *Carbohydr. Polym.*, 2013, **94**, 345–355.

160 R. Mörck, H. Yoshida, K. P. Kringstad and H. Hatakeyama, *Holzforschung*, 1986, **40**, 51–60.

161 A. P. Lemes, M. A. Soto-Oviedo, W. R. Waldman, L. H. Innocentini-Mei and N. Durán, *J. Polym. Environ.*, 2010, **18**, 250–259.

162 S. S. Y. Tan, D. R. Macfarlane, J. Upfal, L. A. Edye, W. O. S. Doherty, A. F. Patti, M. Pringle and J. L. Scott, , DOI:10.1039/b815310h.

163 H. Yoshida, R. Mörck, K. P. Kringstad and H. Hatakeyama, *Holzforschung*, 1987, **41**, 171–176.

164 R. C. Sun, J. Tomkinson and G. Lloyd Jones, *Polym. Degrad. Stab.*, 2000, **68**, 111–119.

165 A. M. da Costa Lopes, K. G. João, A. R. C. Morais, E. Bogel-Łukasik and R. Bogel-Łukasik, *Sustain. Chem. Process.*, , DOI:10.1186/2043-7129-1-3.

166 D. Klemm, B. Heublein, H. Fink and A. Bohn, 2005, 3358–3393.

167 J. Tang, J. Sisler, N. Grishkewich and K. C. Tam, *J. Colloid Interface Sci.*, 2017, **494**, 397–409.

168 B. Liu, T. Li, W. Wang, L. M. C. Sagis, Q. Yuan, X. Lei, M. A. Cohen Stuart, D. Li, C. Bao, J. Bai, Z. Yu, F. Ren and Y. Li, *Nat. Sustain.*, 2020, **3**, 448–458.

169 Z. Hu, H. S. Marway, H. Kasem, R. Pelton and E. D. Cranston, ,

DOI:10.1021/acsmacrolett.5b00919.

170 Y. Li, X. Liu, Z. Zhang, S. Zhao, G. Tian, J. Zheng, D. Wang, S. Shi and T. P. Russell, 2018, **100193**, 13560–13564.

171 B. M. Trinh and T. Mekonnen, *Polymer (Guildf).*, 2018, **155**, 64–74.

172 E. Ojogbo, C. Tzoganakis and T. H. Mekonnen, *Compos. Part A Appl. Sci. Manuf.*, 2021, **149**, 106580.

173 J. M. Jardin, Z. Zhang, G. Hu, K. C. Tam and T. H. Mekonnen, *Int. J. Biol. Macromol.*, 2020, **152**, 428–436.

174 L. Kong, C. Zhang, J. Wang, D. Long and W. Qiao, *Mater. Chem. Phys.*, 2015, **149**–**150**, 495–504.

175 Y. Shin and G. J. Exarhos, 2007, **61**, 2594–2597.

176 M. S. Islam, L. Chen, J. Sisler and K. C. Tam, *J. Mater. Chem. B*, 2018, **6**, 864–883.

177 G. Kandhola, A. Djioleu, K. Rajan, N. Labbé, J. Sakon, D. J. Carrier and J. W. Kim, *Bioresour. Bioprocess.*, , DOI:10.1186/s40643-020-00302-0.

178 S. Beck-candanedo, M. Roman and D. G. Gray, 2005, 1048–1054.

179 X. Fu, H. Ji, B. Wang, W. Zhu and Z. Pang, *Cellulose*, 2020, **27**, 1289–1299.

180 X. Fan, H. Yu, D. Wang, Z. Mao and J. Yao, , DOI:10.1021/acssuschemeng.9b05081.

181 F. Hemmati, S. Mahdi and R. Ali, *Int. J. Biol. Macromol.*, 2019, **137**, 374–381.

182 W. Jia and Y. Liu, *Cellulose*, 2019, **26**, 8351–8365.

183 L. Chen, J. Y. Zhu, C. Baez, P. Kitin and T. Elder, *Green Chem.*, 2016, **18**, 3835–3843.

184 H. Bian, L. Chen and H. Dai, *Cellulose*, 2017, **24**, 4205–4216.

185 H. Bian, J. Luo, R. Wang, X. Zhou, S. Ni, R. Shi, G. Fang and H. Dai, , DOI:10.1021/acssuschemeng.9b05766.

186 D. Lv, H. Du, X. Che, M. Wu, Y. Zhang, C. Liu, S. Nie, X. Zhang and B. Li, , DOI:10.1021/acssuschemeng.9b00714.

187 D. Li, J. Henschen and M. Ek, *Green Chem.*, 2017, **19**, 5564–5567.

188 J. Henschen, D. Li and M. Ek, *Carbohydr. Polym.*, 2019, **213**, 208–216.

189 J. C. P. de Melo, E. C. da Silva Filho, S. A. A. Santana and C. Airoldi, *Colloids Surfaces A Physicochem. Eng. Asp.*, 2009, **346**, 138–145.

190 N. L. Mai, K. Ahn and Y. Koo, *Process Biochem.*, 2014, **49**, 872–881.

191 X. Qi, L. Li, T. Tan, W. Chen and R. L. Smith, *Environ. Sci. Technol.*, 2013, **47**, 2792–2798.

192 X. Y. Tan, S. B. Abd Hamid and C. W. Lai, *Biomass and Bioenergy*, 2015, **81**, 584–591.

193 J. Lazko, T. Se, N. Landercy, L. Dangreau, J. Raquez and P. Dubois, 2014, 4195–4207.

194 L. Segal, J. J. Creely, A. E. Martin and C. M. Conrad, *Text. Res. J.*, 1959, **29**, 786–794.

195 M. Bousmina, A. Ait-Kadi and J. B. Faisant, *J. Rheol. (N. Y. N. Y).*, 1999, **43**, 415–433.

196 M. N. Belgacem, G. Czeremuszkin, S. Sapieha and A. Gandini, *Cellulose*, 1995, **2**, 145–157.

197 L. S. Johansson and J. M. Campbell, *Surf. Interface Anal.*, 2004, **36**, 1018–1022.

198 R. M. Parker, G. Guidetti, C. A. Williams, T. Zhao, A. Narkevicius, S. Vignolini and B. Frka-petesic, *Adv. Mater.*, , DOI:10.1002/adma.201704477.

199 D. Langevin, E. Raspaud, S. Mariot, A. Knyazev, A. Stocco, A. Salonen, A. Luch, A. Haase, B. Trouiller, C. Relier, O. Lozano, S. Thomas, A. Salvati and K. Dawson, *NanoImpact*, 2018, **10**, 161–167.

200 E. O. Ogunsona, P. Panchal and T. H. Mekonnen, *Compos. Sci. Technol.*, 2019, **184**, 107884.

201 M. S. Mohaiyiddin, O. H. Lin, W. T. Owi, C. H. Chan, C. H. Chia, S. Zakaria, A. R. Villagracia and H. M. Akil, *Clean Technol. Environ. Policy*, 2016, **18**, 2503–2512.

202 H. Kargarzadeh, I. Ahmad, I. Abdullah, A. Dufresne, S. Y. Zainudin and R. M. Sheltami, *Cellulose*, 2012, **19**, 855–866.

203 L. A. S. Costa, D. de J. Assis, G. V. P. Gomes, J. B. A. Da Silva, A. F. Fonsêca and J. I. Druzian, *Mater. Today Proc.*, 2015, **2**, 287–294.

204 M. Lee, M. H. Heo, H. Lee, H. Lee, H. Jeong, Y. Kim and J. Shin, 2018, 2596–2610.

Appendix A

Table A1. ANOVA table for percentage lignin extraction yield

Source	DF	Seq. SS	Adj. SS	Adj. MS	F	P (α = 0.05)
Main Effects	2	165.890	165.890	82.9450	70.89	0.014
2-Way Interactions	1	39.690	39.690	39.6900	33.92	0.028
Curvature	1	0.429	0.429	0.4286	0.37	0.607
Residual Error	2	2.340	2.340	1.1700		
Pure Error	2	2.340	2.340	1.1700		
Total	6	208.349				

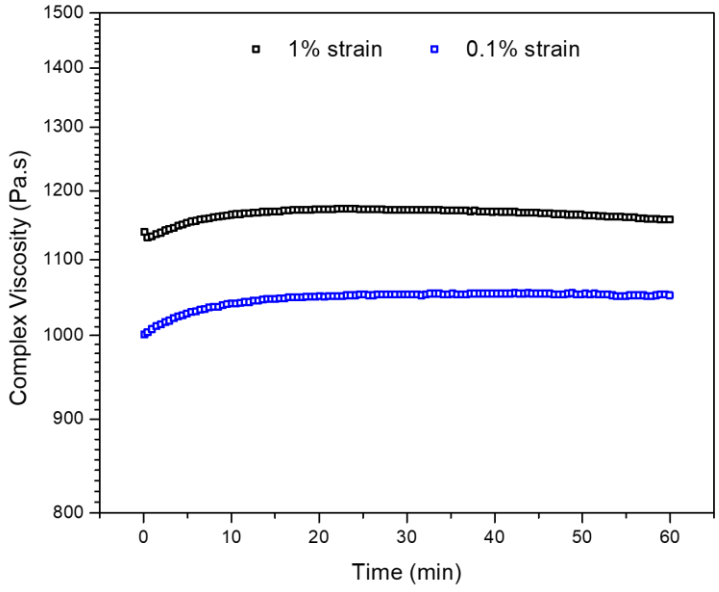

Figure A1. Complex viscosity of 50W-45m after batch processing at 150°C and 100 Hz (625.2 rad/s) over 1 h at 0.1 and 1% constant strain. There is a slight increase in the first 10 min due to integration and swelling of MHF biomass by BmimCl. There is no evidence of other reactions.

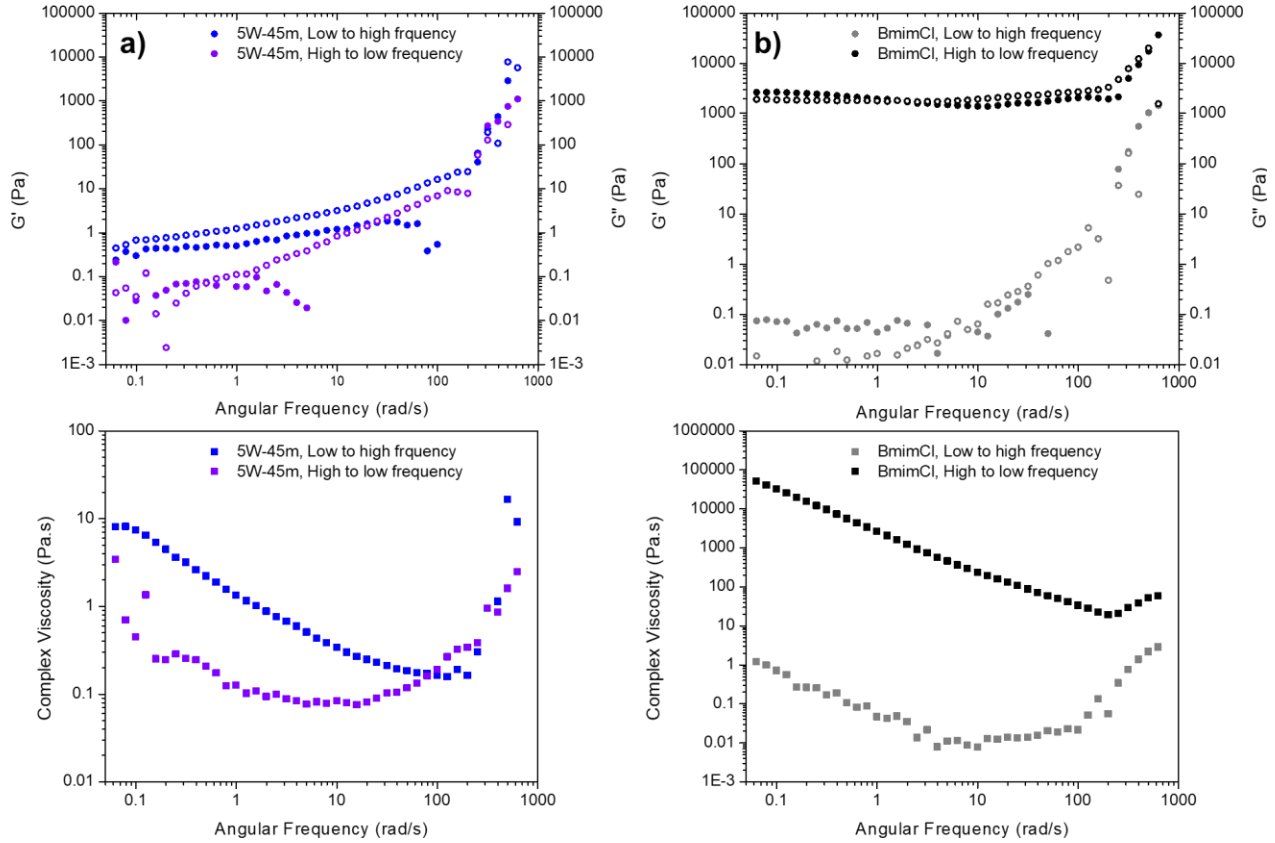

Figure A2. Modulus (G' – closed circle, G" – open circle) and complex viscosity (square) of a) 5W-45m and b) BmimCl after a frequency sweep from low-to-high and high-to-low frequencies for confirmation of apparent shear thickening behavior at high frequencies. Shear thickening behavior remained for all tests. However, during testing at high-to-low frequencies, BmimCl flowed out of the parallel plate set up which led to an erroneous complex viscosity reading that was significantly higher.